12405

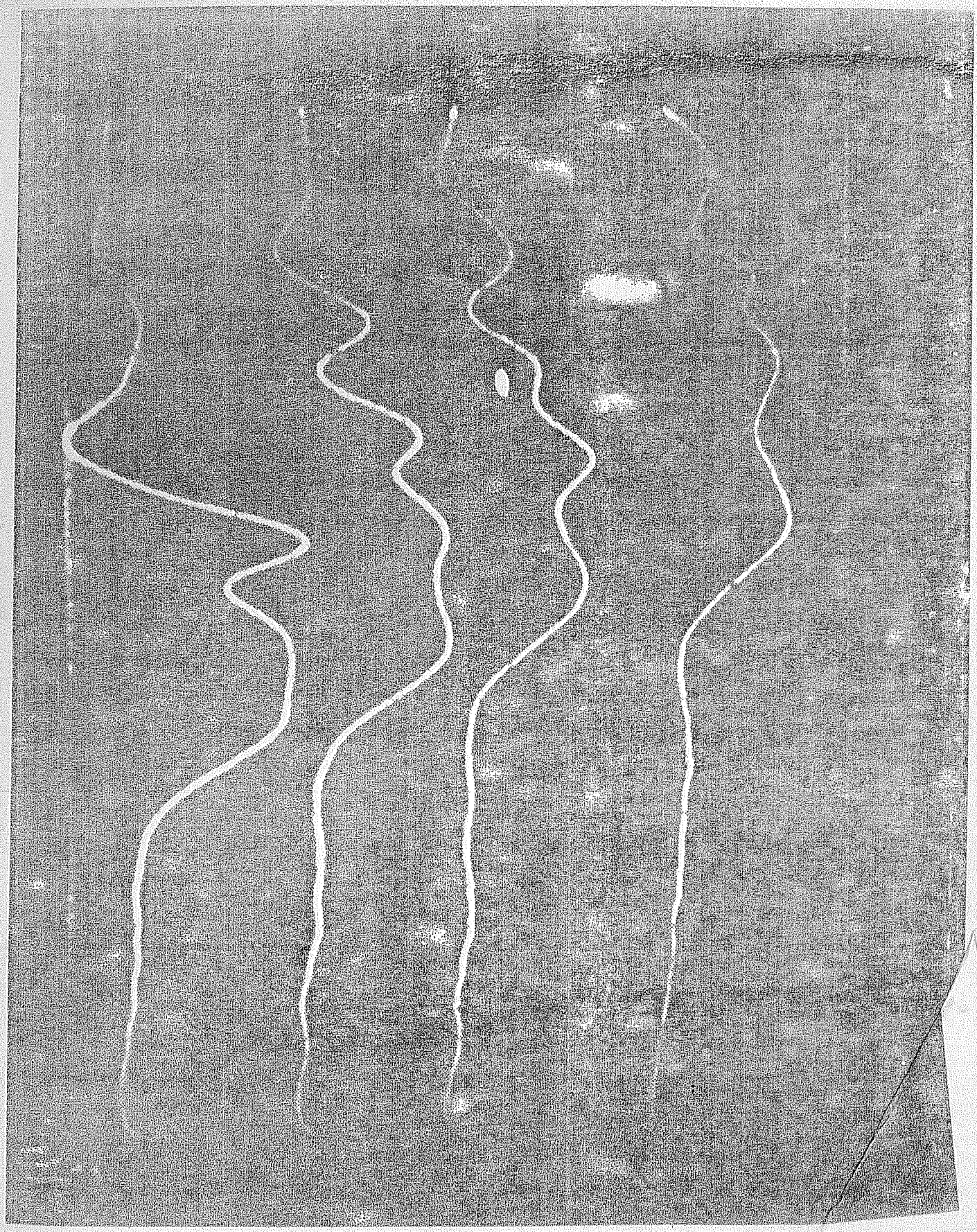

NONLINEAR PROCESSES IN PLASMA

BY

A.N. SEKAR IYENGAR

PHYSICAL RESEARCH LABORATORY

AHMEDABAD 380009

INDIA

A

THESIS

SUBMITTED TO GUJARAT UNIVERSITY

FOR THE DEGREE OF

DOCTOR OF PHILOSOPHY

AUGUST 1984

TO

THEE

MOTHER

"sometimes a scream is better than a thesis"

RALPH WALDO EMERSON

C E R T I F I C A T E

I hereby declare that the work presented in this thesis is original and has not formed the basis for the award of any degree or diploma by any University or Institution.

A. N. Sekar Iyengar

A.N.SEKAR IYENGAR

(AUTHOR)

Certified by :

Y.C. SAXENA

Professor-in-charge

ABSTRACT OF THE THESIS

This thesis describes an experimental study of some nonlinear phenomena in plasmas, like the formation and properties of a double layer, and evolution of a rarefaction waves, in the process of its propagation in plasmas. The experiments on double layers, were performed in a double plasma machine, and the rarefaction wave propagation studies were conducted in a similar device, but modified suitably.

A detailed study of the pseudo-double layers revealed, that it was due to a plasma blob, formed as a result of ionisation of additional neutral gas that leaked into the system, during the probe movement. These effects were observed only when the system was operated at a critical pressure. This led to the formation of potential and density discontinuities. Velocity measurements showed an ion front, moving at a velocity much greater than ion acoustic velocity. Further probing, revealed that it was due to the expansion of a plasma blob, in which was imbedded a double layer, moving almost at the

velocity of the front. From an adiabatic thermodynamic model and a model based on self similar expansion of plasma, we verified that it is possible to accelerate ions to large velocities in an expanding plasma in the direction of electron drift.

Operating the system, below the critical pressures as noted above, we succeeded in generating weak double layers with $e\Delta\phi/T_e \simeq 4$ to 5. We observed criticality in the relative bias conditions too. Beyond a critical bias voltage especially around ionisation potential of the neutral gas, the entire plasma potential in the target region was rendered uniform, by disrupting a double layer.

In the course of our further investigations, we found that on modifying the bias configurations, we could successfully obtain strong double layers. A detailed investigation was carried out, and detected no restraints on the maximum amplitude to the ionisation potential, or electron temperatures. We were able to obtain double layers with $e\Delta\phi/T_e \simeq 50$. A circuit model was carried out, which exhibited an increase in current in the modified configuration. This was verified, by experimentally, monitoring the electron currents in the two configurations. It was found, that the strength of the double

layers mainly depended on the currents involved in the system.

We next carried out a time evolution study of the rarefaction waves in a homogeneous and a current carrying plasmas. In the former case, we observed a phenomena, quite contrary to the fluid theories. The rarefaction wave was found to broaden at the minimum, and developed a shock wave at the trailing edge. The minimum, split into two troughs, one of which propagated at a supersonic speed and the other travelled at a subsonic speed. The KdV equation was numerically solved, with a rarefaction wave, as an initial condition. We did not observe, any result, similar to the experiments. Since the fissioning of the wave, could be due to trapping of charged particles, we have resorted to carry out some computer experiments by solving the ion Vlasov-Poisson equation.

In the presence of a small steady circuit, we pulsed the source plasma of the double plasma machine, and observed a rarefactive wave, to amplify, and also give rise to an ion acoustic type of turbulence. The compressive modes, that formed on the downstream sector damped out, while the dominant rarefactive mode evolved into an ion hole like double layer. Thus we were able to exhibit in the laboratory, for the first time, that

double layers do originate from a rarefactive wave.

LIST OF PUBLICATIONS

1. S.K.Mattoo, Y.C.Saxena, A.N.Sekar.: 1980, Pramana 15 525

   Fake double layers in double plasma devices.

2. Y.C.Saxena, S.K.Mattoo, A.N.Sekar and V.Chandna.: 1981, Phys. Lett. 84A 71

   Propagation and Fissioning of ion-acoustic Rarefaction pulses in a homogeneous Quiescent plasma.

3. S.K.Mattoo, Y.C.Saxena and A.N.Sekar.: Fusion Energy - 1981, Spring College on Fusion energy, Trieste p. 305

   Double Layers with an Expanding plasma.

4. Y.C.Saxena, S.K.Mattoo, and A.N.Sekar.: Fusion Energy - 1981, Spring College on Fusion Energy, Trieste, p. 321

   Fissioning of nonlinear ion-acoustic rarefactive pulse in a homogeneous Quiescent plasma.

5. A.N.Sekar, Y.C.Saxena, S.K.Mattoo, M.Mohan.: 1981, Proc. of All India Plasma Science Symposium 12

   Double layer experiments in Double Plasma Devices.

6. A.N.Sekar.: 1982, Proc. Indian Natn. Sci. Acad., 48A 257

   Plasma Potential measurements using an Emissive Probe.

7. A.N.Sekar, S.K.Mattoo, and Y.C.Saxena.: 1982, Proc. of Int. Conf. on Plasma Physics - Goteborg, Sweden, (eds. Hans Wilhelmsson and Jan Weiland) p. 131

Weak double layers in a double plasma device.

8. A.N.Sekar and Y.C.Saxena.: 1984, Proc. of Int. Conf. on Plasma Physics, Lausanne, Switzerland

Evolution of ion-acoustic rarefaction into a weak double layer.

9. A.N.Sekar and Y.C.Saxena.: 1984, Proc. of Symp. on Plasma Double Layers

Strong double layers in a double plasma machine.

10. A.N.Sekar and Y.C.Saxena.: 1984, To appear in Pramana

Potential double layers in a double plasma device.

11. A.N.Sekar and Y.C.Saxena.: 1984, Submitted to Phys. Letts.

Current driven ion acoustic instability and evolution of a weak asymmetric double layer.

12. A.N.Sekar, and Y.C.Saxena.: 1984, Submitted to Plasma Physics and Controlled Fusion

Development of ion acoustic double layers through ion acoustic fluctuations.

ACKNOWLEDGEMENTS

It is with my heartfelt gratitude I wish to offer the pride of place to my counsellor and companion, Prof.Y.C.Saxena. His constant encouragement in various respects, throughout the dissertation period, made the entire journey a smooth sailing. I take this opportunity to offer him my sincere thanks.

The benefits I reaped from the interactions with Profs.P.I.John and S.K.Mattoo have been boundless and I am grateful to them.

I would like to express my deep sense of appreciation to Prof.Kaw for his mode of converging on a problem from various angles and truly enjoyed his democratic outlook: PHYSICS FOR FUN, PHYSICS BY FUN, PHYSICS IS FUN. I express my sincerest thanks to Profs.B.Buti, R.K.Varma and Abhijit Sen, for their innumerable help and encouragement during my stint as a student.

Words fail me, to express the gratitude I owe the members of the fraternity, Kamlesh, Venkat and Dhiraj for their pleasant company and help in different forms. To my other student colleagues Vijay Shankar and Chenna, I owe a lot thanks for their kind help through useful discussions.

The enlightening and enlivening sessions with Mohan and Parvez, were one of the best phases, in my academic pursuit and I duly acknowledge their everwillingness to help me out, and for the keen interest they exhibited in the experiments.

To Shaikh Saab, I am indebted for the assistance offered to me at all times. No less help was rendered by other colleagues Messrs. Lali, Pujara, Bhatt, Pathak, "Strong man" Suthar and Acharya. I offer my exclusive heartfelt thanks to Krishnamurthi for his kind help with the computations rendered with great enthusiasm.

Hearts are measured by the content of love and affection rather than by diameters in inches. True was this, as I experienced it from my buddies Chandra the pillar of patience, Harish the mountain of magnanimity, Don the Oil Tycoon, Ramesh, Sahu, Jha, Ajai, Nautiyal, Hussein, Veena Venkat, Usha, Chitra, Veerji, Murthy, Robin and Avinash, whose pleasant company diluted the drab hours of monotony and boredom.

To the Banker chums, I reserve my special thanks for the delicacies of all kinds and the humorous Tété-a-Tété provided by them off and on.

I would be unfair on my part not express my gratitude to the Subramaniams, Kotas, Pandyas, Jayakumars, Manians, Narayanans, Chakrabortys and Ashok's parents for their concern in my wellbeing both academically and physically.

To my GURU of martial arts, Pandit Oyabum Kazuyuki Funatsu & his consort Emiko, I humbly offer this piece of work as GURU DAKSHINA for inducting the spirit of a Samurai in me and my sincerest thanks to the NAKAMAHS Kurup, Shivadas and Ashok for the all round conditioning sessions we had together.

It is at this juncture, I would like to thank Messrs. P.S.Shah, Gurang, Darji, P.R.Shah and Rastogi, for the kind cooperation extended to me in the long hour computational jobs.

I would like to thank Mrs.Bharucha, Mrs.Ghia, Mrs.Pannaben, Miss Swadha and the other staff members of the PRL Library and Mrs.Das and Miss Pathak for their extensive cooperation, by going out of their way to help me in the completion of this thesis.

I am truly indebted to D.R.Ranpura and J.M.Patel for having outdone themselves in getting the diagrams

ready within the stipulated time.

If this could be executed successfully it was mainly due to the big hand lent to me by the personnel of all the offices, both technical and non-technical. I am truly grateful for all the help extended to me.

It is time I remember the funtime with my cute little enchanting playmates Jillu, Jittu, Viju, Kartik, Anshu, Rani, Archana, Sidharth, Prashant, Pooja, Yasha and Kanishk, for the grand time I had with them and the annual entertainments they provided, that was probably enjoyed more by me than them.

Messrs. Sourabhan and Murlidhar - the synonyms of diligence and meticulousness. I offer my grateful thanks to you for the excellent jobs done in the completion of this thesis. Vinod's cautious proof reading was an invaluable help.

As one cannot omit his family, I finally thank my father, sister and Rajan for having patiently borne with me, with utmost grace and understanding. I am truly indebted to them and other kith and kin for their constant encouragement, which was a source of

inspiration at the needed hour.

The advent of PPP brought me new friends, and it is my bounden duty to thank them for the mighty help, and cooperation provided to at all times.

Lastly I thank all the friends who have been instrumental directly or indirectly in the successful completion of this thesis.

C O N T E N T S

Chapter 1

INTRODUCTION

1.1 Nonlinear processes in plasma physics

Plasma Physics research, both theoretical and experimental, has undergone a tremendous surge of activity, in the last few years. Plasma effects are finding an ever increasing application in astrophysics, solid state physics, laser physics, gas discharges, and finally the most important of them all being the quest for controlled fusion as a replacement for the existing sources of energy. Depending on the complexity of the various processes taking place in a plasma, they have been classified as Linear, Quasi-linear and Non-linear phenomena.

Plasma possesses the property of sustaining collective oscillations, which in turn provide an interface to transfer energy into a plasma from an external source. Both the linear and nonlinear properties of these collective modes are important and fascinating. They are classified on the basis of some field quantity. When the amplitude of the disturbance in a field quantity is small compared to either the mean value of the field or other appropriately chosen quantity, pertaining to the medium (in case the mean value is zero), then one can obtain linearized field equations which gives linear waves and instabilities. A linear wave can continue to propagate with constant amplitude temporally, at all points of space or spatially as it propagates in space. In either of the latter two cases, the amplitude of the waves, after a sufficiently long time can grow to an extent, that the assumption of linearity breaks down. Obviously, since in almost all cases in nature, enough time is usually available, most disturbances end up in a nonlinear state, in which case, one must use the field equations, without any linearization.

Nonlinear equations, though hard to tackle, describe a rich variety of nonlinear phenomena, that are being explored in the recent years. Thus, we find that the

study of nonlinear phenomena is fascinating as it requires an amalgamation of various branches of physics, like astrophysics, biophysics, particle physics and solid state physics. Some of the amazing processes in plasma physics like the saturation of instabilities, trapping of charged particles etc., have been possible only by nonlinear effects.

1.2 Coherent and incoherent structures

Two subclasses, the coherent and incoherent phenomena belong to the nonlinear processes. The former is a very scarcely found property, but the latter seems to be the most probable state. One of the most difficult problems, has been the understanding of the transition from an incoherent or turbulent state to a coherent structure. What exactly is the process or mechanism, whereby such a transition takes place? What are the factors governing such a transition? Are there systems, at least in a mathematical sense, where such a transition can occur? It is these queries which still remain unexplored.

Amongst the various coherent nonlinear structures found in a plasma, a couple of examples are the Double Layers and Ion Acoustic Solitons. Double layers belong

to the class of a highly nonlinear laminar electrostatic shocks, which have been found to be responsible for the acceleration of charged particles in many regions of space plasmas. They have been suggested to be the end result of certain class of instabilities like the ion acoustic instability or Buneman instability (Buneman 1959). They have been found to be stable even in the presence of fluctuations, driven by the accelerated particles.

The ion acoustic solitons, which are regions of local density maxima, also belong to the class of coherent structures. These waves exhibit the fascinating property of maintaining their shape and amplitude, and still propagate long distances without damping. In these waves, the effect of nonlinearity is to cause a steepening, whereas dispersion broadens the wave. Even if one of the effects dominate, the result would be a distortion of the wave. But in these compressive ion acoustic solitons, both nonlinearity and dispersion, operate on the wave in such a way, that their effects are opposite, and equally balanced. As a consequence, the wave maintains a stable structure, for long distances and times. This fascinating property, has been one of the main reasons, for the extensive study of these waves.

On the contrary, a rarefactive wave, does not possess the same properties of a compressive wave. Instead, both nonlinearity and dispersion operate on the wave in such a way, that there exists no balance between them. As a result, it leads to the steepening of the wave, and finally damps out due to dispersion. Hence, a detailed study of rarefactive waves, has not been carried out to the similar extent, as that of compressive waves.

Of recent, rarefactive waves have been invoked, in the formation of double layers. This has been proposed, mainly, because of its ability to reflect electrons and trap ions in the potential wells. In the presence of a current especially, these rarefactive waves have been observed in computer simulations, to develop into a double layer.

In order to understand the phenomena of some nonlinear coherent structures, this thesis is aimed to investigate some of their properties via double layers, and propagation of rarefaction waves, both in a homogeneous and a current carrying plasma.

1.3 Plasma Double Layers

1.3.1 Historical background

Theoretical plasma astrophysics is usually based on a formalism, that broke down in the laboratory about 25 years ago. Its application to the magnetosphere, has proved to be invalid during, the last few years (Alfvén 1968, 1975, 1976, 1977 and Alfvén and Arrhenius 1976). In this "pseudo plasma" formalism one neglects a number of important plasma phenomena (e.g. electrostatic double layers, current sheaths, pinch effect, critical velocity), which are generally recognised to be of decisive importance. (Alfvén 1968; Fälthammar 1977; Block and Fälthammar 1976; Block 1972, 1975, 1978; Sherman 1973; Danielsson 1973).

Electric fields perpendicular to the magnetic field or Tranverse electric fields, can be easily upheld in a plasma, and are intimately related with the state of motion. Nevertheless, transverse electric fields have proved to be important for some kinds of particle energization, in the magnetosphere.

Electric fields in the direction or parallel to the magnetic fields are termed field aligned or parallel electric fields. These electric fields are particularly

interesting both from a plasma dynamic point of view (e.g. unfreezing of magnetic field lines) and with respect to direct energization of charged particles. For a long time, the importance and even the existence, of magnetic field aligned electric fields in most cosmical plasmas, were disregarded. The main reason for this, was the unjustified extrapolation of the conductivity concept from a medium to a low density plasma. In reality, the conductivity concept losses its meaning and the actual behaviour of the plasma may be more similar to a situation with $\sigma = o$ than $\sigma = \infty$ (Alfvén and Fälthammar 1963, Alfvén 1968, 1977, Fälthammar et al., 1978).

1.4 The double layer phenomena

An interesting phenomena, belonging to the class of parallel electric fields, is that of double layers. The study of double layers also called as double sheaths can be dated to the days of Langmuir (1929). He studied these phenomena of Sheaths, that form around the hot anodes and cathodes, where an excess of negative charges are found around the cathode (negative) and accordingly, an excess of positive charges are found around the anode (positive). These excess charges shield out the long-range coulomb potential and thus produce a sheath so

that a potential plot across the space between the conductors appears as an arctan (fig. 1.1). Langmuir coined the word "Double Layers" to these phenomena.

1.4.1 Free Double Layers :

Of recent double layers have been used to describe the region of transition, between two plasmas at different potentials, far from any boundaries. The number of investigations of these free electric double layers has increased rapidly during the last few years. In many cases, the investigations have been stimulated by the strong evidences from space experiments, that double layers exist in the magnetosphere, above the auroral zones (Wescott et al., 1976; Mozer et al., 1977; Temerin et al., 1982) and other cosmical applications (Alfvén and Carlquist, 1967; Alfvén 1978). Apart from an academic interest, double layer like potential structures, are beginning to find a large amount of applications, in open ended fusion devices like the thermal barriers in Tandem mirrors. In such devices, these structures, enable an effective confinement of the high temperature, charged species (Fowler and Logan, 1977; Baldwin and Logan, 1977).

1.5 Characteristics of a double layer

Some of the widely accepted characteristics of a

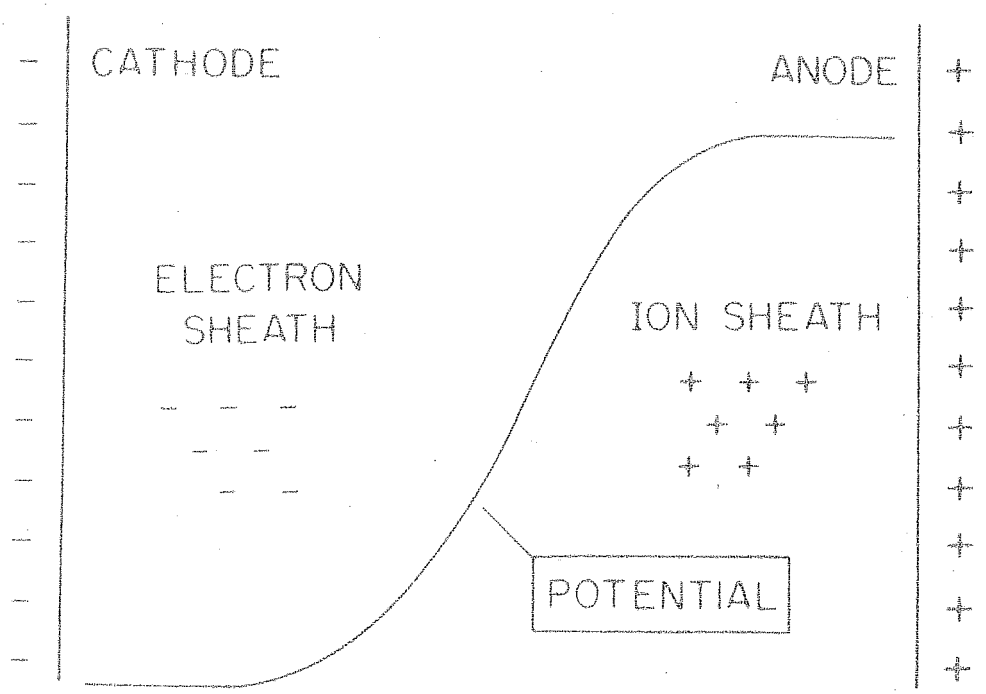

Figure 1.1 A double sheath established between a cathode shielded by electrons, and an anode, shielded by ions. The resulting potential is that of a double layer. After Coakley and Hershkowitz (1979).

double layer are as follows :

1. The double layer is a local region, capable of sustaining a high potential drop ϕ_{dl}, due to space charge separation, and sandwiched between two plasmas. Generally, ϕ_{dl} is larger than the equivalent thermal potential, kT_e/e, of the plasma. Potential drops of the order of 10 - 10^5 volts, have been experimentally found over structures, interpreted to be the double layers.

2. The potential drop ϕ_{dl}, within the double layer is usually assumed to vary monotonically (fig. 1.2a). In some cases, there may be a superimposed fine structure, consisting of several maxima and minima.

3. The electric field, E (fig. 1.2b), which gives rise to the potential drop across the double layer is generated by space charges ρ, according to Poisson's equation. The space charges are primarily concentrated to two adjacent layers of opposite polarity (fig. 1.2c), hence the term double layer. Inside the double layer, the positive charge density produced by the ions may drastically differ from the negative charge density produced by the electrons. Quasi-neutrality, does therefore not prevail in the double layer.

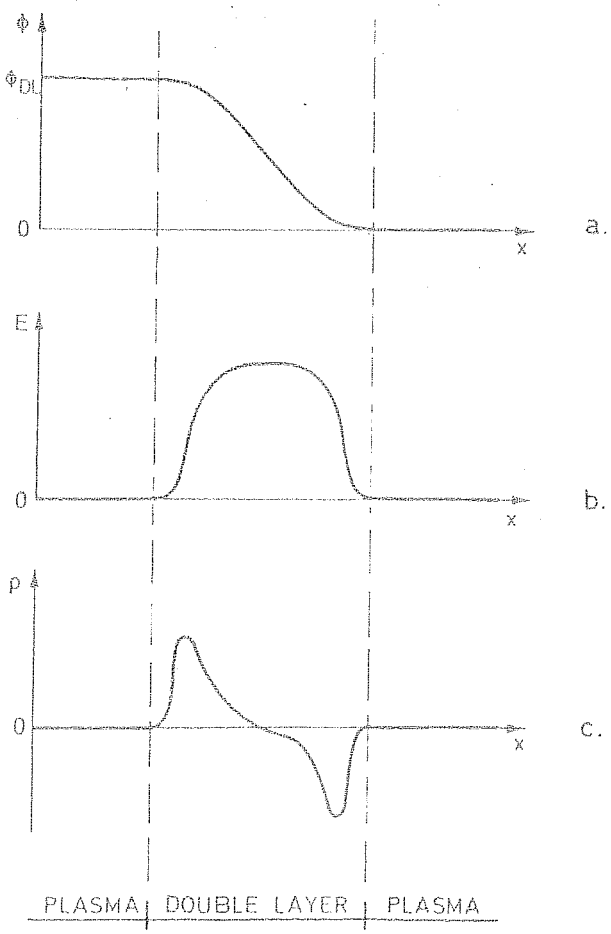

Figure 1.2 Schematic diagram of the variation of a) the potential ϕ, b) the electric field E, and c) the net charge density ρ with the distance x in a double layer surrounded by a plasma. After Carlquist (1979).

4. The electric field is much weaker in the plasma, that surrounds the double layer, than in the layer itself. This implies, that the double layer, taken as a whole, is electrically neutral. It therefore contains an approximate number of positive and negative charges.

5. The thickness of the double layer is generally much smaller than the mean free path of the ions and electrons.

6. Inside the double layer, the ions and electrons, which account for the space charge, are acted upon by the electric field. Some of the particles, are accelerated and form beams on both sides of the layer, while the rest are either decelerated or reflected.

7. Most double layers, which have been experimentally investigated, have carried an electric current, I_{dl}. This does not mean that the current is a necessary condition for the formation of all types of double layers. However, in case electric energy is released, in the double layer, a current must flow through it, since the power developed is

$$P_{dl} = I_{dl} \phi_{dl} \qquad (1.1)$$

1.6 Double Layer formation

It is well known, that electric current densities, exceeding certain threshold values, will drive instabilities, and that the end result can be a state, that constitutes anomalous resistivity. Linear theory is sufficient to determine the onset criteria of these instabilities. But to follow the development of the instabilities into the non-linear regime and through, to the final state is forbiddingly difficult. Yet to do this and take appropriate account of the mutual interaction of the particle and wave distribution functions, is in principle necessary, to calculate the value of the anomalous resistivity. In order to make some progress, one often assumes, that the steady state is one of spatially uniform and time stationary "turbulence" with certain properties, and from there one calculates the corresponding anomalous resistivity.

However, it has become clear from the laboratory experiments, and numerical simulations, that the end result of current driven instability need not be the turbulent state, and the associated distributed voltage drop, characteristic of anomalous resistivity. Instead, the end result can be a localised space charge structure, "a double layer", where essentially, the whole potential

drop occurs over a distance of only some tens of Debye lengths.

With a view to understand the various processes, that goes into the formation of a double layer, and determine what the end result would be, it is necessary to carry out laboratory experiments, and numerical simulations, in addition to the theoretical analyses.

1.7 Review of the Theoretical analysis and numerical computer experiments

1.7.1 Theory : Double Layers with a relative electron drift velocity

Due to the inherent difficulty in carrying out a detailed time dependent theoretical analysis, most of the work has been carried out as a time independent phenomena. One of the first theories can be traced back to Langmuir (1929). It was first demonstrated by Bernstein, Green and Kruskal (1957), that by adding appropriate number of particles, trapped in the potential energy troughs, essentially arbitrary travelling wave solutions could be constructed. These waves were henceforth termed as BGK waves. Montgomery and Joyce (1969) obtained laminar collisionless shock like solutions of the electrostatic Vlasov equation, without invoking a

dissipation mechanism. Assuming a monotonically varying potential, they determined the different sorts of time independent solutions to the electrostatic collisionless plasma equations, that would exist with the following distribution functions, for the electrons

$$f_e(x, v) = f_{ef} + f_{et}(x, v) \tag{1.2}$$

$$f_{ef}(x, v) = n_0\left(\frac{m_e}{2\pi k T_e}\right)^{1/2}\begin{cases}\exp\left[-\frac{m_e}{2kT_e}\left(\sqrt{\left(v^2 - \frac{2e\phi}{m_e}\right)} + V_0\right)^2\right] & v > 0 \\ \exp\left[-\frac{m_e}{2kT_e}\left(\sqrt{\left(v^2 - \frac{2e\phi}{m_e}\right)} - V_0\right)^2\right] & v < 0\end{cases} \tag{1.3}$$

where f_{ef} - free electron species and f_{et} - trapped electron species. The ions were treated to be cold. The trapped particle species for electrons were defined, a distribution function, such that the trapped particle density n_{et}, is always a non-negative, non-decreasing function of the potential. With these, they were able to obtain, shocks, whose amplitudes were unlimited, in contrast to the fluid theories.

Block (1972) derived, from fluid equations, a number of self consistency conditions for stationary double layers. But it was not clear from this work, whether plasma on both sides of the double layer was stable. Knorr and Goertz (1974) constructed strong and

weak stationary shock solutions from the one dimensional Vlasov equation. They derived the necessary conditions for the existence of a double layer and investigated the stability of the plasma in the regions where the potential is constant. The distribution functions of the charged particles both free and trapped, were determined as functions of total energy

$$W = \frac{1}{2} m_j v_j^2 + q_j \phi(x) \qquad (1.4)$$

where m_j, v_j and q_j are the mass velocity and charge of the specific species respectively and $\phi(x)$ is the potential as a function of x.

The density of the free and trapped species, was determined from

$$n_j(x) = \int \frac{f_j(W)\, dW}{\sqrt{2m_j}\sqrt{W - q_j \phi(x)}} \qquad (1.5)$$

Substituting these values in the Poisson equation they were able to obtain a solution of the type

$$\phi(x) = \phi_o \, \mathrm{tgh}\,(x/\xi) \qquad (1.6)$$

They had determined the stability, by evaluating the Penrose criterion. But since Penrose criterion is applied to only homogeneous plasma, the stability analysis is not complete, because it does not cover modes due to

the inhomogeneity. Nevertheless, it has helped in understanding better some of the observations of double layers in space and laboratory experiments.

Wahlberg (1979) investigated the stability problem, of the double layers, in the presence of electron oscillations. It was found that in the weak-field limit, the oscillations are adiabatic and mode coupling is negligible, but becomes significant, if the field is stronger.

Hasan and Ter Haar (1978) obtained solutions of the Vlasov-Poisson equations, resulting in a double layer, with power law distributions for the electrons. This theory was suggested to explain partially, the phenomena of solar flares.

Levine and Crawford (1980) presented a theoretical model to obtain double layers from fluid theory, by choosing appropriate charged species, consisting of both free and trapped electron and ion species.

In most of the works mentioned above, it was necessary, for the current through the plasma to exceed a critical value. This condition was favourable to initiate Buneman instability, before the double layer formation. Some investigations of double layers,

especially the numerical simulations, revealed, that the condition of relative electron drift velocity to be greater than the electron thermal velocity was not necessary. Perkins and Sun (1982), were able to obtain double layer solutions, of Vlasov-Poisson equations, in which no relative electron-ion drift was included.

1.7.2 Double Layers from a rarefactive initial conditions:

There are quite a few theoretical models, which have predicted the formation of double layers, from a rarefactive initial condition. Block (1972), has shown that in a system, possessing rarefactive and compressive waves, it is possible in the presence of a current, to amplify the rarefactive waves, by ejecting out particles, while the compressive modes would damp out, as a result of particles filling the region. But for this to occur, an important condition to be satisfied is that

$$m_e u_d^2 \geq \gamma T_e + T_i \qquad (1.7)$$

where u_d is the relative electron drift velocity, and T_e and T_i are the electron and ion thermal energies.

Carlquist (1972) demonstrated, that in the presence of a current, the plasma was rendered unstable, if the current density exceeded a critical value. As a

result, a small one dimensional disturbance, in the form of density dip would then give rise, to a progressive local evacuation of the plasma. When the particle density in the dip reduces to a certain value, a double layer is formed in the evacuated region. Hasegawa and Sato (1980) showed that in a current carrying plasma, if it was possible to generate a negative potential well, it would result in a double layer, due to reflection of electrons. Raadu and Carlquist (1981) discussed an evacuation process, due to the growth of current driven instabilities in a plasma. The evacuation process was found to work very effectively in the nonlinear phase and leads to an extreme, density reduction, within the dip. It was suggested, that the growth of such structures produced weak points within the plasma, that could lead to the formation of double layers. Hudsen et al. (1983) examined the time-stationary solutions to the Vlasov Poisson equations for ion holes and double layers. From their analysis, it was observed, that double layers evolve from holes in ion phase space.

Lotko (1982) drawing a clue from Buti (1980), suggested that atleast under conditions in space plasmas,

where two electron temperature plasmas were present, it was possible to have rarefactive solitary waves resonantly amplifying into a final structure of a double layer, whereas the compressive modes would damp out. Schamel (1982) reported analytical proofs of the existence of two distinct classes of double layer solutions of the Vlasov-Poisson equations. One class, consists of a strictly monotonic transition of the potential and needs distributions with a beam component. The potential profile and the phase space diagrams are shown in fig. 1.3. The second class has, in addition, a negative potential spike at the low potential side of the double layer and needs distributions which are distorted in the thermal range. The latter, ion acoustic type of double layer, has been identified with an asymmetric ion hole. The potential profile and the phase space diagrams are shown in fig. 1.4. Kim (1983) obtained two different double layer analytic solutions, one related to the electron solitary hole and ion acoustic solitary hole, and has shown, that they are the nonlinear extensions of the slow electron acoustic wave and the slow ion acoustic wave respectively.

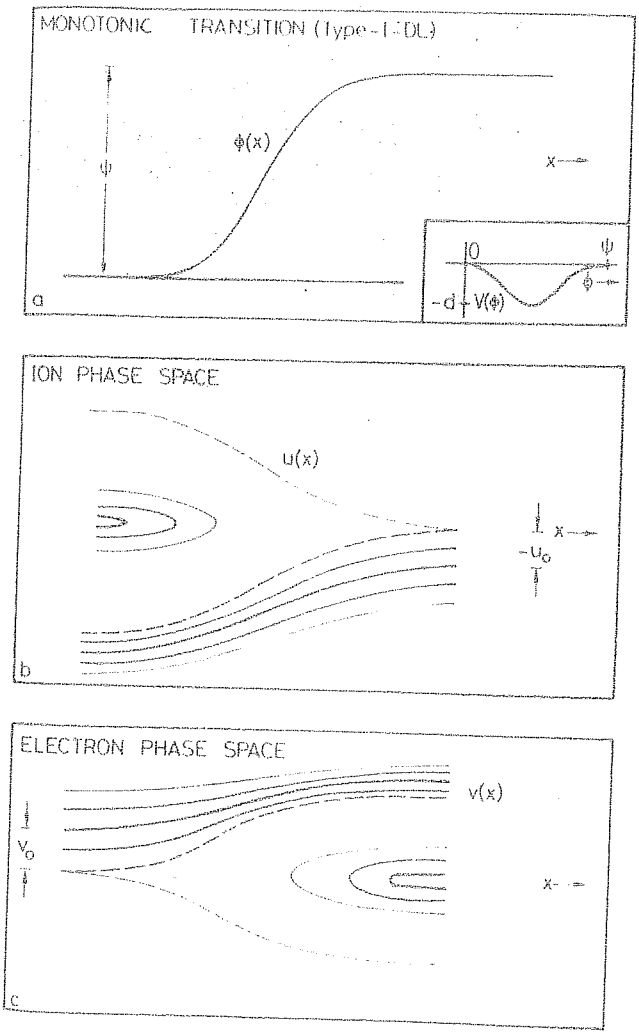

Figure 1.3 a) A qualitative plot of the electrical potential $\phi(x)$ of a monotonic double layer as a function of x.

b) Ion trajectories in the ion phase space exhibiting two species of ions. The dashed line marks the separatrix. Free ions enter into the double layer region from the high potential side with a normalised drift velocity $-U_o$

c) Electron trajectories in the electron phase space, Free electrons enter into the double layer from the low potential side with a normalised drift velocity $+V_o$. After Schamel (1982)

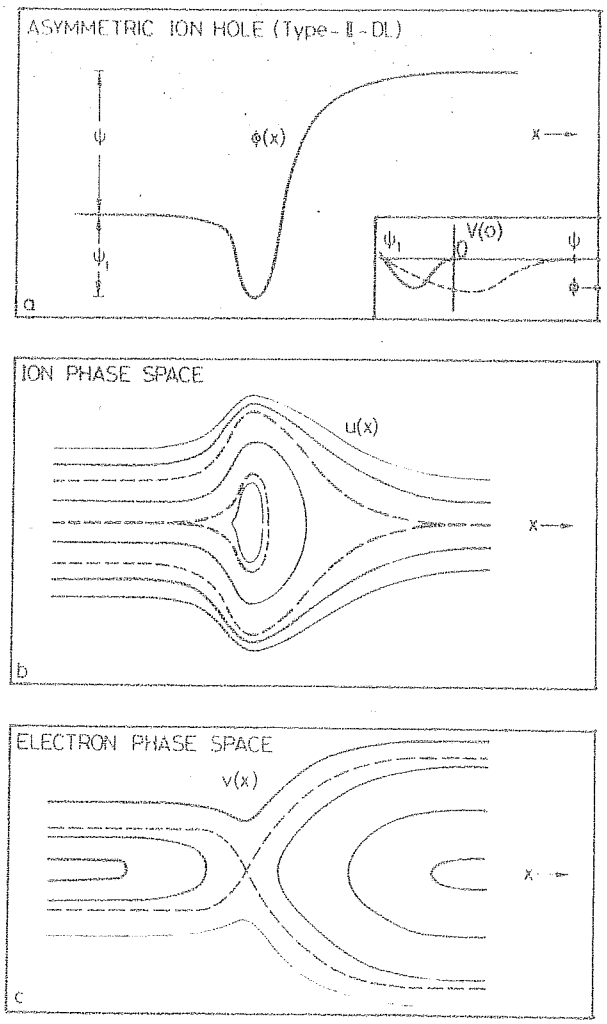

Figure 1.4 a) A qualitative plot of the electrical potential ϕ (x) of the ion acoustic double layer as a function of x.

b) The ion trajectories in the ion phase space, one separatrix respresenting ion trapping in the hole, whereas the other one refers to the reflection of ions at the potential jump.

c) The electron trajectories in the electron phase space, which does not exhibit significant changes. The negative potential on the low potential side reflects the slowly moving electrons. After Schamel (1982).

1.7.3 Computer Experiments :

Though most of the theoretical analyses mentioned above, relate the equilibrium state to the imposed boundary conditions, they are unable to address questions about the accessibility of the steady state to a system in dynamical evolution or its stability. Though the experiments reveal fascinating physics, within the context of laboratory conditions, they are also influenced by such factors as grids, wall sheaths, ionisation of background neutrals etc., they provide limited implications about the accessibility of d.c. state, under space conditions.

In many cases and particularly, in nonlinear fluid or many body systems, numerical simulations are useful for investigation at a level intermediate between the analytical and experimental modelling. Simulations too, have inherent limitations, in the scale and complexity of the descriptions they may economically provide, but subject to these they offer a means to do "experiments" with controls and diagnostics limited to mainly, by the ingenuity of the investigator.

A variety of double layer simulations have

already been carried out, marked by a diversity of approaches, parameter regimes, and results. Because the double layer evolution involves microscopic phase-space phenomena, such as particle trapping, only the particle in cell and Vlasov-Poisson solution methods are appropriate for studying its dynamics, and both methods have been employed.

The different methods and techniques can be classified into distinct groups :-

Group A:1-D, fixed potential simulations
Group B:1-D, floating potential Buneman regime
Group C:1-D, ion acoustic regime, floating and periodic potential
Group D:2-D simulations

The works in group A include those of Joyce and Hubbard (1978), Hubbard and Joyce (1979), Singh 1980, 1982) and Johnson (1980). The common features in these simulations being first, the obtained potentials ϕ_{dl} are "strong"; $\phi_{dl} \gg T_e/e$. Second, they are initialized in a nonequilibrium state; the transient response of the plasma to the initialization is violently nonlinear and dominates the entire evolution. At the outset of the run, a large amplitude solitary pulse, forms near the

low potential end and propagates towards the high potential end. This structure resembles an electron hole propagating towards the high-potential boundary and is a characteristic dynamic feature of all the fixed potential simulations. The pulse relaxes into a monotonic double layer as it traverses the system. A central result in the double layer simulations is the existence of a scaling law relating the width L and potential of the double layer :

$$\frac{e\phi_{dl}}{T_e} = \alpha \left(\frac{L}{\lambda_{eo}}\right)^2 \qquad (1.8)$$

λ_{eo}, is the upstream Debye length. The physical content resides in the constant α, and is essentially determined by the necessity that the distribution function of the reflected particles, to be positive definite (Goertz and Joyce 1975).

Group B includes papers by Goertz and Joyce (1975), Smith (1982), Belova et al. (1983), which are quite different from one another both in their approaches and observed dynamics. Goertz and Joyce (1975) carried out a particle in cell simulation, with stationary Maxwellian electrons. The double layer evolution is marked by the appearance of a solitary pulse near x = 0, which propagates towards x = L, and exhibits an overshoot before

settling into a stationary double layer. Smith (1982) employed a circuit model in a Vlasov simulation. The evolution of the double layer clearly depends on wave instabilities. The unstable modes grow in the direction of the electron drift. As electrons become trapped, the potential rectifies and quasi-stationary solitary pulses develop, with alternating ion and electron holes. As the double layer evolves, the magnitude of the current density decreases. Since no waves were observed outside the double layer, the double layer is stable.

Belova et al. (1980) intialised the simulation in the ion frame, in a longer system than Goertz and Joyce (1975). They observed recurrent explosive instability of the ion acoustic caviton.

Particle in Cell simulations of Ion Acoustic double layers, in group C have been performed by Sato and Okuda (1980, 1981), Kindel et al. (1981), and Hudson and Potter (1981). They exhibit a different phenomenology and dynamics, from that of Buneman double layers, discussed above. In these experiments a long, gentle potential drop is seen in the leading region, which is interpreted as being due to anomalous resistivity developed as the drifting electrons lose their momentum to the excitation of ion-acoustic waves. The striking

characteristic, which is always evident, is the existence of a sharp negative potential spike, immediately preceding the double layer, which resembles an ion hole. The ion acoustic double layer observed in these simulations are all "weak", the central potential jump being of the order of $e\phi_{dl} \leq T_e$.

Under group D, very less of simulations, has been carried out, except for Kindel et al. (1981) and Borovsky and Joyce (1981a,b). Kindel et al. (1981) noted, that in 2-D unmagnetized simulations, double layers do not really form because, electrons are free to scatter around localised potential fluctuations, instead of being trapped. In the presence of a magnetic field, the double layer develops independently on neighbouring bundles of field lines with a perpendicular correlation length of about twice the double layer thickness.

Borovsky and Joyce (1981a,b) obtained U shaped 2-D structures in their simulations. An interesting result of these structures is that both parallel and normal to the magnetic field, and regardless of the magnetic field strength, they scale with the Debye length and not with the ion gyroradius as might be expected.

Inspite of the numerous simulations, there has been no simulation truly applicable to double layers in space. The principal reason concerns the plasma reservoirs, which may be assumed to be unaffected by the double layer in the present simulations in which current closure is implicitly, at the system boundaries. In space, however, the true plasma reservoirs are far from the immediate vicinity of the double layer, and so the distributions of the injection sources must be modelled in such a way that they depend on the evolution of the double layer itself.

As regards to comparisons between simulations and laboratory experiments, many interesting fruitful work could be done in this regard. Though there are a couple of experiments of Baker et al. (1981), and Iizuka et al. (1982), wherein such detailed comparisons have been made, there are more experiments which could be interesting subjects for simulation. Finally simulations may also be exploited to study some of the fundamental paradigms, which seem to be important for double layers, such as the development of ion acoustic cavitons and ion holes.

From the theoretical models and numerical simulations we can conveniently distinguish double layers into

two classes, one, the Buneman type strong double layers with $1 < e\phi/T_e < 1000$ and second, the ion-acoustic weak double layers $0 \leqslant e\phi/T_e \leqslant 1$. The first class of double layers consists of a strictly monotonic transition in the potential. This kind double layer is found in beam and voltage driven plasma. In this class there is no limit on the upper bound of the amplitude of the double layer. The second class of double layers, predominantly found in current driven plasmas has in addition a hole at the low potential side. The potential drop is weak $0 \leqslant e\phi/T_e \leqslant 1$ and covers the range, which was excluded for the first type of double layer. The other synonyms for this could be, ion-acoustic double layer, asymmetric ion hole or weak double layer.

1.8 Review of Space and Laboratory Experiments

1.8.1 Space Observations

The electrostatic double layers may now be considered a well established phenomenon in laboratory plasmas which was stimulated by space observations, by means of rockets and satellites. From the study of Cosmic plasmas, it has been increasingly clear, that such plasmas do not usually differ in any fundamental way from those produced in the laboratory. In

accordance with this view, it was suggested that double layers may exist in cosmic sites such as in the solar atmosphere (Alfven and Carlquist 1967; Carlquist 1969, 1979), in the ionosphere and magnetosphere of the Earth, in the magnetosphere of Jupiter (Shawhan et al. 1975; Shawhan 1976; Smith and Goertz 1976), and in double radio sources (Alfven 1978). Several mechanisms, based on parallel electric fields have been proposed to explain how auroral particles are accelerated (Falthammar, 1977, 1978). One of the most interesting of these mechanisms is constituted by the double layer (Block, 1969, 1972 , 1975, 1978; Akasofu, 1969; Kan et al. 1979; Goertz, 1979).

The first measurements indicating the existence of double layers were obtained by Albert and Lindstorm (1970), from the pitch angle distribution of electrons in the ionosphere above the visible aurora. Wescott et al. (1976) and Haerendel et al. (1976), studied the electric fields in the magnetosphere, by means of artificially injected barium plasmas. Though they were able to monitor the electric fields, it was not evident, if some of the phenomena was essentially due to double layers.

Further, evidence for the occurrence of double layers in the magnetosphere comes from direct (in situ) measurements of the electric fields made on board the S3-3 satellite (Mozer et al. 1977; Temerin et al. 1982). Mozer et al. interpreted their results on the parallel electric fields, in terms of oblique double layers (or electrostatic shocks) similar to that studied theoretically by Swift (1975). Temerin et al. (1982), have observed some new results of the electric field measurements which reveal two types of structures. The first was the double layer which predominantly consists of one polarity, which accelerates ions upwards and electrons downwards. The second type was that, consisting of two opposite polarities and called solitary wave structures. To explain their observations they suggested a mechanism similar to that of Hudson et al. (1983), wherein a rarefactive solitary wave can reasonably amplify into a double layer.

1.8.2 Laboratory Experiments

During the last two decades a great number of experiments have been performed, showing that free double layers of various types can arise under widely different plasma conditions (including both magnetized

and non-magnetized plasmas) (Torven, 1971; Babic, Sandahl and Torven, 1971; Torven and Babic, 1975; Torven, 1979; Torven and Lindberg, 1980; and Sato, 1982). In some plasma experiments, refined equipments and techniques have been required to study the double layers. In other plasma experiments again(though not aimed for the investigation of double layers) it has been difficult to avoid the occurrence of double layers.

According to the methods used for double layer generation, the experiments can be classified into four categories :

Category I :- Double Layers generated by driving a large discharge current between the Cathode and Anode

Torven and Babic (1975) carried out the first clear experiment on the double layers generated in an uniform positive column with a large discharge current between the cathode and anode. At a critical current, a visible boundary was detected across the positive column and this was attributed to a double layer. Though stationary, the voltage was fluctuating, but below the critical value, there appeared periodic pulses that propagated towards the anode at ion acoustic speed.

Levine and Crawford (1980) carried out a similar experiment, wherein they observed an abrupt increase in potential at a critical current. Lutsenko et al. (1976) also observed a current limitation as above, associated with a double layer formation. In this case the double layer always propagated towards the anode after its initial formation, at the cathode.

Category II :- Double Layers generated by applying a large positive potential to an electrode immersed in a plasma

In this case a large positive potential was applied, to a metal electrode immersed in a discharge plasma, (Torven and Andersson, 1979; Torven, 1980). Above a critical value of the plate potential relative to the the plasma, additional ionisation occurred in front of the plate. At this instant a double layer was found to separate out from the anode sheath. Beyond the critical value, the double layer was found to move towards the left. A similar experiment was carried out by Hatakeyama et al. (1980), in a strong magnetic field. A large potential was applied to the end plate, which resulted in the formation of a double layer when the applied potential was greater than the ionisation

potential. Andersson (1977, 1981) investigated the formation of double layers in a similar type of experiment. He was able to obtain double layers, which was found to separate from the anode sheath similar to those of Torven. An important conclusion was that volume ionisation at the anode was necessary to generate these double layers. Stenzel et al. (1982) carried out an experiment to simulate magnetic substorms and solar flares. A potential was applied to a plate to drive a current in the centre of a neutral sheet of magnetic field topology with a discharge plasma. When the current was increased to a critical value, a spontaneous current disruption was observed. The disruption induced a large inductive spike in the plate voltage, which was confirmed to drop off in the plasma forming the transient double layer. In the experiments, belonging to this category, ionisation effects cannot be neglected, since a large positive potential is applied to the electrode immersed in a low density plasma.

Category III :- Double Layers generated by applying a potential difference between two plasmas

Two plasmas produced independently, can lead to two plasmas with different potentials, if a potential

difference is applied between their sources. Hollenstein et al. (1980, 1983) produced two independent plasmas by argon discharge and a potential difference was created by applying a potential between the two sources. In this experiment since the electron drift was smaller than the thermal velocity, ion acoustic instability was considered to give rise to the double layer generation. Torvén and Liting (1982), in a similar Argon discharge, but with some modifications succeeded in obtaining double layers with potential drops upto 1000 volts, in a weakly magnetized plasma column. This value is the highest reported to date. The double layer was stable for a wide range of plasma parameters, though instabilities could be introduced for certain parameter conditions. Sato et al. (1981, 1982) performed some experiments in a Q machine under a uniform magnetic field. Stationary double layers were generated by applying potential differences between the two heated plates on which the plasma is produced by surface ionisation. They were able to obtain potential drops upto 150 volts. An added advantage in their experiment was the very low electron temperature, which led to a large ratio of the potential to the thermal energy. Hatakeyama et al. (1982) also carried out some experiments in similar machines, but with non uniform

magnetic fields like mirrors. It was found that the double layer position was very closely associated with mirror position and mirror ratio. Kanazawa et al. (1981) were able to obtain double layers, with three dimensional configurations under a strong magnetic field. The double layers had a two stage structure in the axial direction and 3 dimensional configuration in the radial direction. Hatakeyama et al. (1982) performed an experiment with a bump in the magnetic field, in which a potential difference was applied between two plasmas. At a position where the two plasma pressures are balanced, a stable potential minimum was observed. The magnetic bump was found to enhance the potential dip. The dip is surrounded by two regions with higher potential of an order of corresponding electron temperature. This potential dip could be correlated to a kind of thermal barrier employed in open ended fusion devices.

Category IV :- Double Layers generated by beam Injection into a plasma

The double layers were generated by the injection of either an electron beam or an ion beam into a plasma. In case of electron beam injection, above a critical

beam current, the pierce instability (Pierce, 1944), gives rise to a potential drop near the beam injection, limiting the beam current. This local potential drop develops into a double layer. Ion beam reflection by a metal plate, biased positively results in an increase of potential near the plate, which leads to the formation of a double layer under a certain condition.

Quon and Wong (1976) obtained the first measurements of the double layers generated by an electron beam injection into a low density plasma. The experiments were performed in a modified double plasma machine. The double layers were obtained only when the electron drift (V_d) was almost equal to the thermal velocity (V_e). Below this critical value only an ion acoustic instability could be excited. The double layers were rendered unstable above the critical value. A similar experiment was performed by Coakley et al. (1978, 1979), in a Triple plasma machine. They were successful in generating strong double layers $e\phi_{dl}/T_e \approx 14$. A clear electron beam generation due to the double layer was reported. Leung et al. (1980) generated double layers, by injecting an electron beam from the source inte the target plasma. The experimental system was a triple plasma

machine, operated in the double plasma mode. As in the experiment of Quon and Wong (1976) they were only able to obtain weak double layers with $e\phi_{dl}/T_e < 10$. They were also limited by the ionisation potential, of the neutral gas.

Iizuka et al. (1979) injected an electron beam into a non-discharge plasma. At a critical value of the beam density, Buneman instability was observed. Above this value, it resulted in Pierce instability. As a result a potential well was created, which developed into a double layer. Baker et al. (1981) used a triple plasma machine of a larger dimension. They used a Kaufman source to produce a plasma, and a strong magnetic field. They were also able to obtain strong double layers with $e\phi_{dl}/T_e > 10$ and thickness of one metre.

Jovanovic et al. (1982) generated double layers in a Q machine, by injecting an electron beam into a plasma produced at a hot plate by surface ionisation of Caesium vapour. The measurements demonstrated a two dimensional configuration of double layers under a strong magnetic field.

Apart from the above experiments, Stenzel et al.

(1980, 1981) performed a novel experiment to generate double layers by injecting an ion beam into a plasma. The ion beam was injected along a converging magnetic field towards a positively biased plate in front of a permanent magnet. They were also able to obtain strong double layers, without being limited by the ionisation potential of the neutral gas.

1.9 Time evolution of double layers :

In addition to the stable double layer experiments, a number of experiments have investigated the formation processes of double layers. Quon and Wong (1976) studied the temporal evolution of the double layer by pulsing the electron drift on and off. They obtained a solitary E-field structure at about 80 μsecs after the electron drift was turned on and reached a steady state was at about 50 μ secs after the passage of the solitary pulse.

Leung et al. (1980) applied a negative potential pulse between the grids and monitored the time evolution of the double layers. At a large voltage, the potential in the target chamber underwent a transient development. They obtained a double layer like structure, which was not stationary, but propagated towards the anode grid, which showed that it was due to moving double layers.

Sato et al. (1981) investigated the double layer formation process, and monitored both the potentials and currents. They also observed a moving double layer like structure with a negative potential dip associated with it. This observation was similar to that of Iizuka (1982), wherein they found a negative potential dip on the low potential side of the double layer. They attributed the decrease in current, in the system, to the formation of this potential dip. This dip was not stationary, but disappeared on reaching the anode and again formed at the cathode end. This phenomena was also attributed to moving double layers, due to plasma expansion from a higher density region to a lower density region. In one of the recent experiments Fujita et al. (1983), in their attempt to investigate the double layer formation process, observed the double layer to separate from the anode sheath and associated with it was a negative potential dip on the low potential side. It propagated from the anode to the cathode region. On reaching the cathode the negative potential dip vanished leaving a stationary double layer structure behind.

Amongst the experiments in group IV wherein double layers were formed by electron beam injection, most of

them were carried out in double or triple plasma machines.

1.10 Experiments in double plasma machine

The first of these experiments were by Quon and Wong (1976). In this experiment, they were unable to produce strong double layers, with $e\phi_{dl}/T_e > 10$. The double layers were rendered unstable, whenever, the electron drift velocity (V_d) exceeded 3 V_e. One restriction in these systems to achieve strong double layers, could have been the large electron temperatures, which were about 2-3 eV. As a result they could never overcome $e\phi_{dl}/T_e > 4$-5, though the potential drops were about 10-12 volts.

Coakley et al. (1978, 1979) were able to observe strong double layers with $e\phi_{dl}/T_e > 10$. They could achieve this only by using specially designed sources. They had deployed surface magnets to contain the primary electrons. As a result they were able to obtain a bulk electron temperature of 1 eV. This enabled them to achieve strong double layers with $e\phi_{dl}/T_e \approx 14$. They had to resort to triple plasma machines, since they had earlier failed to produced even weak double layers in the double plasma machine. But instead,

they had observed another interesting phenomena. As they moved to collecting probe axially, they observed the entire plasma potential to switch from a low state to a high state. As they did not find any signature of an accelerated component, they attributed this phenomena, to plasma itself, to possess two metastable states. Even in their triple plasma device, they were not able to produced stable double layers of amplitudes larger than 22 volts. Beyond $e\phi_{dl}/T_e > 18$, the double layers were rendered unstable.

Leung et al. (1980), investigated the double layer formation in a triple plasma machine, but operated in the double plasma mode. In this experiment too, the electron temperature was about 2 eV, and though they were able to obtain double layers of amplitude of about 15 volts, the ratio $e\phi_{dl}/T_e$ was always less than 10. They also observed that the double layers were unstable for amplitudes greater than the ionisation potential of the neutral gas. Hence they concluded that in terms of experimentally produced double layers, in a multiple plasma device, a strong double layer is one whose potential drop is comparable to the ionisation potential and is not necessarily large with respect to electron temperature.

1.11 Non-linear ion acoustic waves

1.11.1 Theory of Ion Acoustic Waves

Theoretical models for ion-acoustic solitary and laminar shock waves have been discussed by a number of authors (Sagdeev, 1966; Washimi and Tanuiti, 1966; Tanuiti and Wei, 1968; Moiseev and Sagdeev, 1963; Yajima et al. 1966; Mason, 1970; Montgomery and Joyce, 1969; Biskamp, 1969; Otto and Sudan, 1969). Using the equations Sagdeev (1966), first predicted the existence of ion acoustic solitary wave, in a plasma of cold ions and isothermal hot electrons. Using the same equations Washimi and Tanuiti (1966) and Tanuity and Wei (1968) showed that the propagation of weakly nonlinear solitary waves can be described by the K.dV equation, that had been studied extensively by Zabusky and Kruskal (1965).

The KdV equation which describes a weakly non-linear dispersive system is given by

$$\frac{\partial \phi}{\partial \tau} + \phi \frac{\partial \phi}{\partial \xi} + \frac{1}{2} \frac{\partial^3 \phi}{\partial \xi^3} = 0 \qquad (1.9)$$

where ϕ is the density or potential perturbations $\xi = \epsilon^{1/2}(x-t)$, and $\tau = \epsilon^{3/2}t$ are the stretched coordinates. In this equation the convective term

$\phi \cdot \frac{\partial \phi}{\partial \xi}$ describes the nonlinearity and the third-derivative term $\partial^3\phi/\partial\xi^3$ reflects dispersion. Compressive ion-acoustic pulses evolve into ion acoustic solitons (Gardner et al. 1972; Whitham, 1974), which are a stationary solution of the KdV equation and result from the balance of nonlinear steepening and dispersive broadening.

A rarefactive pulse of finite amplitude is also subjected to nonlinear steepening, but unlike the compressive pulse, it does not evolve into a soliton as a balance between non-linearity and dispersion cannot be achieved for it. According to KdV equation a rarefactive pulse should evolve into a wave train.

1.11.2 A rarefactive pulse in a current carrying plasma

Contrary to the propagation of rarefaction pulses in a homogeneous plasma the same has gained a lot of importance in a current carrying plasma in the last few years due to the study of double layers.

Block (1972) determined from fluid equations a condition for an instability containing both rarefaction and compression regions, and also determined the direction of plasma motion in the rarefaction and compression regions, and also determined, the direction of plasma

motion, in the rarefaction and compression regions. He obtained a condition for the electron drift velocity to satisfy

$$m_e v_d^2 \gg r\, T_e + T_i \qquad (1.10)$$

in order to attain a sheath of unlimited strength. Under this condition, plasma particles are ejected out of the rarefaction regions. This leads to a growth of the rarefactive wave and finally transforms into a double layer. Kan and Akasofu (1978) proposed a current interruption mechanism in a collisionless plasma with $T_e < T_i$. They suggested that when a current exceeds the Buneman instability threshold, the instability leads to the growth of Bernstein-Greene-Kruskal (BGK) waves in the form of a row of solitary negative potential wells, in the direction of the current. As these waves grow, they trap an increasing number of current carrying electrons between the neighbouring potential wells. This trapping process was proposed as a possible mechanism for current interruption in a collisionless plasma. Carlquist (1972) considered initially a homogeneous plasma of density $n_e = n_i = n_o$ and carrying a constant current density i. As a result, a small dip in the density occurs at time t = 0. From the equation of

motion for electrons, the electric field, was calculated to be

$$E = \frac{m_e}{e^3} \frac{i^2}{n^3} \frac{\partial n}{\partial z} \qquad (1.11)$$

This electric field ejects out plasma particles, thus accentuating the dip. The result is a progressive evacuation of the dip, and finally the potential resembles a double-double layer. When the density depletion reaches a critical value, the double-double layer disintegrates and evolves into a single double layer.

Schamel and Bujabbarua (1980), showed that the stationary, ion-vortex (plasma hole) is a solitary BGK solution and derived the conditions for its existence. Lotko and Kennel (1981) and Lotko (1982) and Lotko and Kennel (1983) have examined the propagation of solitons along the direction of the field aligned currents and suggested that the upward field-aligned currents in the ionosphere-magnetosphere regions causes rarefactive solitons to amplify, through inverse reflection dissipation, a process which also transforms the initially symmetric soliton into a spatially asymmetric structure resembling a non-monotonic double layer. Schamel(1982)

reviewed the time-stationary theory of phase space holes and double layers and concluded that an ion-hole consisting of a negative potential can in the presence of a current evolve into an asymmetric double layer. Hudson et al. (1983), examined time stationary solutions of Vlasov-Poisson equations for ion holes and double layers, pertaining to recent space observations of Temerin et al. (1982). From their analysis it is suggested that double layers evolve from holes in ion phase space.

Hasegawa and Sato (1982), supposed a negative potential spike to be formed in an electron stream by some mechanism. Then, those streaming electrons whose kinetic energies are less than the peak potential energy can be reflected by the potential spike, thus leaving an electron void in the velocity space on the downstream side of the spike. With this electron void, the potential would swing to a positive value on the downstream side forming a double layer structure.

From flux and energy conservations, the density of beam current was evaluated to be

$$n_b = n(1 + \phi/\phi_s)^{1/2} \qquad (1.12)$$

n is the density, and ϕ is the potential and $\phi_s = \frac{m_e u_o^2}{2e}$.

The density of the thermal electrons was described as

$$n_{th} = n_2 \exp(e\phi/kT_e) \qquad (1.13)$$

The density of ions was assumed to be

$$n_i(\phi) = \frac{2n_o}{\sqrt{\pi}} \exp\left(\frac{-e\phi}{kT_i}\right) \int_{\sqrt{-e\phi/kT_i}}^{\infty} e^{-t^2} \, dt \qquad \phi \leq 0 \qquad (1.14)$$

$$= n_o \qquad \phi > 0$$

These values were substituted in the Poisson's equation and obtained a double layer structure, with a negative potential well on the low potential side.

There are four independent one dimensional computer simulations (Sato and Okuda, 1980; Kindel et al. 1981; Hudson and Potter, 1981; Chanteur et al. 1982), which indicate that a double layer evolves from an initially small amplitude, negatively polarised soliton, which is apparently amplified by coupling, to the electron current. Thus the study of rarefactive waves has generated immense interest in the recent few years in order to explain the formation of double layers.

1.11.3 Experiments on rarefactive waves

Because of the interesting characteristics, a number of experiments have been performed on ion

acoustic solitons, in uniform quiescent plasmas (Ikezi et al. 1970; Hershowkitz et al. 1972; Ikezi, 1978; Watanabe, 1975; Nakamura, 1982; and Longren, 1983), and in plasmas having density gradients (John and Saxena, 1976; Dahiya et al. 1978; John et al. 1977).

Ikezi (1970) and Watanabe (1975) launched a rarefaction pulse in a plasma, which evolved into a wavetrain. Okutsu and Nakamura (1979), have observed ion-acoustic soliton-like pulses evolving from rarefactive initial conditions. Their observations were interpreted in terms of the solution of the KdV equation for an initial rarefactive pulse which evolved with the steepening of the trailing edge into a wave train moving slower than the ion acoustic speed. It has been observed that the width of the pulse launched into the plasma modifies the shape of the profile considerably (Saxena et al., 1981).

As regards, the experiments on the evolution of ion acoustic double layers, from a rarefactive pulse in a current carrying plasma, no laboratory evidence has been attained, except some computer simulations Chanteur et al.1981; Sato and Okuda, 1980; Hudson and Potter, 1981). In our experiment on the time evolution

of double layers, we observed evidences, showing the development of double layers from a rarefactive ion acoustic wave. This will be described later, in this thesis.

Chapter 2

EXPERIMENTAL SETUP AND DIAGNOSTICS

The experiments were performed in a double plasma machine modified accordingly, for the different experiments. A schematic of the device used in the double layer experiments is shown in fig.2.1. The entire vacuum system was made of stainless steel cylindrical chamber, pumped down to a base pressure of about 1×10^{-5} Torr. In the following sections, we describe the plasma sources, the diagnostics etc., that were housed inside the vacuum system, also dealing briefly with the construction of these diagnostics and the electronics circuitry necessary.

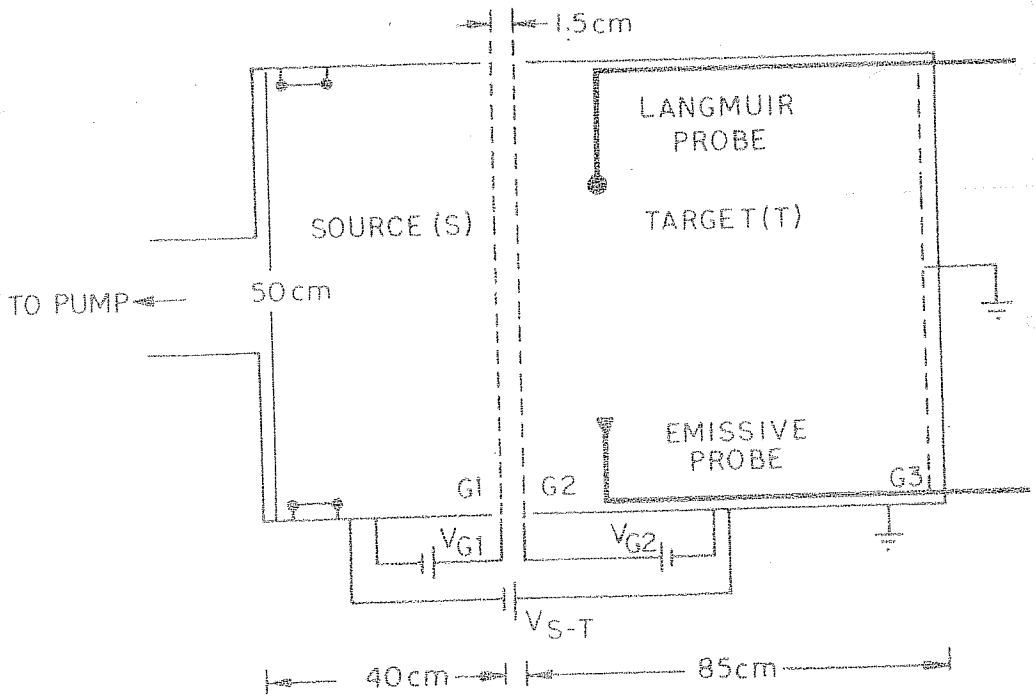

Figure 2.1 Schematics of the double plasma device. Drifting electrons are produced by biasing the source chamber negative with respect to the target chamber. Filaments are placed in the source chamber only. Collecting Langmuir probe and the emissive probe are placed in the target chamber. Grids G1 and G2 are maintained at oV in the normal mode of operation, and are maintained positive with respect to the adjacent sources. Grid G3 is usually grounded.

2.1 Plasma Sources

The double plasma machine comprised of two plasma chambers. One is the source plasma and the other target plasma. The source plasma, was made of a cylindrical mesh chamber of 30 cms long and 30 cms diameter. The mesh chamber itself served as the anode. About 20 tungsten filaments, 8 cms long, were mounted inside the cylindrical chamber. To achieve uniformity of the plasma, the filaments were positioned at equal intervals in a circular configuration, along the periphery of the chamber. The filaments were electrically isolated from the anode body, by porcelein washers. This structure was in turn housed in the vacuum system of 50 cms diameters and 125 cms long. The tungsten filaments were heated to thermionic emission and a steady state discharge was maintained between the filaments and the anode mesh, by accelerating the electrons to about 50-60 volts. The filament heater current was about 150 Amperes at about 10 volts.

The target region did not contain a separate filament source. The high energy drifting electrons from the source maintained the plasma in the target region, by electron-neutral impact ionisation. The target and the

source plasmas were electrically isolated by a grid assembly consisting of two wire meshes of about 70% to 80% transparency. This grid assembly was mainly used as an accelerating structure for the electrons, and also prevent density gradient, that could be present with a single grid. The cross flow of charged particles is prevented by appropriately biasing the grids. As a result, the source and target plasmas could be maintained at different potentials. Depending on the nature of the experiment, we could inject an electron or ion beam by appropriately biasing the source plasma. An end grid G3 was provided at the end of the target plasma, and grounded. The sheath around this grid, helps in maintaining the trapped particle population.

The whole vacuum unit was pumped down to a base pressure of 1×10^{-5} Torr. Different pumping arrangements like pumping from the target section, or source section, were deployed. Their advantages are explained in detail, later in the thesis. The grids were usually biased positive, with respect to their adjacent chambers. For e.g. G1 was biased positive with respect to the source, and G2 biased positive with respect to the target. In some cases, both the grids G1 and G2, were

biased positive with respect to the source. The results, obtained from both the configurations are described later chapters of the thesis.

The experiments on rarefaction waves, in a homogeneous plasma, were carried out in an uniform plasma produced as explained above. A grid of a diameter of 20 cms was used to launch the waves. The experimental set up will be explained in detail in Chapter 5 of this thesis.

2.2 Diagnostics

The diagnostics comprised of a hot emissive probe for plasma potential measurements, a cold Langmuir probe for density, temperature and electron energy distribution measurements. A retarding potential analyser was deployed for ion energy distribution measurements. A detailed account of each of these diagnostics is described below.

2.2.1 Plasma potential measurements using an emissive probe

Electron emitting probes have been used to determine the plasma potential quite accurately to the order of the wire temperature. Its advantage in potential measurements lies in the fact, that it responds to only

particle potential energy unlike the collecting Langmuir probe, which senses both the potential and kinetic energies, of the particles.

An emissive probe forms a diode with a plasma in which it is immersed, but in addition to electrons, we also have ions which are collected by the probe depending on the bias voltage. When the probe is hot and biased below the space potential it emits electrons into the plasma and also collects plasma ions. When biased above the plasma potential it collects electrons from the plasma. The point at which the transition from hot to cold probe takes place is called the inflection point and this point gives the plasma potential.

Several authors (Chen 1965, Kemp and Sellen 1966, Smith et al. 1979) have proposed various methods to determine the plasma potential. The floating potential (Kemp and Sellen 1966) method can be used to determine the space potential of the plasma. The point at which the hot probe deviates from the cold probe (cross-over point) gives the plasma potential. The plasma potential determined from the emission characteristic also gives a good measure of the plasma potential. The double cross technique (Smith et al. 1979), where the plasma potential

is measured from the collection and emission characteristics gives an accuracy of the order of wire temperature.

Both plasma and wire temperatures are obtained from the same probe characteristic. In the experiments on potential double layers, we used the hot probe, for space potential measurements, with high spatial resolution. Some preliminary investigations were carried out to determine the best method of measurement as presented below.

2.2.2 Probe construction and mode of measurement

The probe construction is shown in fig. 2.2. The Block diagram of the electronics used to determine the probe characteristic is given in fig. 2.3, with the timings diagram presented in fig. 2.4. The probe is heated by a half-wave rectifier output which also triggers the comparator, and the measurements are carried out during the off-half cycle to keep the probe at a uniform potential. The probe is biased by a sweep of - 28.0 volts to + 14.0 volts of 5 seconds duration. The probe current is sampled at various bias voltages, using pulses of 50 microseconds width, using a Boxcar integrator operated in the sampling mode. The output or its differential can be directly recorded on a X-Y recorder.

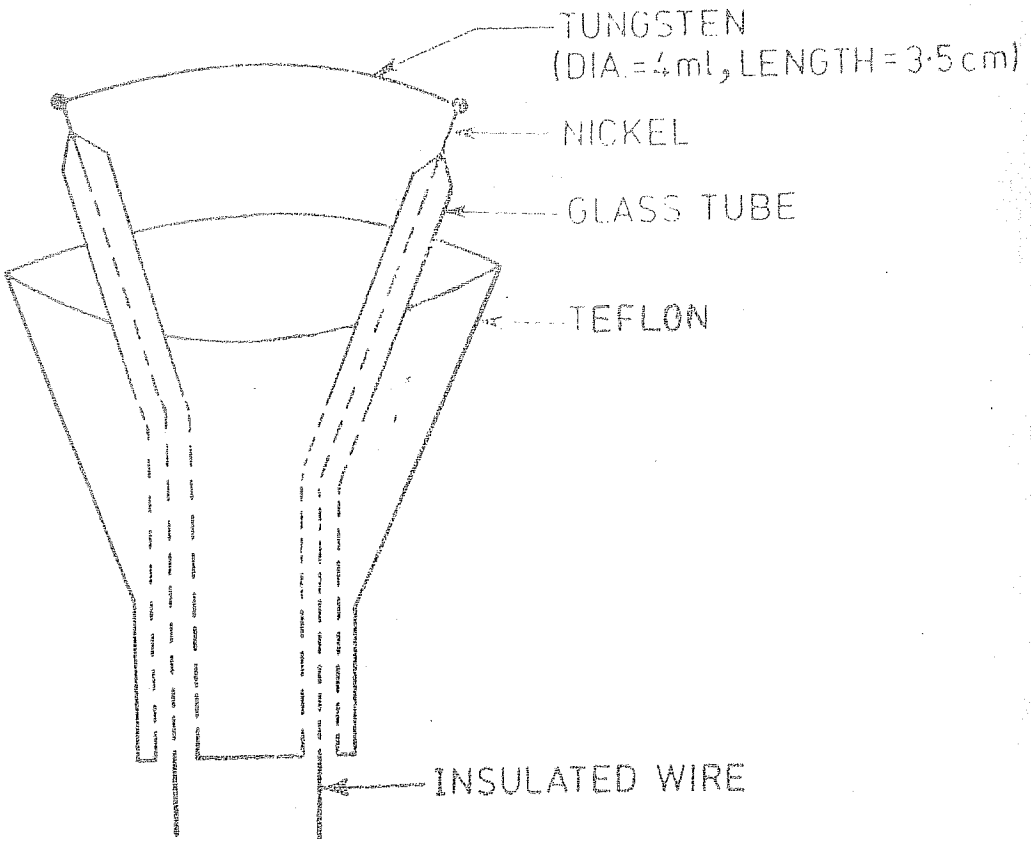

Figure 2.2 Design of the emissive probe construction.

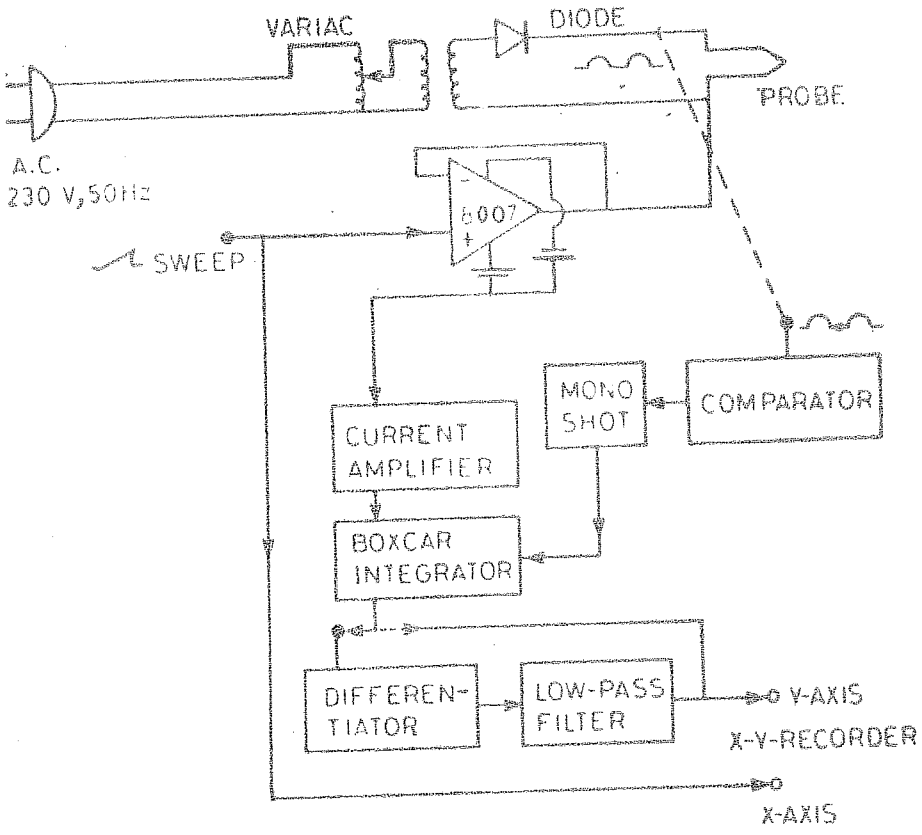

Figure 2.3 Block Diagram of the electronics used in the probe characteristic determination. The probe is heated by a half-wave rectifier output which also triggers the comparator, and the measurements are carried out during the off - half cycle to keep the probe at uniform potential.

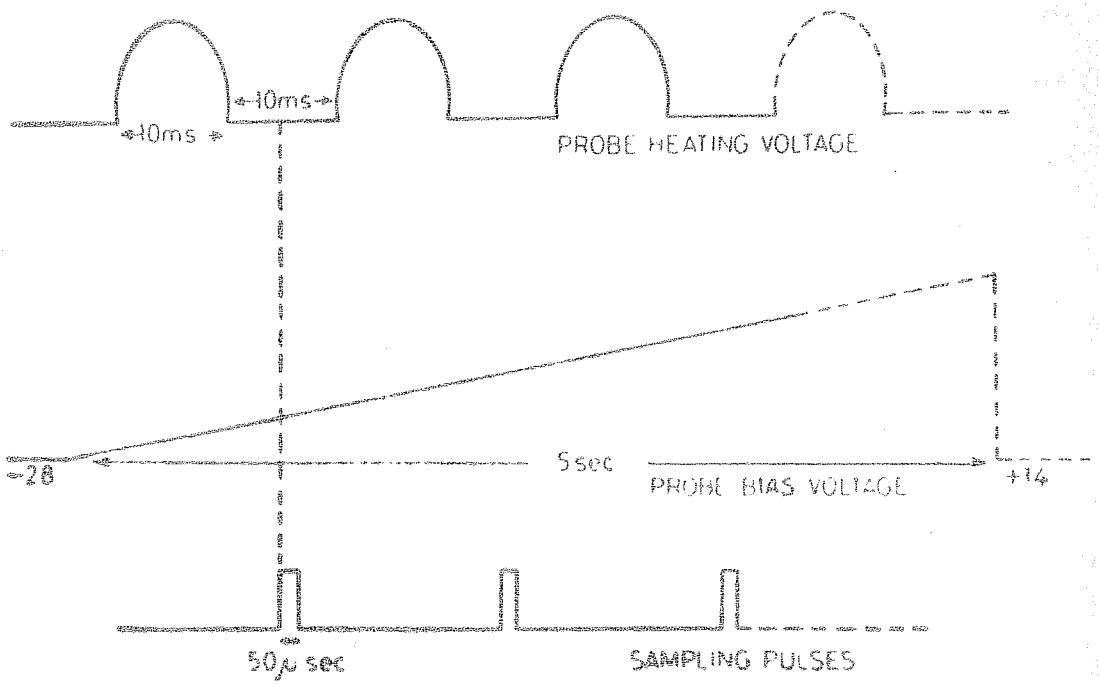

Figure 2.4 The timings diagram for probe current sampling. The probe is biased by a sweep of -28 V to +14 V of 5 seconds duration. The probe current is sampled at various bias voltages using pulses of 50 seconds width, using a Boxcar in the sampling mode. The output is directly recorded on a X-Y recorder.

The characteristics have been obtained in the plasma sources described above. The differentiated curve is also recorded on the same graph. The density is varied by varying the discharge current from 1.8 Amp to 0.3 Amp resulting in a density change by an order of magnitude. The plasma potentials determined by double cross technique are compared with that obtained by the first differential.

2.2.3 Results and Discussion

The probe emission data for 150 volts is given in Table 2.1. Fig. 2.5 shows the probe characteristic at a density of $10^9/cm^3$ and fig. 2.6 at a density of $10^8/cm^3$. It is found that at a density of $10^9/cm^3$, $I_e Sat/I_c Sat < 1$, and the plasma potentials determined by the three methods i.e. from the collection characteristic, emission characteristic and the peak of first differential, are almost of the same order only differing by an order of the wire temperature. At a density of $10^8/cm^3$, I_e Sat/I_c Sat ≈ 1, the three methods yielded three different potentials. This has been found to be prominent only at low densities i.e. at $10^8/cm^3$ and increasing the probe filament voltage does not affect much, since the collection saturation characteristic does not change much though I_e Sat/I_c Sat < 1.

TABLE 2.1

PROBE EMISSION 150 VOLTS

Collection saturation I_c Sat	Emission saturation I_e Sat	I_e/I_c (Saturation)	Plasma potential V_p volts (Collection characteristic)	Plasma potential V_{pe} volts (Emission characteristic)	Plasma potential V_p volts (First differential)	Electron Temperature (eV)	Wire temp. (eV)	Ion saturation current μA	Density n/cm^3
6.7	4.7	0.7	4.0	4.3	4.8	2.5	0.4	100	1.8×10^9
5.0	4.5	0.9	3.8	4.2	4.2	2.4	0.4		1.6×10^9
3.1	4.4	1.4	1.5	3.2	3.2	2.0	0.4		1×10^9
2.5	3.4	1.4	1.3	2.3	2.4	1.6	0.4		9.0×10^8
2.5	2.5	1.0	-2.2	+1.2	-1.0	-1.8	0.4	25	4.5×10^8
6.3	6.7	1.06	-3.2	+0.2	-2.6	2.0	0.4		-
4.5	2.0	0.44	5.6	5.1	5.3	2.8	0.4		10^9
3.3	3.3	1	-1.9	-0.5	-0.1	2.6	0.4		10^8

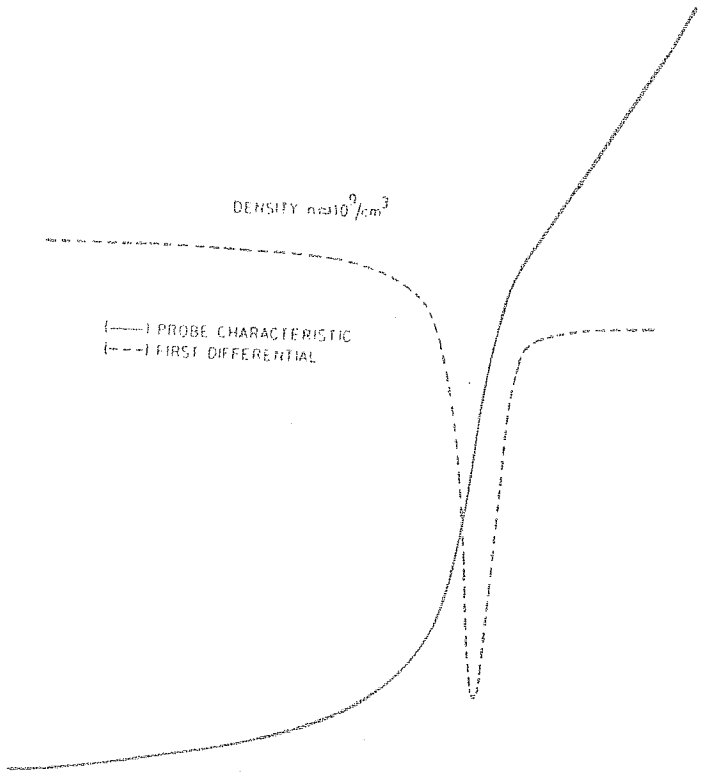

Figure 2.5 I-V characteristic of the emissive probe and the first differential at a density $n \approx 10^{9}$ cm^{-3}.

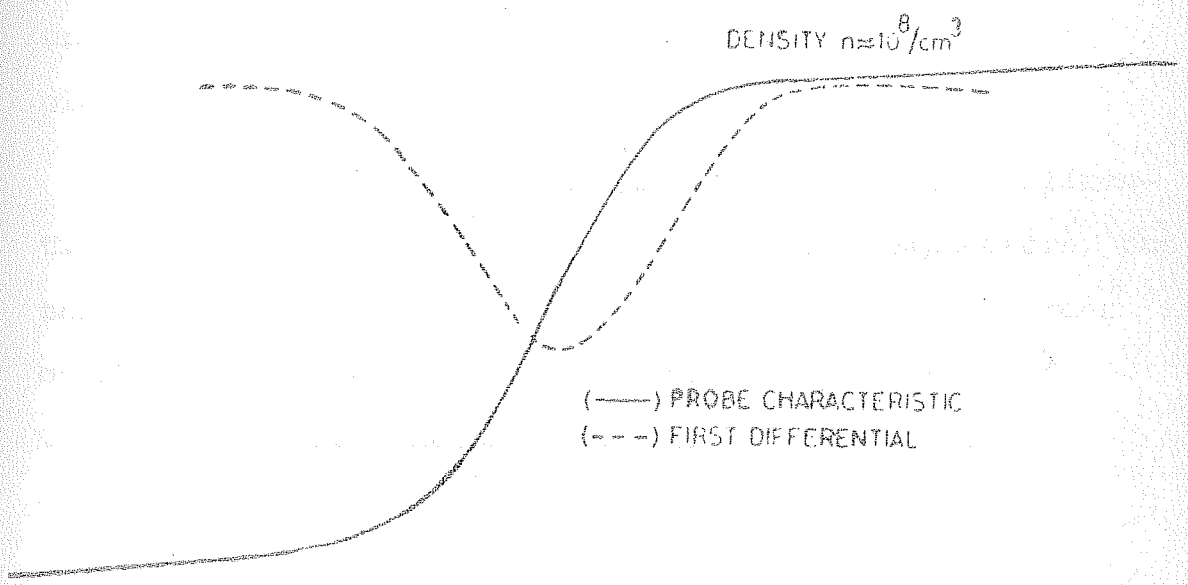

Figure 2.6 I-V characteristic of the emissive probe and the first differential at a density $n \approx 10^8$ cm^{-3}.

The discrepancy in this result at low densities is that the sheath size increases and hence presents almost a planar surface to the plasma. Thus there is a transition from cylindrical probe characteristic to a plane probe characteristic.

The Half width Half maximum (HWHM) of the diffrentiated peak is supposed to give the probe temperature, but this is also true only at higher densities of the order of $10^9/cm^3$, whereas at low densities of the order of $10^8/cm^3$, the width becomes very broad, leading to incorrect determination of probe temperature directly.

It is also noted that between densities $10^8 - 10^9/cm^3$, I_e Sat/I_c Sat > 1, where the emission characteristic gives the same potential as the first differential. From the above observations, we can conclude that the double cross technique is useful at higher densities $\geq 10^9/cm^3$ with I_e sat/I_c sat < 1, where the measured potentials are of the same order as that of the first differential. Finally we observed that the floating point method (Kemp and Sellen,1966) yielded potential measurements as accurate as the first differential method even at low densities. Hence we employed this scheme of measurement in all our observations.

2.3 Cold Langmuir Probe

The cold collecting probe of 1.2 cms diameter, made of tungsten disk, was used to measure plasma density, electron temperature and distribution functions.

2.3.1 Temperature measurement

The block diagram of the electronics used to determine the I-V characteristic, and distribution functions is shown in fig. 2.7. The probe was applied a ramp voltage from -20V to + 20 volts, and the current-voltage characteristics (I-V) were directly obtained on the X-Y recorder or the oscilloscope. The temperature was obtained from the formula

$$kT_e \text{ (eV)} \approx \frac{d(eV_p)}{d(\ln I_{probe})} \qquad (2.1)$$

k is the Boltzman constant, V_p probe bias potential, I_p is the probe current.

2.3.2 Density measurement :

The probe was biased to large negative values to collect ion saturation current. The density was obtained from the eqn. (2)

$$N_e = \frac{(I_{ion})_{sat}}{ev_i \cdot A} / cm^3 \qquad (2.2)$$

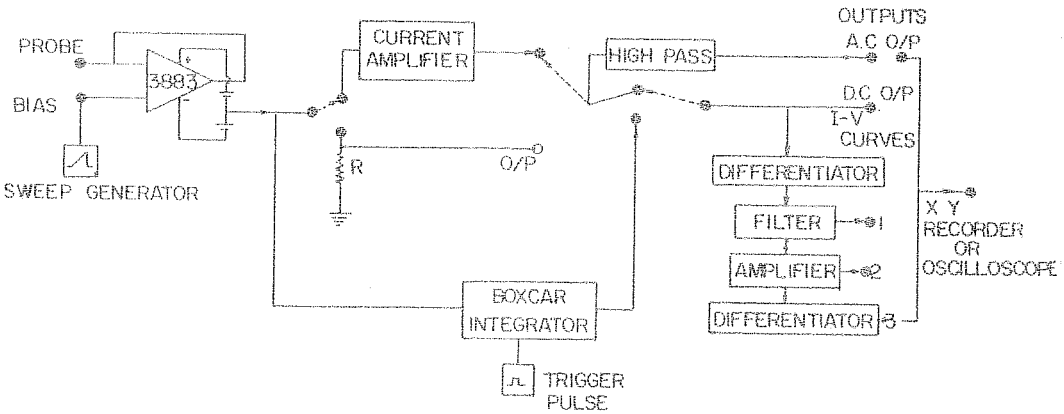

Figure 2.7 Block diagram of the electronics deployed in obtaining the I-V characteristic and the distribution function of a collecting Langmuir probe.

$(I_{ion})_{sat}$ - Ion saturation current, v_i - ion acoustic velocity = $\frac{2kT_e}{M_i}^{1/2}$ cms/sec. A - Area of the collecting probe in cm^2, M_i = Mass of argon ion.

2.3.3 Electron Energy distribution

The I-V characteristic, thus obtained as mentioned above, was differentiated electronically, to yield the energy distribution function f(V), as explained below :

Let the electron current collected be

$$I_p = nev \tag{2.3}$$

where I_p is the current,

n is the density

v is the velocity of the electrons due to the applied potential.

In terms of the velocity distribution function, density n can be written as

$$n = \int f(v)dv \tag{2.4}$$

Substituting this in eqn. (2.1)

$$I_p = e\int f(v)vdv \tag{2.5}$$

This can be written in terms of energy due to the applied potential as

$$I_p = \frac{e^2}{m} \int f(V_p) dV_p \qquad (2.6)$$

V_p is the potential applied to the probe

Differentiating equation (6) we get

$$dI_p = \frac{e^2}{m} f(V_p) \quad dV_p \qquad (2.7)$$

$$\text{Hence} \quad \frac{dI_p}{dV_p} = \frac{e^2}{m} f(V_p) \qquad (2.8)$$

In general, equation (8) can be written as

$$f(V) = \frac{m}{e^2} \frac{dI}{dV} \qquad (2.9)$$

Hence from equation (9), we find that the first differential of the I-V curve yields the electron energy distribution.

2.4 Gridded Energy Analyser

A retarding potential analyser (RPA) consisting of grids and a collecting disk was deployed to monitor the ion energy distribution functions. The dimension of the RPA was about 3 cm long and 2 cm diameter. The RPA used in our system consisted of one grid and a collecting disk. The outer enclosure was left at floating potential to repel ions. The grid mesh was applied a negative potential to collect ions, but repel electrons. The potential

on the collector was varied and the ion current was monitored with respect to the collector potential. The first differential of this I-V curve yielded the ion distribution function. The ion temperature measured with this analyser was about 0.2 eV.

2.5 Probe Configurations

In addition to the individual probes, we had mounted a cold Langmuir probe and a hot emissive probe, on the same shaft one slightly above the other. The shaft was insulated and placed along the wall of the system, to minimise the disturbances, to the bulk plasma. The advantage in this arrangement, is that, in the presence of a double layer, the plasma potential and the corresponding distribution function can be measured simultaneously, at a particular point.

Chapter 3

MOVING DOUBLE LAYERS IN AN EXPANDING PLASMA AND WEAK DOUBLE LAYERS

3.1 Moving double layers

In our efforts to form double layers, we found that as the emissive probe was moved axially to scan the axial plasma potentials, there occurred abrupt potential jumps in a distance of about a Debye length. These results were similar to those observed by Coakley and Hershkowitz (1979). In order to understand the physical process involved, we carried out further investigations, which are explained in the following paragraphs of this chapter.

3.1.1 Experimental setup and diagnostics

The experiment was performed in a double plasma machine, similar to that described in 2.1. In this assembly the grids were biased positive with respect to the adjacent chambers, i.e., the grid G1 was biased positive with respect to the source plasma and the grid G2, was biased positive with respect to the target plasma. The base pressure in the system was $\approx 10^{-5}$ Torr, whereas the working pressure was between 8×10^{-5} Torr, to 2×10^{-4} Torr. The essential diagnostics, were collecting Langmuir probe, to measure plasma density, electron temperature, and distribution functions. The emissive probe was deployed to monitor plasma potentials directly by the floating potential method (Sekar 1982). The plasma parameters in the system were $N_e \approx 10^{+7} - 10^{+9}$ cm^{-3}, $T_e = 2eV$, $T_i = T_e/20$. Three Langmuir probes spaced at equal distances, as shown in fig. 3.1, were mounted on the same shaft, and biased to collect electron saturation currents.

3.2 Experimental Results

3.2.1 Axial variation of plasma potential

A large electron current was made to flow, from the source to the target chamber, by means of a relative

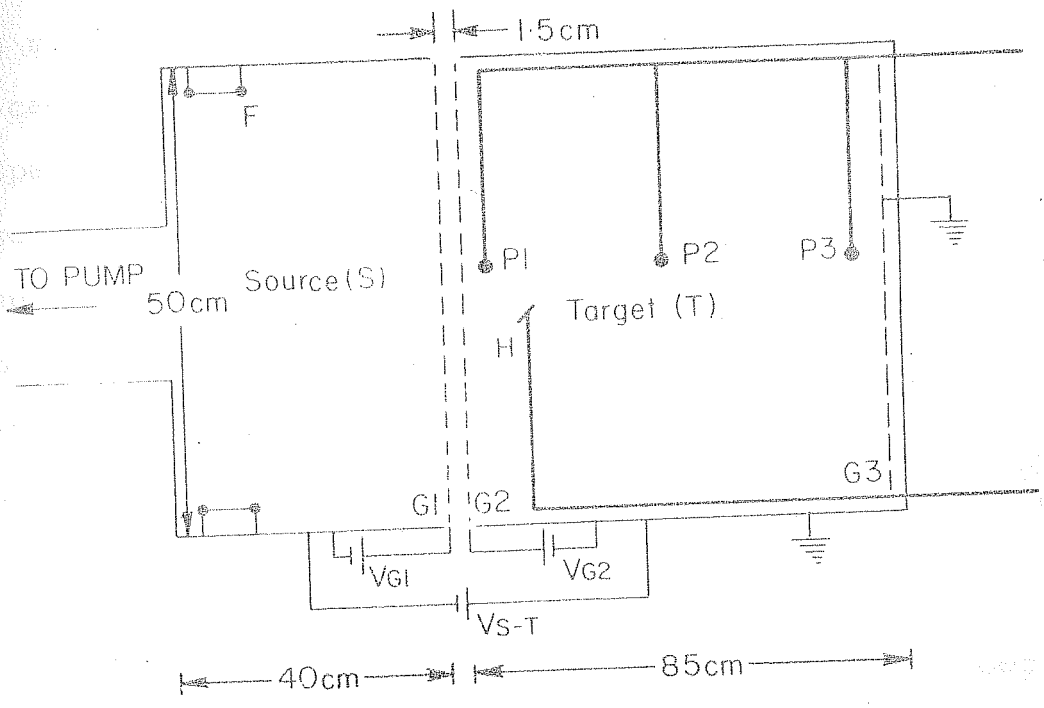

Figure 3.1 Schematics of the double plasma device. Drifting electrons are produced by biasing the source chamber negative with respect to the target chamber. F-Filaments, P_1, P_2 and P_3 - collecting Langmuir Probes, H-Emission probes. Grid G1 is biased at oV with respect to the source, potential of grid G2 is varied between 0-10V with respect to the target and end grid G3 is grounded.

bias between the source and the target. The space charge effect of this current, lowered the plasma potential in the target region close to the grid G2 and was negative with respect to the ground. The pressure of argon gas was carefully adjusted to prevent complete neutralization of space charge of electron current. In a certain range of neutral pressures, below a critical pressure, plasma potential changes $e\Delta\phi > kT_e$, extending over several tens of Debye lengths, were observed. This will be shown in the next subsection. At a critical neutral pressure, determined by the relative bias on grids and between target and source chambers, the plasma potential made an abrupt transition (over a distance $\approx$ Debye length), as the position of emissive probe was changed in the target region. Fig. 3.2 illustrates the observation of such a sharp potential jump in one typical case.

The profile A was obtained while the emissive probe was moved away from the grid G2. It can be seen that at a certain position in the target chamber the plasma potential makes a sharp transition from a low-state of -6V to a high-state of + 4.4V in a distance of $\approx$ 0.2 cm. At this instance, there occurs a visible increase in the plasma glow indicating that the plasma density has

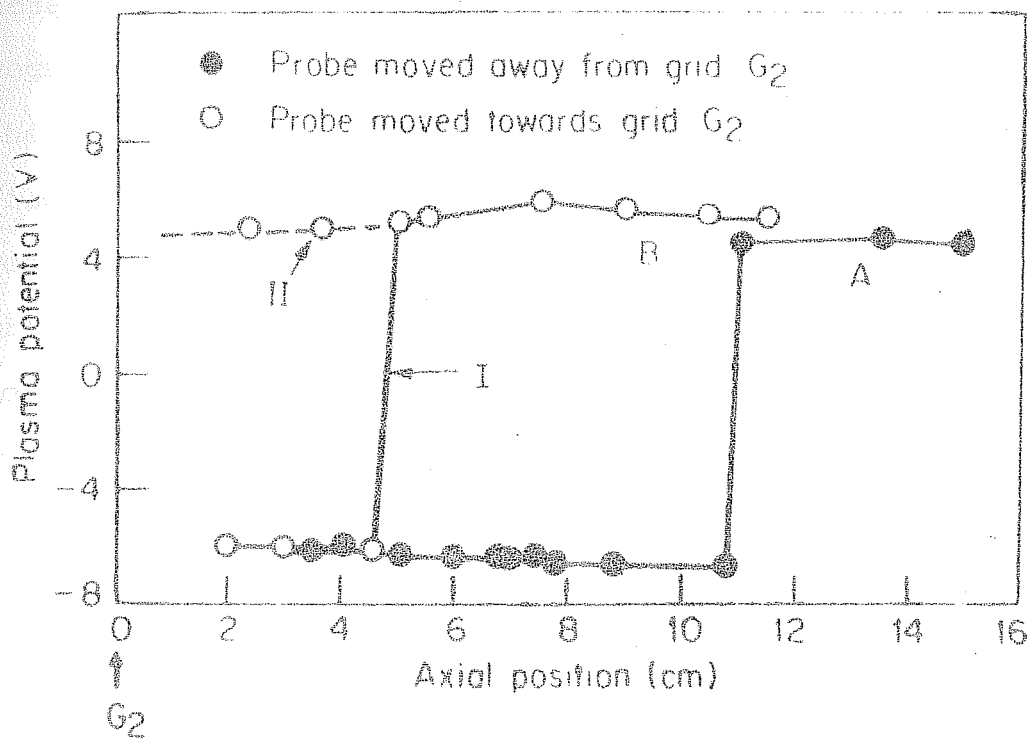

Figure 3.2 The plasma potential is plotted for various axial positions of the emissive probe. Profile A corresponds to when the emissive probe is moved away from the grid G2 and profile B when the probe is moved towards the grid G2. The dashed line (branch II shows that occasionally the entire plasma remains at high potential state).

increased. Also collecting Langmuir probe shows that the plasma density increases from 2.4×10^8 cm^{-3} to 4×10^8 cm^{-3}. The profile B corresponds to the measurements obtained while the emissive probe is moved from the region of the high-potential state towards the grid G2 and different from the position of transition in the profile A. This is indicated by branch I of profile B. Occasionally, the plasma potential did not make any such transition and the entire plasma remained at the high potential state (branch II of profile B). To realise the initial conditions it became necessary to disturb the device controls like the needle valve which maintained the gas flow or the relative bias between the source and the target chamber. Apparently resetting of the device controls enabled us to reduce the ionisation of the neutral gas in the target chamber to an extent that space charge of the electron current was not completely neutralised. From the analysis of Langmuir probe traces we did not find any indication for the presence of beam electrons with energies less than or equal to the potential jump as shown in fig. 3.3 after the transition was effected. The probe characteristics before and after the transition, only exhibited a change in the electron temperature.

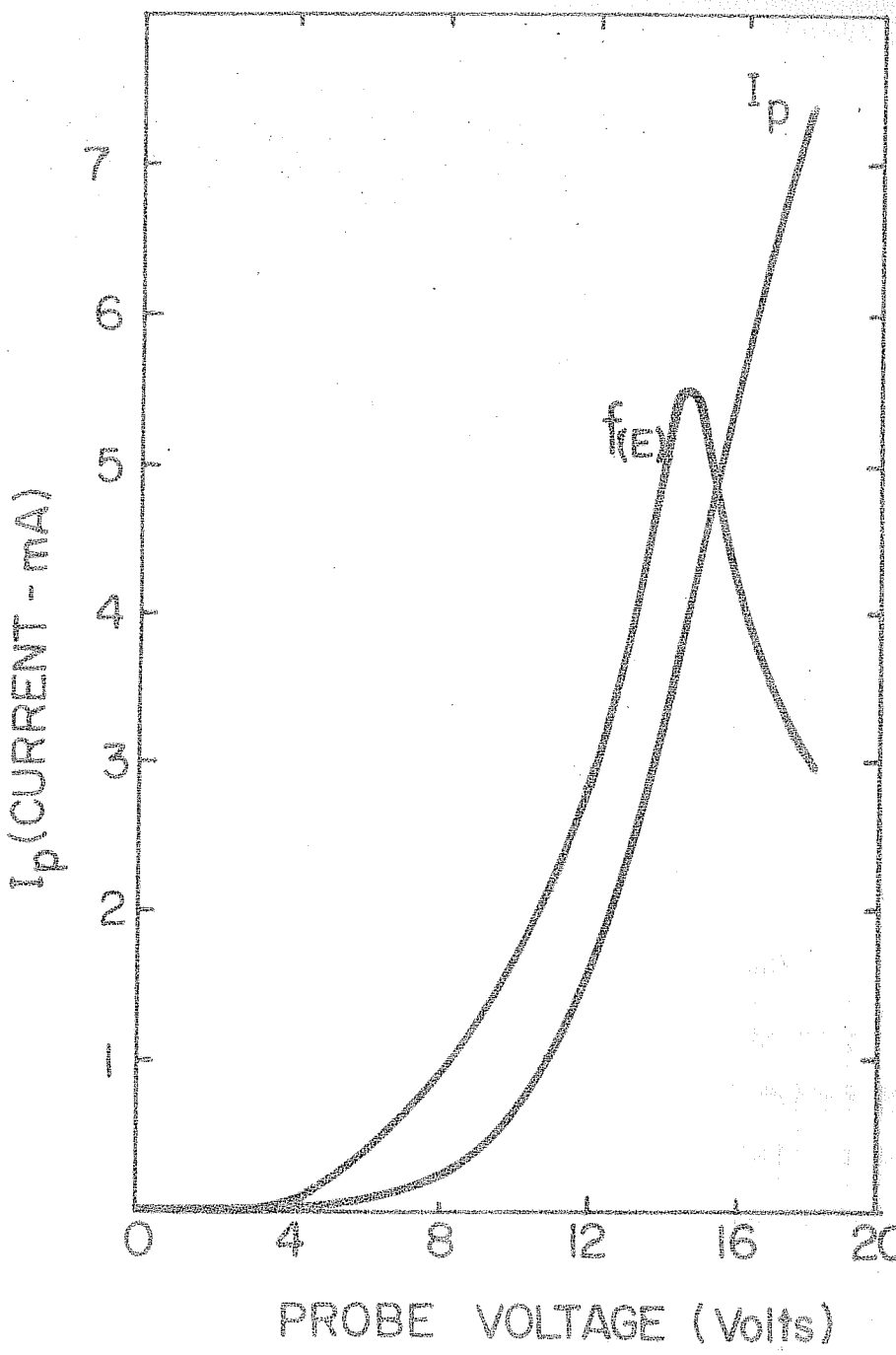

Figure 3.3 The I-V characteristics and the electron distribution function obtained with a Langmuir probe, after the transition in plasma potential was effected by the movement of the emissive probe. There is no indication of the beam component in the plots.

3.2.2 Variation of plasma potential profiles at different Neutral pressures

Fig. 3.4 shows the variation of plasma potential axially at different neutral pressures. The inset is the one shown earlier in fig. 3.2. As mentioned earlier, the effect of biasing the source plasma negative with respect to the target, was to cause a large electron current to flow from the source to the target chamber. Depending on the pressure of neutral gas, the net effect was to lower the plasma potential in the entire target region.

As seen from the fig. 3.4 at low pressures (7×10^{-5} Torr) an extended potential structure, corresponding to a drop of $\simeq$ 12 volts over 20 cms is formed with a potential minimum adjacent to the grid G2. Of the applied potential between the chambers nearly half appears across this extended potential structure, and the rest appears across the sheath formed around the end grid G3.

The measured electron distribution does not contain any beam component, but it could be represented by two population of electrons, hot and cold. As the hot plasma component is increased by increasing the relative bias voltage, to accelerate electrons from the source, the

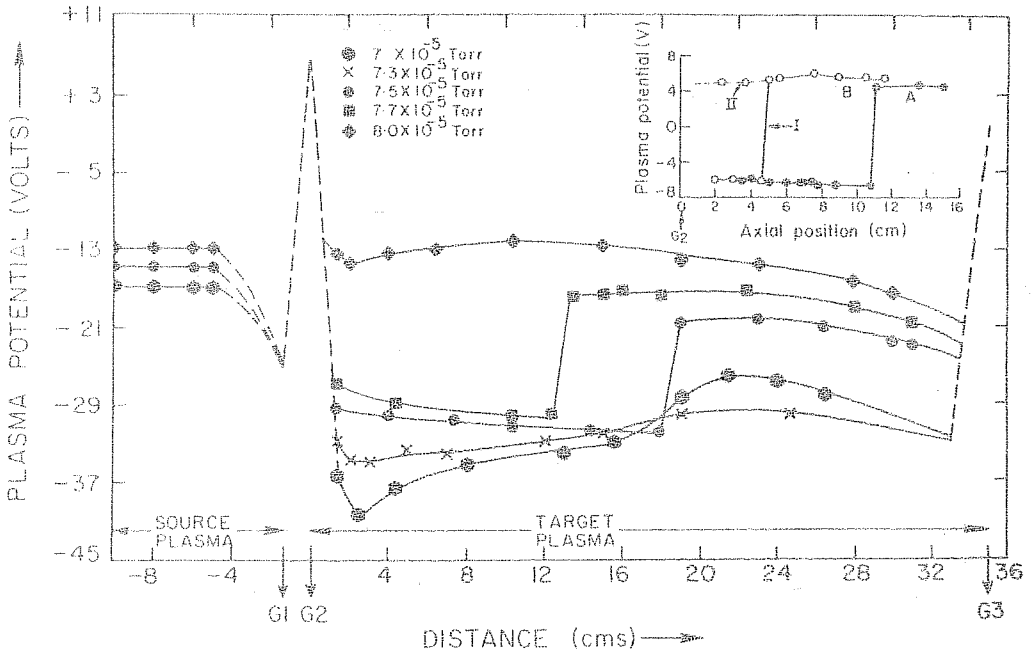

Figure 3.4 The axial plasma potential distribution in the target chamber at various indicated pressures, obtained by the emissive probe. The inset is the same as that in fig. 3.2.

spatial variation gets modified. The potential near G2, becomes positive, and potential near G3 more negative. At the critical pressure, the entire plasma potential undergoes a rise in potential. This transition occurs over a distance of one Debye length. At 8×10^{-5} Torr, the entire plasma attains uniform potential. The difference between the source and the target potentials become very small. Any increase, in the neutral gas pressure makes very little change in the spatial variation of the plasma potential profile, in both the source and the target chambers.

3.2.3 Variation of plasma potential at different relative biases

Similar effects were observed with different relative biases at a constant pressure, as shown in fig. 3.5. At about 10 volts applied to the source, the electron current injected into the target plasma lowers the potential of target plasma due to the excess space charge. The result is an extended potential structure. At a critical threshold value of bias the entire potential of the target plasma undergoes a sudden transition as the probe was moved. The potential jump observed at regions close to the grid G2 was larger

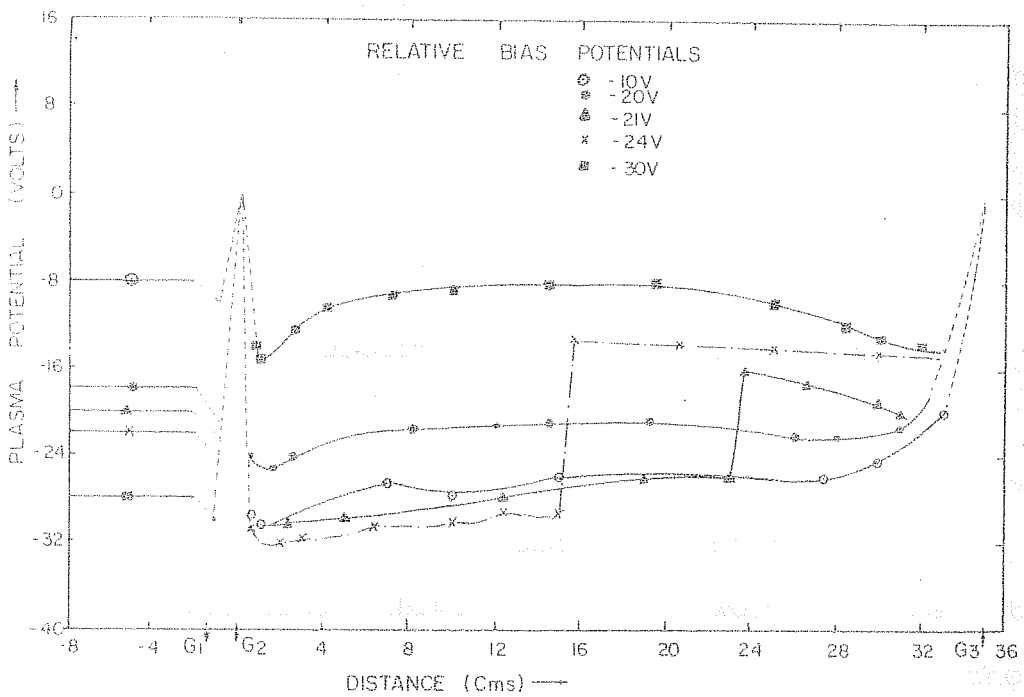

Figure 3.5 The axial plasma potential distribution in the target chamber at various indicated relative bias voltages, monitored with the emissive probe.

than the potential changes near grid G3. Upto about 24 volts, it was observed that the target plasma potential was lower than the source plasma potential. But at about 30 volts, the potential change took place very close to grid G2. At this instant the potential of the target plasma was more positive than the source plasma. Another interesting result was that at lower potentials, the plasma attained its original state as the probe was moved towards G2, resembling the results shown in fig. 3.2.

It was also observed that the value of the relative bias needed to trigger these transitions was lowered as neutral pressure was increased. In all these cases the maximum potential jumps were of the order of the ionisation potential. Similar effects were observed at different G2 bias voltages also. It was found that the high state plasma potential was almost close to the potential of grid G2. It increases with the bias voltage of grid G2 as shown in fig. 3.6.

3.2.4 Location of initial ionisation

Since the maximum potential drops occured near the grid G2, we carried out an investigation to locate the source of ionisation. Hence we monitored the variation of the plasma potential, near the grid G2, as the neutral

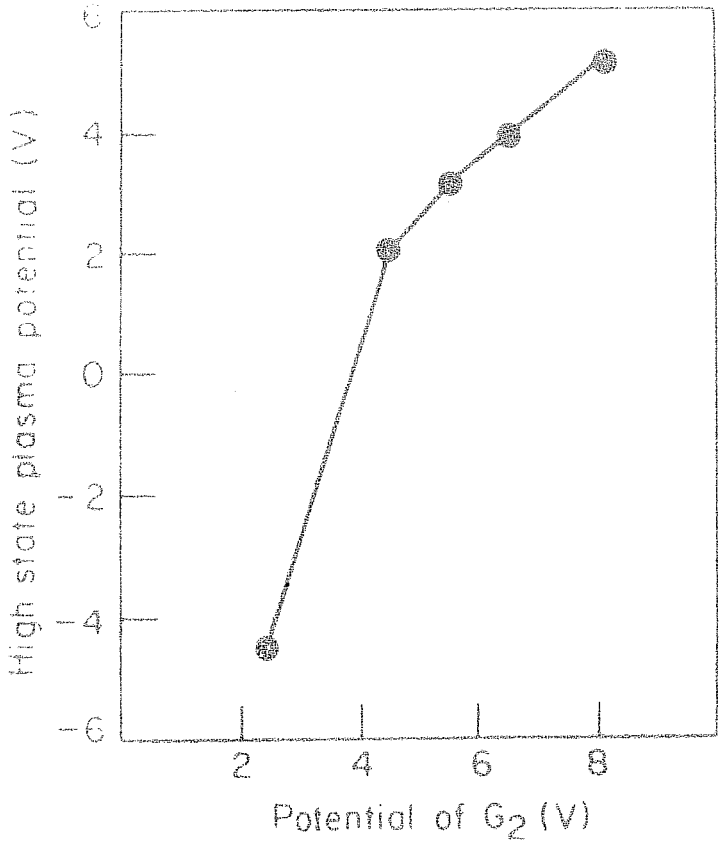

Figure 3.6 A plot between the high-state potential and the potential of the grid G2.

gas pressure was varied. This is shown in fig. 3.7. It shows that as the pressure of the neutral gas is changed from 1.3×10^{-5} Torr to 1.35×10^{-5} Torr, the plasma potential makes an abrupt jump, from -13.2 volts to 6 volts. The implication of this result, is that a sharp transition of the plasma potential can be effected by a minute amount of the neutral gas, and it occurs, only when the device is tuned to a critical pressure. The value of the critical pressure depends upon the relative bias between the two chambers. At larger bias voltages, the critical pressure depends upon the relative bias between the two chambers. At larger bias voltages, the critical pressure is lower. It thus appears, that during the movement of the probe, a very minute amount of neutral gas leaks into the device, and ionisation of this gas, on reaching the grid G2, leads to the source of the moving plasma.

Having ascertained that maximum ionisation occurs near the grid G2, and this blob expands towards grid G3, we carried out a time of flight measurements. Two collecting Langmuir probes P1 and P3, placed near G2 and G3, separated by about 30 cms, are biased to collect, the saturation electron current. Fig. 3.8 shows that the

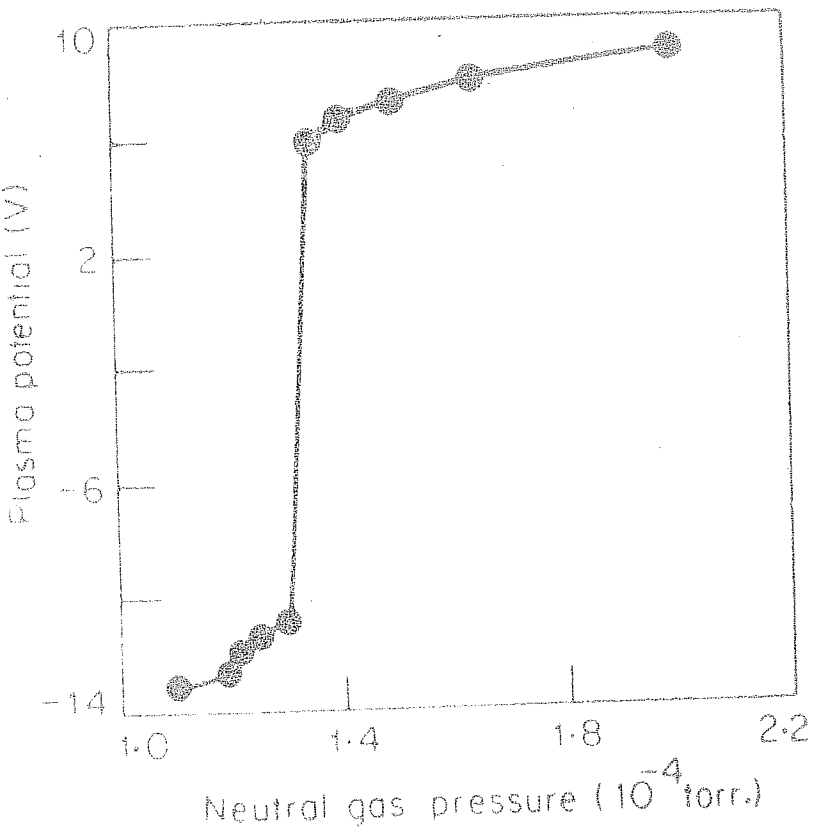

Figure 3.7 The plasma potential at 10 cm from the grid G2 is plotted for various gas pressures. The device control setting are G1 = 0V, G2 = 10V, G3 is grounded, V_{S-T} = -8.3V. A sharp transition in the plasma potential is observed between 1.3 - 1.35 x 10^{-4} Torr.

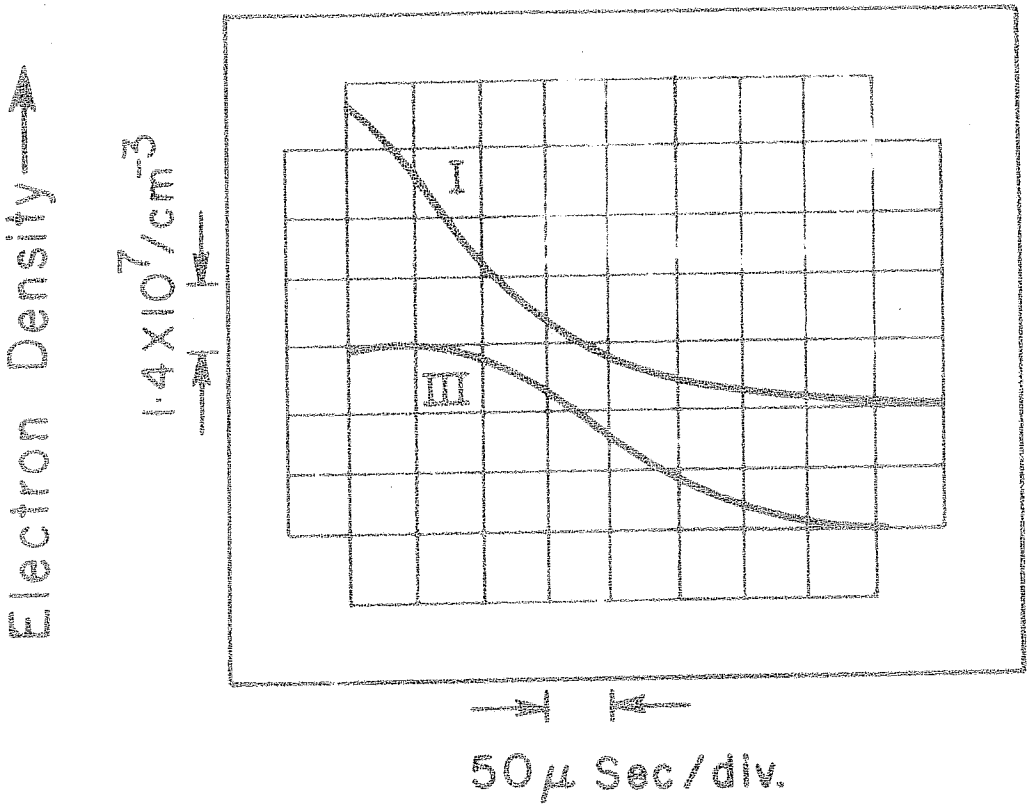

Figure 3.8 Oscilloscope trace of time profile of saturation electron currents obtained by collecting Langmuir probes P_1 and P_3, separated by 30 cms. Fig. shows that the arrival of the plasma blob at P_3 is delayed by 30 μs with respect to the same at P_1.

onset of the increase in electron density occurs earlier at the probe near G2 than grid G3, when a transition in the plasma potential is effected by moving the emissive probe, away from G2. From the I-V curves, the electron temperatures at P1 and P3, before and after ionisation were 10.5 eV and 4.5eV, respectively. This indicates that the plasma potential jump is accompanied by a moving plasma. The plasma moves in the direction, away from grid G2, and towards G3, at a velocity $\gtrsim 10^6$ cms/sec. At a given position in the target region, the onset of the increase in the electron density occurs simultaneously, with an increase in the plasma potential at that position. Thus the plasma potential jumps, shown in figs. 3.2 to 3.4 are not stationary structures.

3.3 Discussion

3.3.1 Role of neutral gas pressure

Below a critical pressure, the electron current extracted from the source, establishes an extended potential structure in the target region. This has a potential structure continuously varying in space and does not correspond to a double layer. What seems to be sustaining these structures in our case is the variation

in the electron temperature of the hot component of the electron distribution.

If a potential double layer is to exist, the ion density in the low potential region, must be less than the electron density. This explains, why a critical adjustment of pressure, of the neutral gas is required to produce a double layer (Leung et al. 1980).

We have demonstrated that the observed potential jumps, are accompanied by a moving plasma. Fig. 3.7 suggests, that the origion of the plasma blob may be in the enhanced ionisation of a very minute amount of the gas that leaks into the system, by the movement of the probe. That the plasma blob is formed in the region adjacent to the grid G2, is evidenced from the time resolved measurements of the density made at different spatial points simultaneously. This also rules out in our experiment the formation of double layers from an anode sheath, as observed in experiments of Torven (1979). The measured velocity of the leading edge of the created plasma is 5 C_s (C_s is the ion acoustic velocity).

3.3.2 Expansion of plasma

The observed high velocity is due to the expansion

of plasma. The expansion results, in due to thermal pressure in the plasma. The initial response of the plasma to the thermal pressure, is that the warm electrons will separate out to form a region of space charge concentrated near the density discontinuity. The electrons on an average will separate out from the ions to form a region of electron space charge, by a distance of a Debye length, so that at the boundary there will be formed a double layer of thickness of the order of a Debye length. The electrons cannot go further due to the electric field, and the ions which immediately follow will be accelerated. This would mean that the leading edge of the ions in the double layer, will be moving at a faster velocity, than the ion acoustic speed. An interesting outcome of our explanation of the observed potential jumps and the large velocities is that they can be correlated to the electron temperature. This is presented below in the model based on the adiabatic expansion of plasma and hence acceleration of ions by the ambipolar fields.

3.3.3 Thermodynamical model for the expansion of plasma

Following Hendel and Reboul (1962), a thermodynamical collisionless model leads to an adiabatic transfer of

energy from electrons to ions. The conditions necessary for such a mechanism to exist being

(1) The existence, in the discharge, of a constant source of electrons, with adequate energies.

(2) The concentration of charged particles at the front, of the expanding cloud, capable of accelerating ions.

As both the conditions are satisfied, in our experiment, the above model is applicable. The electrons gain relatively high energy from the applied field, while the energy transferred to the ions from the external field, and electron-ion collisions are negligible. Randomization of electron velocity is obtained in a few microseconds. High velocity electrons, attempt to escape isotropically from the plasma, but are restrained by the electric field of the ions to a distance of a Debye length.

The space charge set up by the electrons accelerates a spherical ion piston radially, outward. Since, we are considering a one dimensional case, we can treat this as a plasma expansion in a single direction. The energy needed for the ions is supplied, by the initial

energy content of electron gas. During the short period of ion acceleration by space charge, only a negligible amount of heat can be delivered to ions by collisions with electrons, due to a limited transfer of momentum in such a collision. So energy transfer is adiabatic.

The work done, by the electron gas at T_{e1} and pressure P on the ion piston, during the expansion from volume V_1 to V_2 is given by

$$W = \int_{V_1}^{V_2} P \, dV \qquad (3.1)$$

This work done, sets up a space charge field, accelerating ions towards electrons and simultaneous deceleration of electrons.

Using Poisson's adiabatic law

$$PV^r = C \qquad (3.2)$$

with r = 5/3, and the general gas law

$$PV = nkT_e \qquad (3.3)$$

From (3.2) and (3.3) we get

$$V^{-2/3} = \frac{nkT_e}{C} \qquad (3.4)$$

Differentiating (3.4) we get

$$-2/3\ v^{-5/3}\ dv = \frac{nkdT}{C} \qquad (3.5)$$

From (3.2)

$$-Pdv = 3/2\ nkdT \qquad (3.6)$$

Substituting (3.5) into (3.1) we get

$$W = \frac{1}{2} nMv^2 = \frac{-3}{2} nk \int_{T_1}^{T_2} dT$$

Hence, we obtain

$$V = \sqrt{3k} \left[\frac{T_{e1} - T_{e2}}{M_i} \right]^{1/2} \qquad (3.7)$$

Eqn. (3.7) is the drift velocity acquired by the ions.

Thus, when ions and electrons, finally drift at almost the same velocity, electron energy is transferred to the ions, the final ion energy being almost equal to the initial electron energy. Momentum is conserved, since the centre of Mass of the expanding plasma is at rest.

From the I-V characteristics, at the probe P_1, we have electron temperatures, before and after ionisation to be 10.5 eV and 4.5 eV respectively.

From eqn.(3.7),

$$V_{ion} = \sqrt{3}\left[\left(\frac{T_{e1} - T_{e2}}{M_i}\right)\right]^{1/2} \approx 8 \times 10^5 \text{ cms/sec.} \approx 4 \text{ Cs.}$$

This is quite in agreement with the experimental result of 5 Cs.

3.3.4 Self Similar expansion of plasma

The observed high velocity of the ions, due to the expansion of plasma can also be approximately modelled on the basis of self-similar expansion of plasma into vacuum, though expansion of plasma from a high density into a low density region would be more appropriate.

In our experiment, the ionisation of additional neutral gas that leaks into the system during the probe movement, leads to a steep increase in density. We can study the motion of this front, through a self-similar analysis.

For this purpose, we can start from the equation of motion for ions

$$\frac{\partial N_i}{\partial t} + \frac{\partial}{\partial x}(N_i V_i) = 0 \qquad (3.8)$$

$$\frac{\partial V_i}{\partial t} + V_i \frac{\partial V_i}{\partial x} = -\frac{e}{M_i}\frac{\partial \phi}{\partial x} \qquad (3.9)$$

As a result of thermal pressures, a charge separation between electrons and ions will be set up, with a distance of about one Debye length. Since, this distance is very small, compared to the dimensions of the system, into which, the plasma expands, we can assume quasi-neutrality i.e.

$$N_e = N_i = N_o \exp\left(\frac{-e\Phi}{kT_e}\right) \tag{3.10}$$

Following the techniques of Ames (1972), Longren (1977) and Gurevich and Pitaevsky (1975), we can from simple Lie groups determine the self similar variable to be

$$\xi = x/t \tag{3.11}$$

A transformation using this variable converts the partial differential equation of two variables, given by (3.8) and (3.9) into an ordinary differential equation of one variable. This simplifies, the mathematical complexities.

Substituting (3.11) into (3.8) and (3.9), we get

$$(v_i - \xi) + N_i \frac{dv_i}{d\xi} = 0 \tag{3.12}$$

$$(v_i - \xi)\frac{dv_i}{d\xi} = -\frac{e}{M_i}\frac{d\Phi}{d\xi} \tag{3.13}$$

Solving (3.12) and (3.13) we get

$$(U_i - \xi)\frac{dU_i}{d\xi} = -\frac{C_s^2}{N_i}\frac{dN_i}{d\xi} \qquad (3.14)$$

Hence

$$(U_i - \xi)^2 = C_s^2$$

and

$$U_i = \xi + C_s \qquad (3.15)$$

Substituting (3.15) into (3.14) we get

$$dU_i = -C_s \frac{dN_i}{N_i}$$

$$\therefore \quad U_i = -C_s \frac{\ln N_i}{N_0}$$

From (3.10) we get

$$U_i = C_s \left[\frac{e\Delta\phi_{pl}}{\Delta T_e}\right] \qquad (3.16)$$

Hence we have derived an expression for the velocity of the ions in terms of the potential jumps ($\Delta\phi_{pl}$).

In our experiment, the potential jumps, we observed were $\gtrsim$ 20 volts.

Setting $\Delta \phi_{pl} \approx 20$

$$T_{e1} = 10.0 \text{ eV}$$

and $$T_{e2} = 4.5 \text{ eV}$$

we get $\Delta T_e = (T_{e1} - T_{e2}) = 5.5 \text{ eV}$

$\therefore$ From equation (3.16), we

$$v_i = C_s \left(\frac{20}{5.5}\right) \approx 4\ C_s$$

This agrees quite well with the experimental observations, wherein we observed ions to be accelerated to velocities much larger than ion acoustic velocity. Though we have not included, density gradient etc., it approximately gives us an idea, of the possibility of ions to be accelerated to large velocities in the expansion of the plasma blob. Since this occurs, in the direction of the electron drift, the charge separation and hence, the moving double layers, will persist, till almost the end of the system.

3.3.5 Comparison with computer simulations

Computer simulations (Goldenbaum and Gerber 1973), that do not use Boltzman distribution for the electrons

and charge neutrality, have obtained a maximum velocity of the leading edge to be about 5 C_s, which is the same as that of our observed result. What is important is, not that the measurement can be explained by the expansion of a plasma blob. The important point to note is that the expansion of the plasma is accompanied by a double layer at the leading edge of the plasma blob, and its thickness is of the order of a Debye length. Thus it seems likely that the potential jumps, are corresponding to the moving double layers, formed as a consequence of the expansion of plasma, created due to the ionisation of the leaked gas adjacent to the grid G2.

We have observed that potential jumps occur when the device is tuned to a critical pressure. Having identified the cause of these jumps in the formation of a plasma blob, it means that enhanced ionisation of the gas, that leaks into the system during the movement of the probe occurs, only when the neutral pressure is at a critical value. In view of that, ionisation mean free path of the ionising electrons in the target plasma decreases very rapidly, when the gas pressure changes by a very small fraction of the ambient pressure, an explanation is required for the cause of the enhanced ionisation at the critical pressure. We explain it as follows:

3.3.6 Role of high energy electrons

The energetic electrons, in the target chamber ionize a fraction of the leaked gas, at the high potential end, producing low energy electrons and ions. The low energy electrons are trapped between the sheath around the grid G3 and the potential minimum, located near the grid G2. The ions in the high potential side are accelerated towards the potential minimum and reflected at the sheath of the grid G2.

Thus the potential well near the grid becomes shallower. This in turn allows more electrons to be extracted from the source and hence more ionisation of the gas. The critical effect may be arising due to the fact that, at this pressure, the plasma region adjacent to the grid G2, attains momentarily an accelerating potential of the order of the ionisation potential, of the gas with respect to the source. Since the ionisation cross section of the gas increases rapidly at the ionisation potential, the accelerated electrons, extracted from the source, leads to an enhanced ionisation of the neutral gas, adjacent to the grid G2. This creates a plasma blob in which a double layer develops at the leading edge, at a later stage.

An interesting feature of these results, is the acceleration of ions in the direction of electron drift. Such observations have been made in the space experiments of Chielmetti et al.(1979)and also in the computer simulation of Singh (1982).

3.3.7 Comparison with the experiments of Coakley and Hershkowitz

Coakley and Hershkowitz (1979) in an attempt to form double layers in a double plasma machine, were not successful. As they scanned the plasma axially with a Langmuir probe, they observed, what they termed as pseudo-double layers. As they scanned with one probe, double layers were apparently observed. However, with two collecting probes simultaneously monitoring the plasma, they found that the plasma potential changed simultaneously at both the probes. They ascribed this to the situation of the plasma actually possessing two metastable states, neither of which had double layers. As the axial position of a probe was changed, in the target chamber, a point was reached at which the entire potential of the plasma changed. From their probe characteristics, it is evident, that there could be a change in the electron temperature. But, they did not pursue their investigations

any further, and concluded, by quoting that the phenomena observed were a pseudo-double layers.

From our investigations, we feel that our observations of potential jumps may be similar to those of Coakley and Hershkowitz (1979), and should be able to explain their observations. However, we do not attribute these potential jumps, to the existence of two metastable states in the plasma, for they require much more complicated processes, rather than the simple explanation, we have offered.

3.4 Weak Double Layers

3.4.1 Experimental setup and diagnostics

The experimental system and the diagnostics are similar to that described in chapter 2. The base pressure was $\lesssim 10^{-5}$ Torr, and the operating pressures ranged from 4×10^{-5} Torr to 3×10^{-4} Torr. Plasma was produced in the source and target chambers, as discussed earlier. The plasma parameters in the target chamber were $n_e \approx 3 \times 10^7/cm^3$, $T_e = 2.0$ eV, $T_i \approx T_e/20$. The plasma potentials were monitored directly with an emissive probe by floating point method (Sekar 1982).

3.5 Experimental Results

3.5.1 Double layer potentials at different neutral Pressures

In the normal mode of operation, grids G1 and G2 were biased at OV. The target chamber and end grid G3 were grounded, keeping the source chamber floating. The potential of the source plasma was varied by applying a bias voltage with respect to the target chamber.

The axial potential profiles at a fixed relative bias, but different neutral pressures, are shown in fig. 3.9. The potential drop across the double layer was about 6 to 10 volts, i.e. $e\Delta\phi/T_e \approx 3\text{-}5$. This was possible only at low pressures. At a higher neutral pressure of about 3×10^{-4} Torr the entire potential in the target chamber became uniform as shown by A in figure 3.9.

3.5.2 Electron Energy Distribution

The electron energy distribution in the presence of a double layer in one of the cases (profile C in fig. 3.9) is shown in fig. 3.10. As a result of electron flow which was maintained by a drift velocity $V_D \gtrsim 1.3\ V_{the}$ (V_{the} = electron thermal velocity = $(kT_e/me)^{1/2}$), a

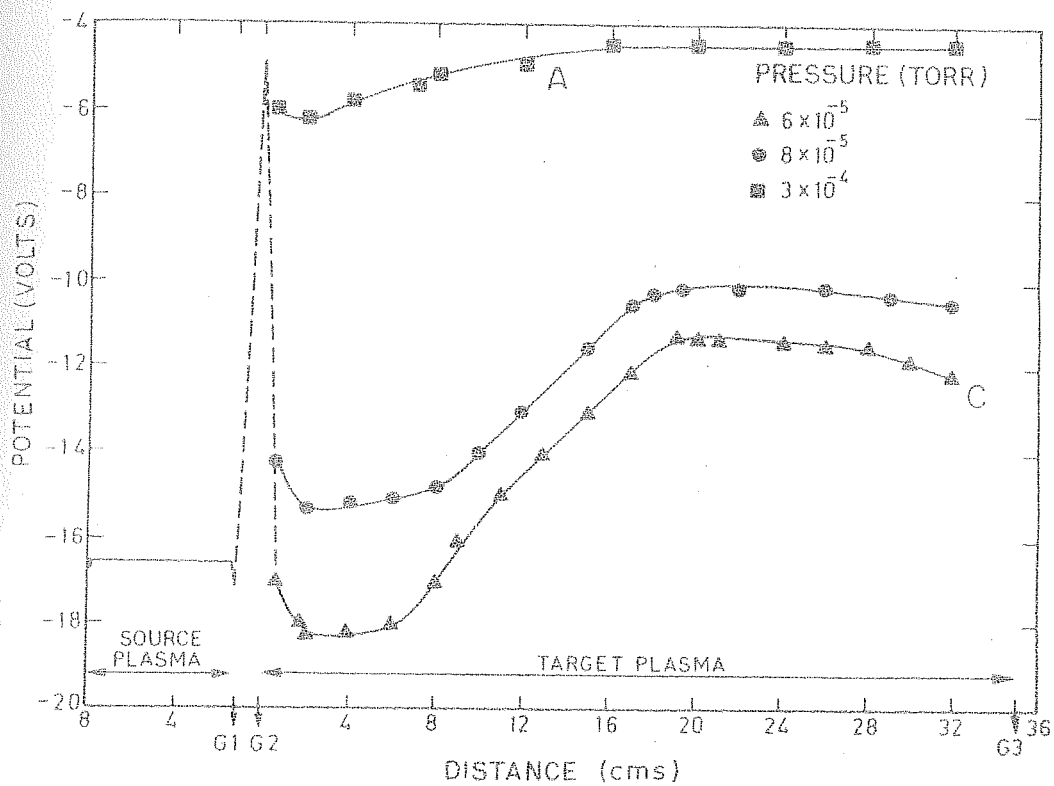

Figure 3.9 Axial potential profiles in the target chamber at different neutral pressures, and a fixed relative bias V_{S-T} = 20 volts. Profile A corresponds to the uniform potential profile and profile C corresponds to the double layer potential profile G1 = 0V, G2 = 0V and G3 is grounded.

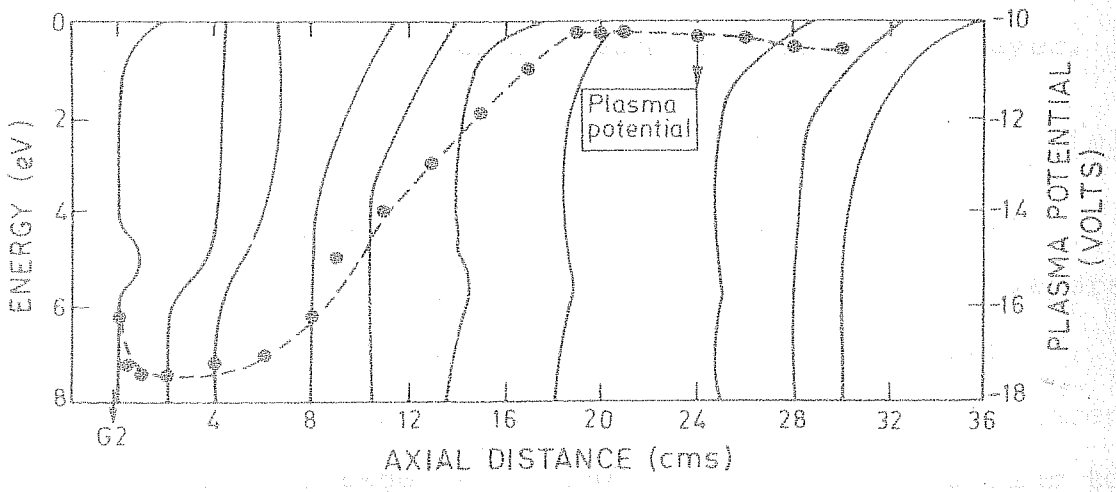

Figure 3.10 Electron energy distribution functions for the double layer corresponding to profile C of fig. 3.9. Drifting electron distrisbution is present at the low potential side and component that is accelerated across the double layer thermalises in a distance of 10 cms on the high potential side.

negative potential well was formed near the grid G2. There was a beam component, near grid G2, which modified to a drifting distribution function at the trough of the potential. Accelerated electrons were observed at the high potential side of the double layer. These components were observed to thermalise in a distance of about 10 cms ($50\,\lambda_D$) on the high potential side of the double layer.

3.5.3 Double layers at different relative bias potentials

Operating the system at low pressures between 4×10^{-5} Torr to 8×10^{-5} Torr, we obtained double layers by varying the relative bias potentials. The axial potential profiles for a fixed gas pressure, but different relative bias voltages are shown in fig. 3.11. Similar to the observations in fig. 3.9, we observed a criticality in the relative bias also. This can be clearly seen from the uniform potential profile of B in fig. 3.11.

3.6 Discussion

3.6.1 Spatial evolution of the electron energy distribution

From the results obtained, it was found that a relative electron drift velocity $V_d \geq 1.3\ V_{the}$, was necessary to form a double layer, which corresponds to the necessary condition to form a double layer, and experimen-

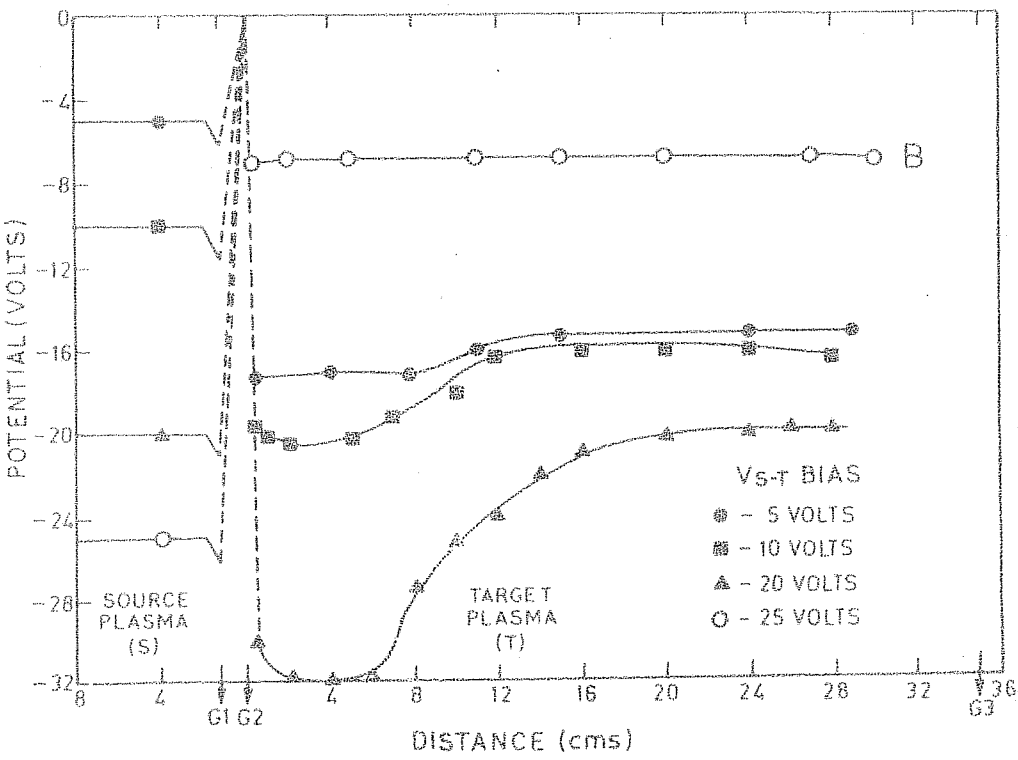

Figure 3.11 Axial potential profiles in the target chamber at different relative bias voltages, maintaining pressure constant at about 7×10^{-5} Torr. G1 = 0V, G2 = 0V, G3 is grounded. Profile B corresponds to the shallow potential structure, at a larger relative bias.

tally observed by Quon and Wong (1976), Coakley and Hershkowitz (1979) and Torven (1979). The relative bias injects an electron beam from the source into the target chamber. The distribution function at the trough of the potential is modified to a drifting distribution. A plausible explanation for this could be that the beam is slightly decelerated at the trough of the potential near G2 and further via fluctuations of the ion acoustic nature (Sekar et al. 1981, Kaw 1982), can redistribute its energy to the low energy components. The resultant drifting distribution leads to the formation of a double layer.

The presence of the electron current, which is maintained by a constant flow of electrons, creates the potential minimum, where ions can get trapped. As the potential rises, the electrons are accelerated, which can be seen from the electron distribution function. We do not provide a separate source of trapped electrons, like the triple plasma device of Coakley and Hershkowitz (1979). Hence the presence of low energy electrons are due to the ionisation of neutral gas, and thermalisation of the beam component. The hot electrons that travel towards the double layer are reflected at the layer, while those moving away are reflected at the end grid

G3, thereby maintaining the necessary trapped population of electrons at the high potential region. Ions that are accelerated from the high potential region get reflected at the grid G2 and together with the ions produced near the grid G2, provide the necessary reflected particles at the low potential side.

3.6.2 Role of Ionisation of neutral gas

Ionisation of neutral gas was found to play a crucial role in deciding the criticality of both neutral pressures as well as relative bias voltages. At low neutral pressures, there was a large potential minimum formed near G2, as a result of the electrons from the source. The potential then rose towards G3 and under suitable conditions of bias voltages, transformed into a double layer. As neutral gas pressure was increased, it led to a larger ionisation. These ions as well as the ions, accelerated from the high potential side, reduced the space charge of electrons at the potential minimum. A further increase of pressure enhanced ionisation and hence a further reduction in the potential drop. The potential change in the entire chamber was about 1 to 2 volts.

Similar results were observed at large relative bias voltages, even at low neutral pressures. Above the critical bias voltage, the beam electrons were energised sufficiently, to ionise the neutral gas in the target chamber. From these observations, the crucial role of ionisation of neutral gas as reported in the earlier experiments (Leung et al 1980, Coakley and Hershkowitz(1979) Mattoo et al. 1980, 1981), in the formation of double layers is clearly observed.

3.6.3 Comparison with the theoretical and computational results

The thermalisation distance of the accelerated electron components, which is about 10 cms ($50\lambda_D$) is comparable to those observed by Quon and Wong (1976). From the theoretical calculations for beam plasma interaction, we obtained a thermalisation distance of 15 cms ($75\lambda_D$). This corroborates to our experimental observations which is of the same order of magnitude.

From the computer simulations of Joyce and Hubbard (1978), it was observed that the spatial extent of the double layer was $L_{dl} = 6(e\Delta\phi/T_e)^{1/2}$, where L_{dl} is the distance measured in terms of Debye length. From the experimentally observed result of $e\Delta\phi/T_e \approx 6$,

width of the double layer = 12 cms and Debye length = 0.2 cms, we get

$$L_{dl} \simeq 25 \left(\frac{e\Delta\phi}{T_e}\right)^{1/2}$$

Coakley and Hershkowitz (1979) obtained $L_{dl} \approx 12 \left(e\Delta\phi/T_e\right)^{1/2}$. The discrepancy in our experimental results with respect to the computer simulations could be due to various reasons, e.g. in the computer simulation, ionisation of neutrals etc., are not considered. Moreover, the double layers in the computer simulation, were strong double layers, with $e\Delta\phi/T_e \approx 50$, whereas, in our experiment, the double layers we had obtained, were weak with $e\Delta\phi/T_e \approx 6$.

Chapter 4

STRONG POTENTIAL DOUBLE LAYERS IN A DOUBLE PLASMA MACHINE

In Chapter 3, we had dealt with the criticality of some parameters like the neutral gas pressures and the relative bias potentials, which controlled the formation of double layers. In Chapter 1, we had discussed that double layers are current dependent phenomena, and the amplitude of the potential drop, depends on the magnitude of the current, in the system. Our further investigations have revealed that the latter is true, rather than the criticality of parameters like the ionisation potential, neutral density etc. In the following we present the results of our observations on strong double layers.

4.1 Experimental Setup and diagnostics

The experiment was performed in a double plasma machine modified in the biasing arrangements, gas feed and pumping arrangements. The double plasma machine consists of a source and a target plasma separated by two grids G1 and G2. The schematic of the modified version of the machine is shown in Fig. 4.1.

Plasma was produced only in the source chamber by heating 20 tungsten filaments, 8 cms long, to thermionic emission. These electrons were accelerated to about 40 to 60 volts, and a steady state discharge was maintained by electron-neutral impact ionisation. The neutral gas used was Argon, maintained at a fixed pressure in the range of 6×10^{-5} Torr to 3×10^{-4} Torr. Though the target region, did not contain a separate source of filaments, plasma was maintained in this chamber by the high energy ionising electrons that drifted from the source.

In order to minimise the effect of additional ionisation the pumping arrangement was shifted from the source region to the target region. The gas was introduced into the source region instead of the target

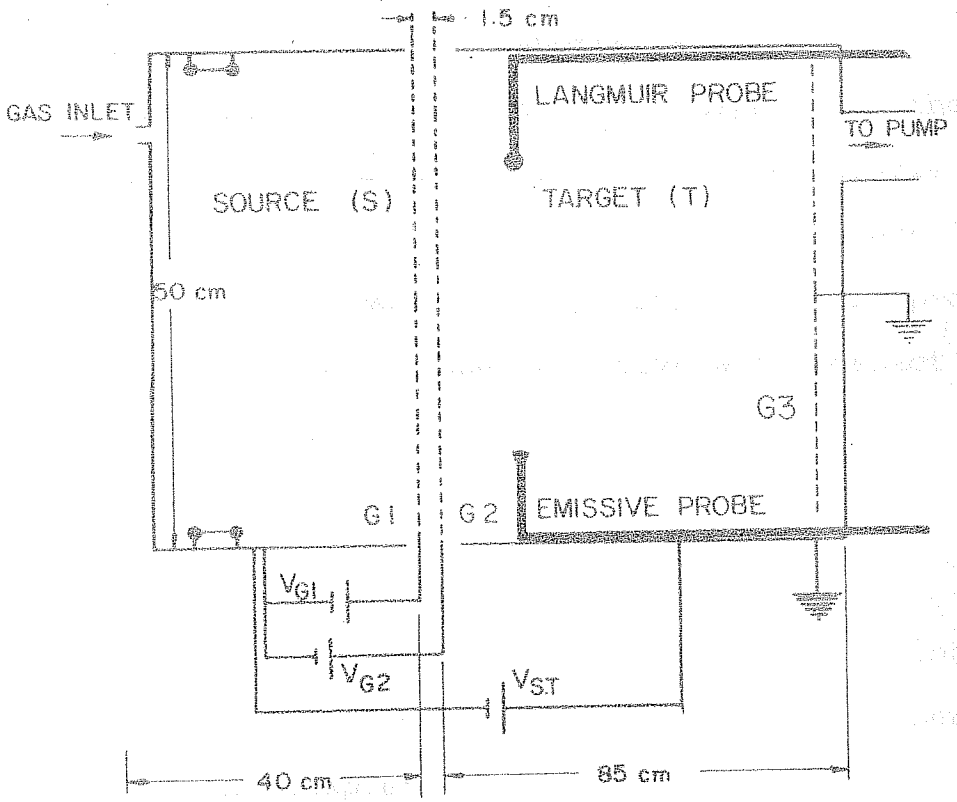

Figure 4.1 Schematic of the modified configuration of the double plasma machine. G1 and G2 have been biased positive with respect to the source and kept at 0V in the normal mode of operation. The system pumping unit is on the target side while the neutral gas is inlet from the source region. Drifting electrons are injected into the target chamber by a relative bias applied between the source and target plasmas.

chamber. The combined effect was to lower the neutral density in the target chamber. Another modification was the biasing arrangement of the grids separating the source and the target chambers. In the earlier configuration (Chapter 3), wherein only weak double layers were generated, grid G1 was biased positive with respect to the source, and G2 was biased positive with respect to the target. But in the modified version, both the grids G1 and G2 were biased positive with respect to the source.

These modifications enabled us to produce strong double layers in this device. These results are presented further in this chapter.

The diagnostics in this experiment, mainly comprised of a hot emissive probe, a cold Langmuir probe and a grid energy analyser. The hot emissive probe, consisted of a tungsten filament sufficiently heated to emit a copious amount of thermionic electrons. The floating potential measured at maximum emission, yielded, the plasma potential directly. A cold Langmuir probe, mounted on the same shaft was deployed to measure plasma temperature, density and electron distribution function.

The advantage in this arrangement of mounting both the probes on the same shaft, was that it made feasible the measurement of both plasma potentials and electron distribution function, simultaneously at different spatial points. The grid energy analyser was used to obtain the ion temperature.

The plasma parameters that were obtained, in the target chamber with these diagnostics were density (Ne)$\approx$ 3×10^{7} cm^{-3}, electron temperature (T_e) $\approx$ 2eV, ion temperature (T_i) $\approx$ 0.2eV and the Debye length$(\lambda_D)\approx$0.2 - 0.3 cm

4.2 Experimental Results

With the biasing arrangements as described above, in a given range of bias voltage, and neutral gas pressures, it was possible to obtain strong double layers with $e\Delta\phi/kT_e > 10$. In the following sections, we describe the results obtained.

4.2.1 Axial plasma potential profiles at different relative bias voltages

Maintaining a fixed pressure, and grid bias voltages, we obtained the axial plasma potential profiles in the target region at different relative bias voltages.

These results are shown in Fig. 4.2. At 0 volts relative bias, the plasma potential in the entire target chamber is uniform, but as the bias voltage is raised to 20 volts, a small amplitude potential drop appears. The potential drop obtained in this case is about 2 volts, in distance of 2 cms. At 30 volts, a larger amplitude potential drop of about 24 volts, with $e\Delta\phi/T_e \approx 12$ is obtained. The spatial extent of this structure is about 14 cms. This structure resembles a double layer with a constant potential, both on the low potential and high potential sides, and an almost monotonic rise in between the two.

Fig. 4.3 shows the potential profiles at relative biases of 40-100 volts. With increase in the relative bias voltages, the potential drop across the double layer also increases. The transition region is found to shift towards the lower potential side i.e. towards grid G2. Till about 40 volts, the potential minimum in the target region is negative than the source potential, but above 60 volts, the potential minimum in the target region is slightly above the source potential. The potential drops obtained at these relative bias voltages vary from 30 - 78 volts thus yielding $e\Delta\phi/T_e \approx 15 - 39$.

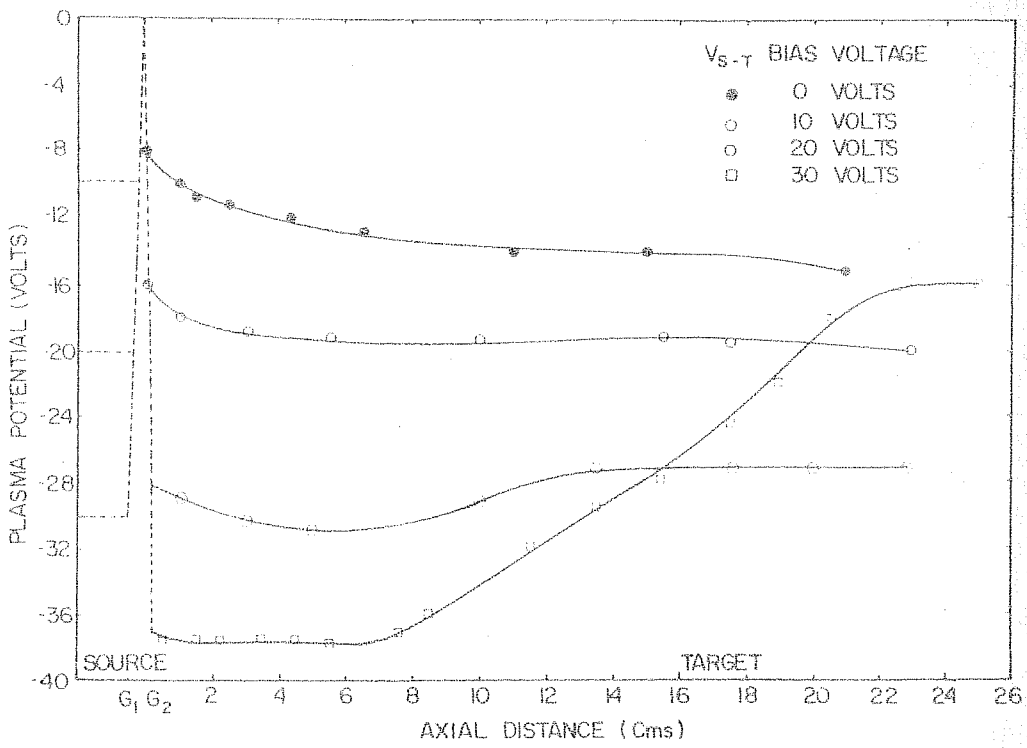

Figure 4.2 Axial plasma potential profiles in the target chamber monitored with an emissive probe at different relative biases from 0 to 30 volts. G1 = 0V, G2 = 0V, G3 is grounded and neutral gas pressure $\simeq$ 8×10^{-5} Torr. A double layer is observed to form at a relative bias of 30 volts.

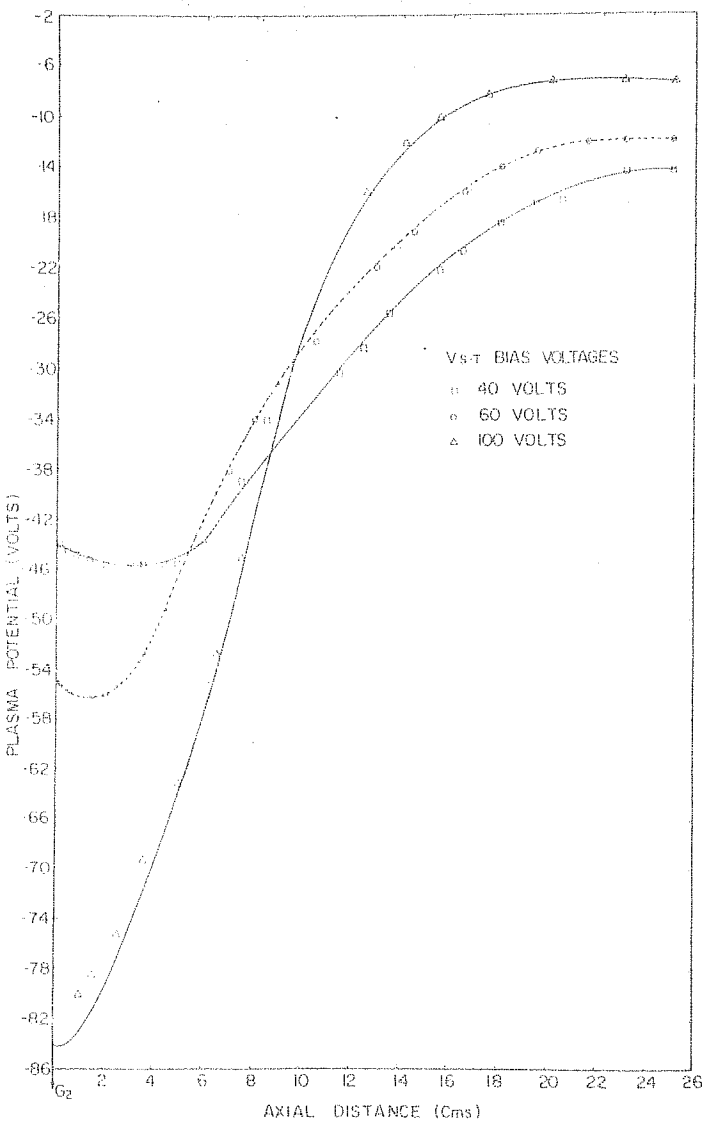

Figure 4.3 Axial plasma potential profile in the target chamber at different relative bias voltages varied from 40 - 100 volts maintaining other conditions same as in fig. 4.2.

Further increase in relative bias voltages, yielded some interesting results, which are shown in Fig. 4.4. The relative bias potentials were varied between 200 - 300 volts. At 200 volts, the potential structure almost resembles a sheath but at about 7 cms from the grid, a knee is observed, beyond which the potential rises monotonically, and possesses an uniform potential on the high potential side. At 250 volt, the knee like structure becomes sharper, with the potential dip resembling a virtual cathode like structure, forming on the low potential side. This structure persists even at higher potentials of about 350 volts. The potential drops obtained at these potentials were about 80 to 96 volts, with $e\Delta\phi/T_e \approx 40 \sim 48$.

Fig. 4.5 shows a plot of the variation of $e\Delta\phi/T_e$ versus relative bias voltages. It initially exhibits a linear increase, with a saturating trend at larger relative bias potentials.

4.2.2 Double layers at different G2 bias voltages and neutral gas pressures

The potentials on G1 and G2 appear to play a crucial role, in the formation and stability of double

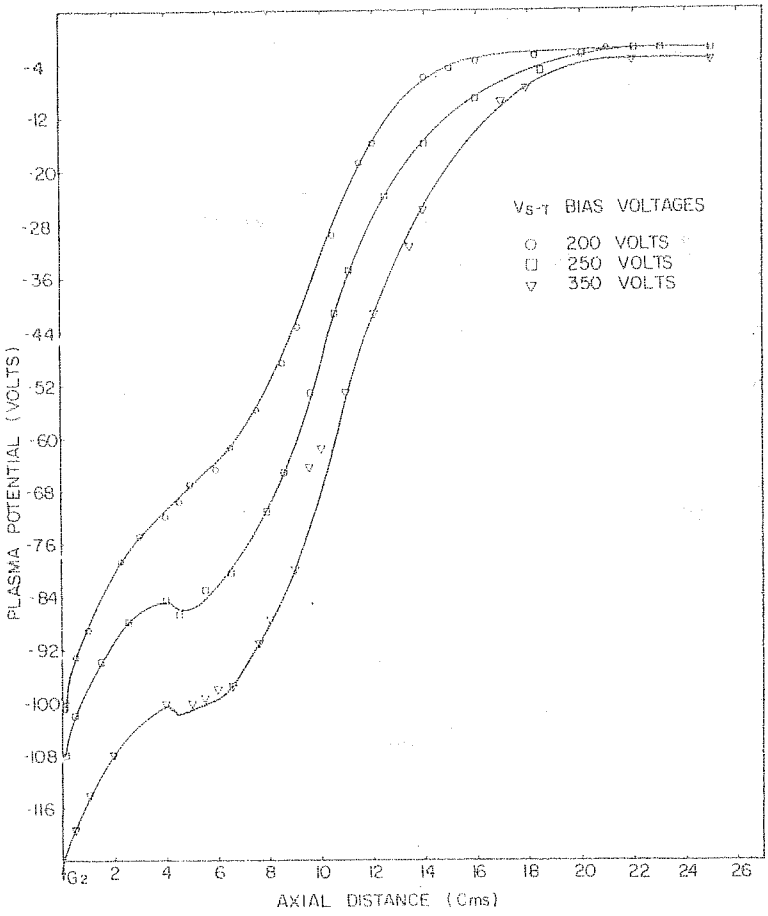

Figure 4.4 Axial plasma potential profiles in the target chamber at higher relative bias voltages from 200-300 volts. A knee like structure appears at 200 volts and manifests into an explicit negative potential dip after the initial increase in voltage. These structures closely resemble multiple double layers.

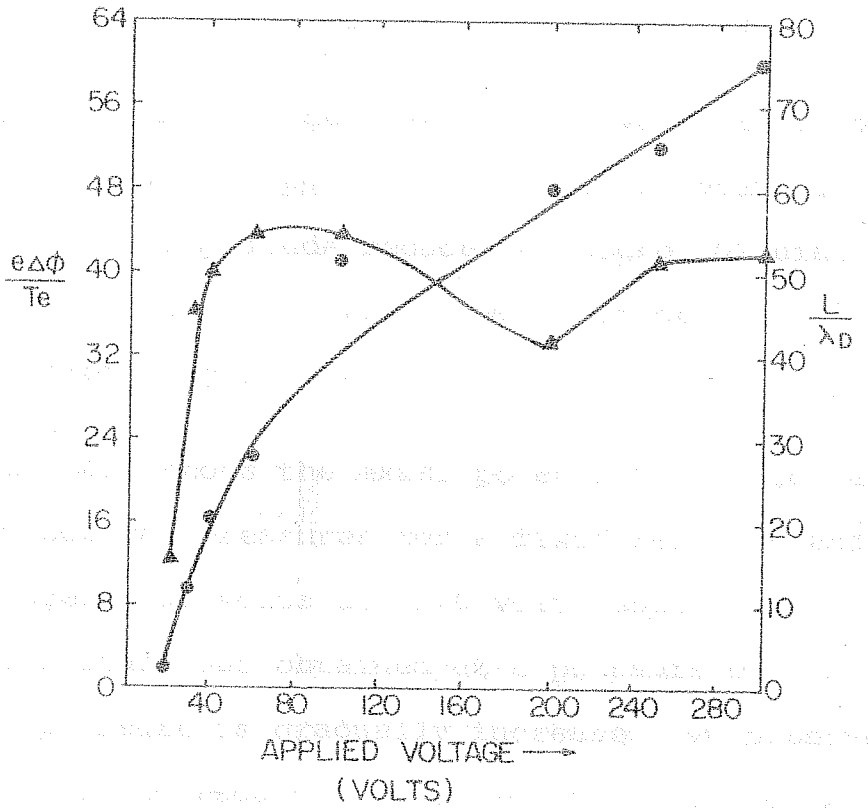

Figure 4.5 Variation of experimentally observed results of:

(1) Potential drop ($\frac{e\,\Delta\phi}{T_e}$) versus applied relative bias voltage (volts).

(2) The corresponding widths of the double layers (L_{dl}).

layers. The potential profiles at constant relative bias ($\approx$50 volts), and neutral pressures (8 x 10^{-5} Torr), obtained by varying the G2 bias are shown in fig. 4.6.

At G2 bias voltages between 0.5 volts to 10 volts, a double layer with a potential drop of 30 volts is observed. This amplitude reduces at higher G2 bias voltages and at about 30 volts, we could obtain a potential drop of only 4 volts.

Fig. 4.7 shows the axial potential profiles at different neutral pressures for a fixed relative and G2 bias voltages (50 volts and 1.0 volt respectively). The maximum amplitude was obtained at a pressure of 6 x 10^{-5} Torr. As pressure is gradually increased, we observe the potential drop to reduce from an initial value of 28 volts at 6 x 10^{-5} Torr, to a voltage drop of 8 volts at 2 x 10^{-5} Torr. One important observation is that in the modified configuration we were able to generate strong double layers, over a wider range of pressures for e.g. from 6 x 10^{-5} Torr to 2 x 10^{-4} Torr, as compared to the earlier experiments (Chapter 3).

4.2.3 Electron energy distribution

Fig. 4.8 shows a plot of the electron distribution

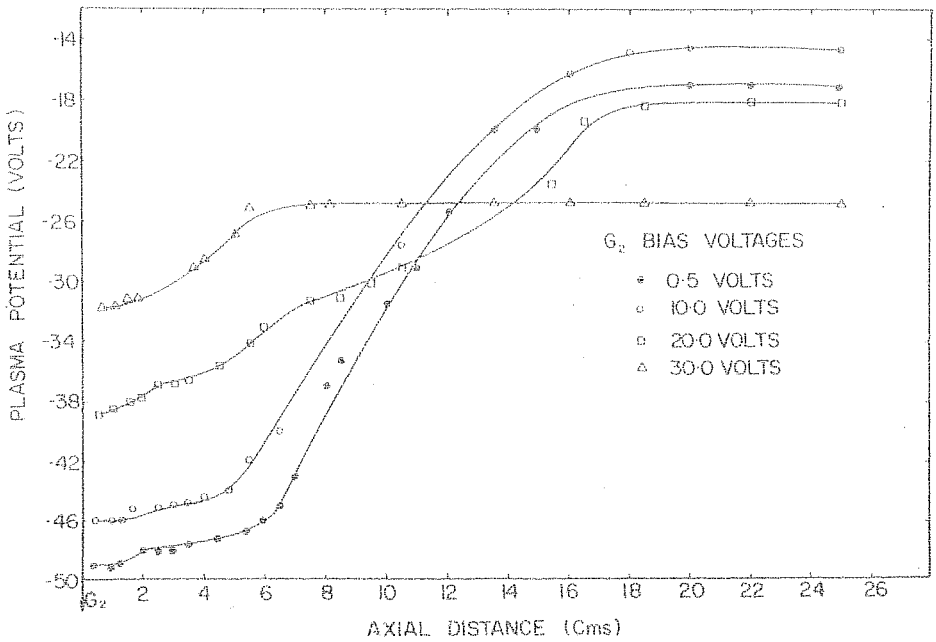

Figure 4.6 Axial plasma potential profile in the target chamber at different G2 bias voltages, keeping the relative bias fixed at about 50 volts and pressure $\simeq 7 \sim 8 \times 10^{-5}$ Torr.

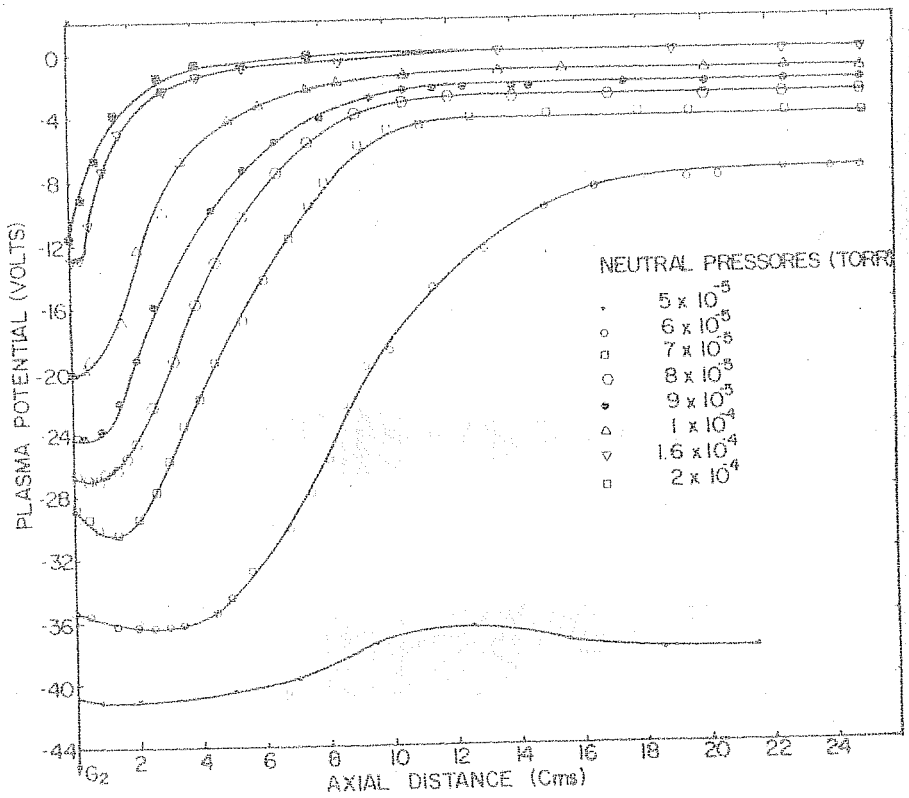

Figure 4.7 Axial plasma potential profiles in the target chamber, at different neutral pressures obtained at a fixed relative bias potential of≃50 volts.

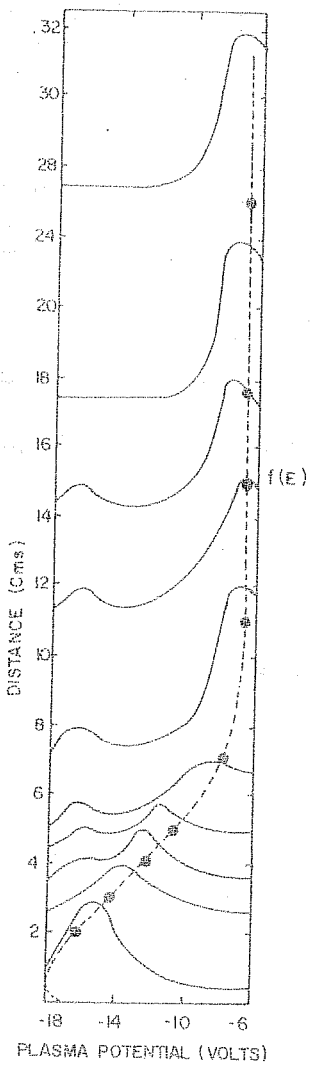

Figure 4.8 Electron energy distribution function in the presence of a double layer, obtained with a Langmuir probe, while the potentials were simultaneously monitored with an emissive probe. (Dotted lines represent the potential profile of a double layer). The accelerated component thermalised in a distance of about 8-10 cms on the high potential side.

function f(E) for one typical case of the observed double layer. These were obtained from the first differential of the I-V characteristics of the collecting Langmuir probe. Since both the emissive probe and the collecting probes are mounted on the same shaft, we could obtain the distribution functions and the plasma potentials simultaneously at all spatial points.

These measurements show an incoming electron beam being slightly decelerated as it creates the negative potential depletion and subsequently accelerated towards the high potential side. There is a large electron component of the main plasma on the high potential side. The accelerated beam components are observed to thermalise in a distance of about 8 - 10 cms on the high potential side.

4.2.4 Electron and ion densities

We monitored the electron and ion densities, in terms of currents, picked up by a Langmuir probe biased appropriately. These measurements were carried out both in the absence as well as in the presence of the double layer.

Fig. 4.9 shows the plot of plasma potential and the electron and ion densities in the target region in the absence of a double layer. The plasma potential initially drops by a few volts near the grid G2 and beyond 2 cms away from the grid, it is uniform, throughout the target region.

The spatial profile of the electron current exhibits an initial increase near the grid but the currents falls off quite sharply beyond 2 cms away from G2. The ion current also shows a similar trend near the grid, but remains almost uniform throughout the target section.

As the relative bias was further increased, a depletion in ion current was observed in the spatial profile and at this instant a small potential drop was also observed. Further increase in relative bias led to a larger potential drop of about 10 volts with $e\Delta\phi/T_e \gtrsim 5$ as shown in fig. 4.10. At this instant, there appeared a well defined depletion in both electron current and ion current. The depletion in ion current occurs on the low potential side exhibiting an excess of electrons whereas the electron current depletion occurs

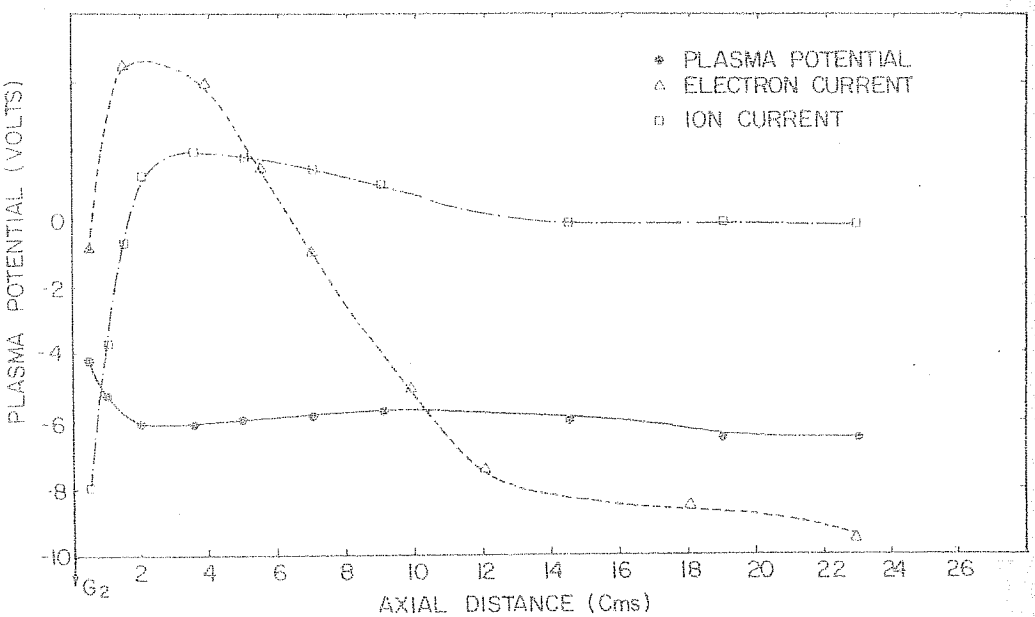

Figure 4.9 Plots of electron and ion densities measured in terms of currents in the absence of a double layer. Electron currents are in milliamps, and ion currents are in microamps.

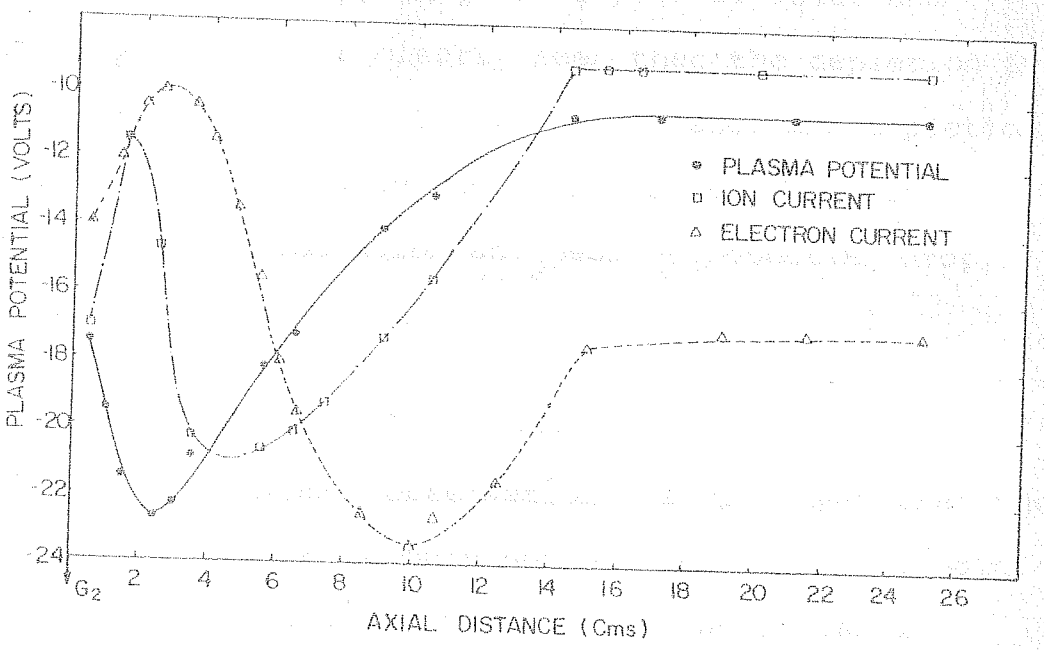

Figure 4.10 Plots of plasma potential, electron current and ion current in the presence of a weak double layer, $\frac{e\Delta\phi}{T_e} < 10$. There is a clear density dip and charge separation in the presence of a double layer.

on the high potential side. This charge separation leading to a potential difference, is a clear indication of the presence of a double layer.

Fig. 4.11 shows the density profile for a strong double layer with a potential drop of 21 volts and $e\triangle\phi/T_e \geq 10$. It is clearly seen that the depletion in density of ions on the low potential side and depletion of electrons on the high potential side, leads to a spatial charge separation and hence a potential drop, across them.

4.3.5 Ion-acoustic fluctuations

From the above observations, it is clear that the double layers could be obtained only above a threshold of the relative bias voltage. Below the threshold voltage, low frequency fluctuations were excited throughout the chamber. To determine the physical processes, we monitored the density fluctuations at about 8 cms away from the grid G2. The monitoring was carried out by a collecting Langmuir probe biased to collect electron saturation currents. The results of the fluctuations obtained at different relative bias voltages are shown in Fig. 4.12.

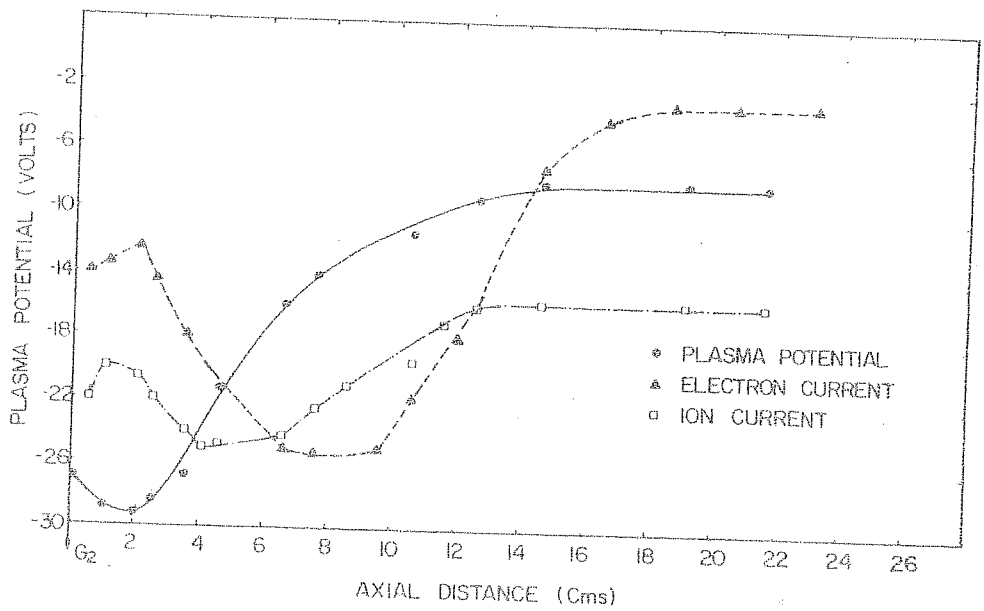

Figure 4.11 Plots of plasma potential, electron current and ion current in the presence of a strong double layer $\frac{e\Delta\Phi}{T_e}$ > 10. The observed dip is larger in this case compared to the weak double layer case shown in fig. 4.10.

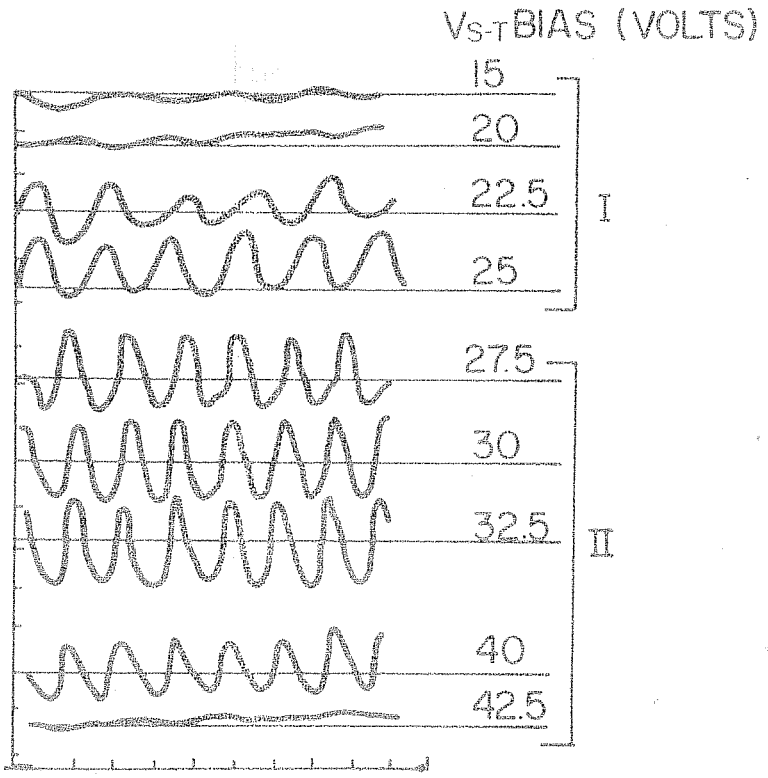

Figure 4.12 Ion acoustic fluctuations triggered at a threshold relative bias voltage before double layer formation. The fluctuations were monitored with a Langmuir probe biased to collect electron saturation current.

$$\text{I } \frac{\delta n}{n_o} = 25\%, \quad \text{II } \frac{\delta n}{n_o} = 50\%.$$

Each division on x-axis is 50 μsecs.

At about 15 volts, we observed some low level fluctuations, which grew in amplitude at about 25 volts. The frequency of these oscillations was about 12 kH_z. At 30 volts the frequency increases from 12 kH_z to 25 kH_z and at higher relative biases the amplitude again reduces, before attaining a very low level, at a bias of about 42.5 volts. At this juncture, a steady state double layer is observed in the target region. The threshold bias voltage for these fluctuations to appear, reduces at higher neutral gas pressures.

4.2.6 3 - dimensional Double layers :

Fig. 4.13 shows the 3-dimensional potential structures in a typical case of a double layer. The potentials were obtained by rotating the emissive probe, through an arc, which intersects the axis of the device. The maximum amplitude along the axis is about 16 volts with $e\Delta\phi/T_e \approx 18$.

The plasma potentials are more negative away from the axis. A representation of the equipotential contours for the date shown in fig. 4.13 is presented in fig. 4.14.

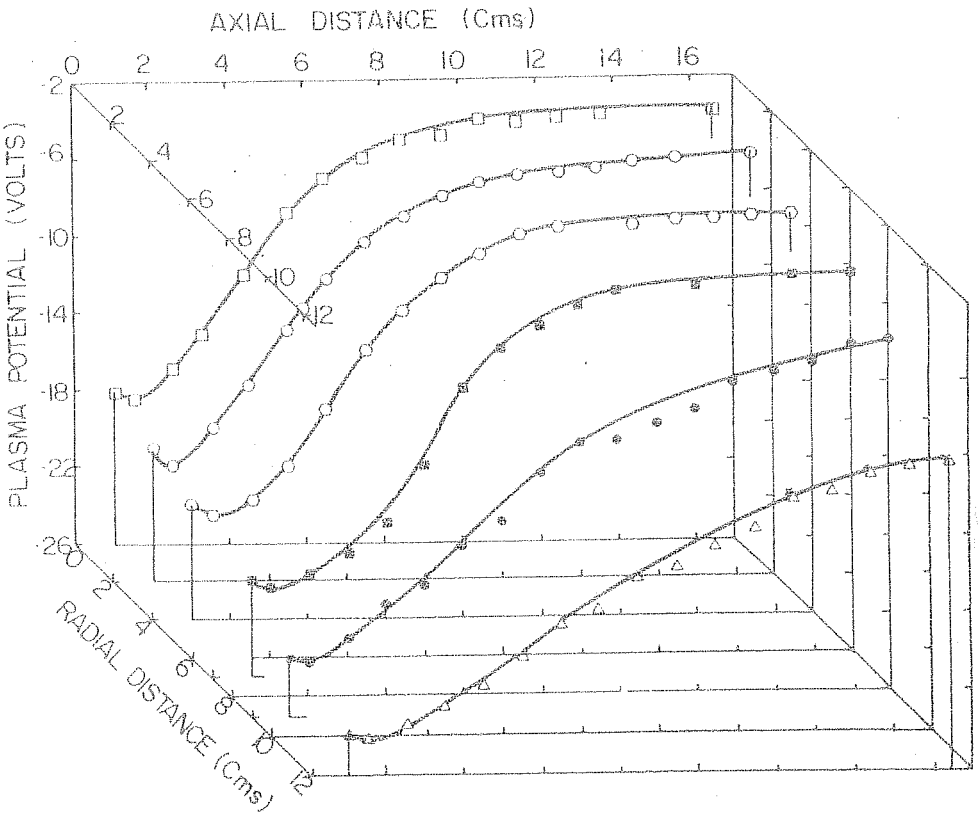

Figure 4.13 Three dimensional characteristics of the double layers. These plots of potential profiles were obtained for different probe orientations in the radial direction.

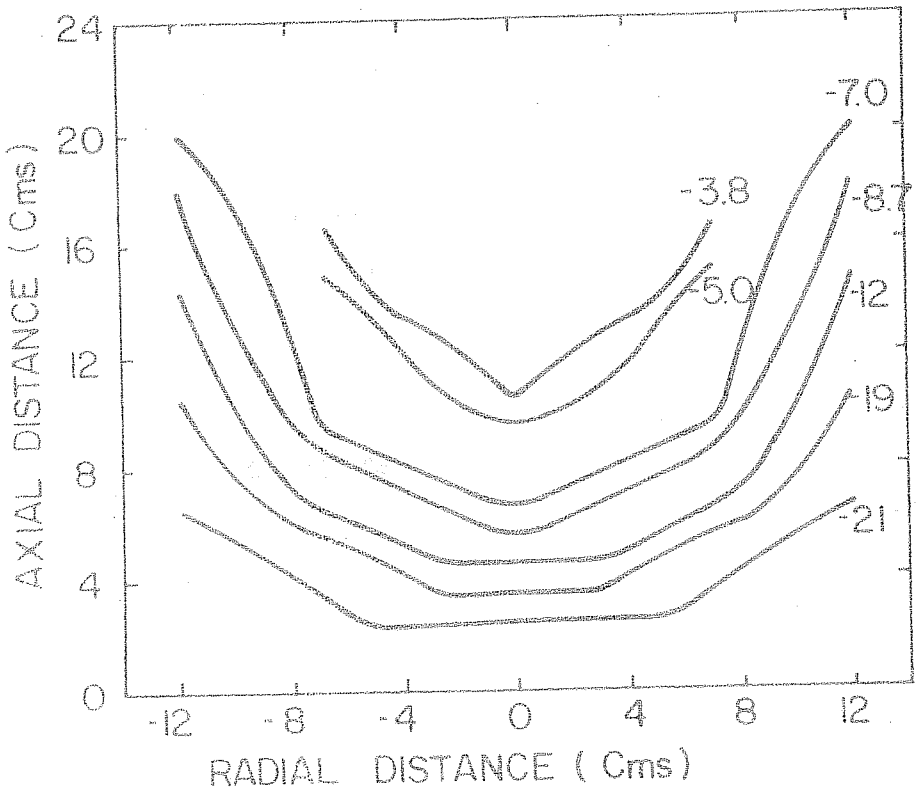

Figure 4.14 The Equipotential contours obtained from the data shown in fig. 4.13.

4.3 Discussions

4.3.1 Dependence of strength of double layers on electron currents

We have shown from the above mentioned results, that it is possible to form strong double layers in a double plasma machine. We have been able to generate double layers over a range of 10 - 100 volts which implies weak double layers with $e\Delta\phi/T_e \gtrsim 5$ to strong double layers with $e\Delta\phi/T_e \gtrsim 50$. From these observations, it is clear that electron temperature or ionisation potential do not constrain the amplitude of the double layers. Quon and Wong (1976), were able to observe only weak double layers in their double plasma machine. Leung et al. later modified their machine into a triple plasma machine and operated it in the double plasma mode. The maximum amplitude of the double layer they could obtain was about 14 volts corresponding to the ionisation potential of Argon; with electron temperature of 2eV, this gave a ratio $e\phi/kT_e \gtrsim 7$. Their attempt to produce potential double layers of larger amplitudes, was not successful, for the larger amplitude potential drops were rendered unstable. Hence they concluded that strong double layers are those, whose potential drop is

of the order of the ionisation potential and not large compared to kT_e. Coakley and Hershkowitz (1979) were unable to produce stable strong double layers $e\phi/kT_e > 10$ in their double plasma machine. They hence resorted to a triple plasma machine using specially designed sources to supply free and trapped particle population on either side of the target region in which double layer was formed. By using surface magnets the bulk plasma electron temperature was reduced to 1 eV. In the triple machine also, the maximum amplitude obtained for stable layers was limitted to a value of 18 volts, with $e\Delta\phi/T_e \approx 18$. Though at times they were able to obtain double layers of amplitudes of 22 volts, these were found to be unstable or irreproducible.

Sato et al. (1981) observed in their Q machines ultrastrong double layers of amplitudes of about 100 - 200 volts. Since the electron temperatures in their machine was 0.1 eV, they were able to generate double layers with $e\Delta\phi/T_e \approx (1-2) \times 10^3$. Baker et al. (1981) were also able to obtain strong double layers with $e\Delta\phi/T_e \approx 50$. Since the plasma was produced in their system by a Kaufman source, the electron temperatures were about 0.3 eV. Hence they were able to obtain strong

double layers with $e\Delta\phi/T_e \geq 10$, though the potential drops were only about 15 volts.

Some of the experimental results mentioned above may lead one to conclude that the strength of the double layer depends on the electron temperature. The lower the electron temperature, the stronger would be the double layer. But this would be true if double layers, were purely resistive in character, where Spitzer's resistivity (Resistivity $\propto 1/T_e^{3/2}$) would hold good. But double layers, unlike anomalous resistivity do not obey the general Ohm's law

$$\vec{E} = \eta \vec{J} \qquad (4.1)$$

and hence no direct relation exists between the currents and voltages (Falthammar, 1978).

According to Block's theory (1972), double layers are current dependent phenomena, and hence larger currents should lead to stronger double layers. This was observed in the experiment carried out by Torvén (1981), where very strong double layers were obtained. For this purpose a triple plasma source was used. The magnetized plasma column was maintained in the central chamber by

two plasma sources, one at each end of the chamber. The high voltage drops were obtained when the background pressure in the chamber was kept so small that ionisation by electron impacts in that region contributed negligibly to the plasma density. The neutral gas that was used in this experiment was Argon. The observed potential drops were of the order of 1000 volts with $e\Delta\phi/T_e \approx 500$ since $T_e \approx 2eV$.

Stenzel et al. (1981) obtained strong stable layers when an ion beam was injected along converging magnetic field lines. The observed potential drops were about 50 volts, with $e\Delta\phi/T_e \lesssim 25$. The electron temperature in this experiment was about 2 eV. One interesting aspect of these results, was that though the experiment was performed in a discharge type of plasma, they were not limited by ionisation potentials of the neutral gas.

Our experimental result indicate that it is possible to generate strong double layers by injecting larger currents into the target plasma, by increasing the relative bias potentials. This very well agrees with Block's theory (1972), that larger currents should

lead to larger potential drops. Another important point to note is that potential drops observed by us were not limited in amplitude to the ionisation potentials, contrary to the observations of Coakley and Hershkowitz and Leung et al. (1981).

One of the main reasons for our being able to obtain strong double layers in the modified configuration is that, we were able to extract a larger current into the target region. In the earlier configuration (Chapter 3), wherein only weak double layers were possible, the biasing arrangements, were similar to those of Quon and Wong (1976), Coakley and Hershkowitz (1976) and Leung et al. (1979). To verify this fact we monitored the electron current close grid G2, with a Langmuir probe in the two different configurations. We term the configuration wherein only weak double layers were obtained (Chapter 3) as configuration I and the modified configuration explained in this chapter as configuration II.

The beam current was monitored at different relative bias voltages. This is shown in fig. 4.15. I indicates the electron current profile in configuration I and II indicates the current profile in configuration II.

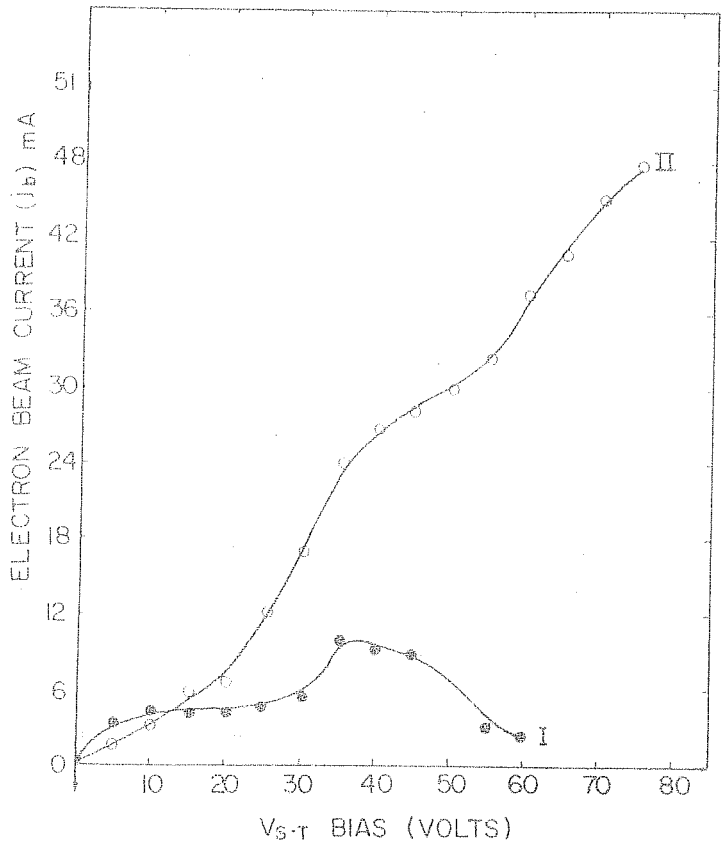

Figure 4.15 Plot of electron beam current in the two configurations I and II. Configuration I corresponds to the case in which grid G2 is biased positive with respect to the target and only weak double layers are possible (Chapter 3). Configuration II corresponds to the case in which G2 is biased positive with respect to the source. The currents were monitored in the target region, with a Langmuir probe biased to collect the energetic electrons.

It is very explicitly observed that, in configuration I, the current initially increases, but further increase in bias voltages reduces the current. It was found that we were able to obtain weak double layers, only in the region where the current showed a trend to increase. Beyond the current cut off, the entire plasma potential was rendered uniform, and no double layer was present.

In case of configuration II, we observed that the current increased with relative bias voltages though it shows a saturating trend at very large potentials. Hence we were able to obtain double layers over a wide regime, ranging from $e\Delta\phi/T_e \gtrsim 1$ -50. This experimental result corroborates the theory that double layers with larger potential drops are generated at larger currents. An interesting observation in our experiments, is the formation of the knee like structure in the potential profile. This type of potential profiles has been mostly observed in numerical studies of heat transfer in laser-pellet problems (Yabe et al. 1981). The potentials could result from the presence of large electron beam current at the low potential side. In our experiment we observe these structures at high relative bias potentials, whence we

could be drawing large electron currents from the source. The sheath like structure could be an additional potential barrier at the low potential side, that may be necessary in limiting the low potential side electron current and/ or provide ion trapping. The experiments of Chen and Hershkowitz (1983) have also revealed such potential barriers on the low potential side.

4.3.2 Relation between the applied voltage and double layer potentials (EMPIRICAL)

From Langmuir's (1929) condition for the double layer, between the electron current (i_e) the width of the double layer d and the double layer potential (ϕ_{dl}), we have obtained an approximate relation between the applied voltage and the double layer potential, for comparison with our experimental results.

The Langmuir's condition as defined by Carlquist (1982) for a double layer is expressed by eqn.(4.2)

$$|i_e|\, d^2 = k \left(\frac{2e}{m}\right)^{1/2} \cdot \phi_{dl}^{3/2} \qquad 4.2$$

where k is a constant.

We can write

$$i_e = e n v_d \qquad 4.3$$

where v_d is the electron drift velocity, and n is the density of the current carrying electrons.

The drift velocity is expressed in terms of the applied potential as

$$v_d = \left(2 e \phi_A / m_e\right)^{1/2} \qquad 4.4$$

where ϕ_A is the applied potential bias. Substituting eqn. 4.4 in eqn. 4.3 we get

$$i_e = e n \left(2e/m_e\right)^{1/2} \phi_A^{1/2} \qquad 4.5$$

This relation for current, when substituted on the LHs of eqn. 4.2, yields

$$e n \left(2e/m_e\right)^{1/2} \left(\phi_A\right)^{1/2} d^2 = k_2 \left(2e/m_e\right)^{1/2} \phi_{dl}^{3/2} \qquad 4.6$$

Further simplification yields

4.7

Since approximately we find O (en) $\approx$ O (K) $\approx$ 1 (Carlquist 1982) we obtain

$$\phi_A^{1/2} \cdot d^2 \approx \phi_{dl}^{3/2}$$

Hence

$$\phi_{dl} \approx \left(\phi_A \, d^4\right)^{1/3} \qquad 4.8$$

We have herewith obtained an approximate relation between the observed double layer potential (ϕ_{dl}), width of the double layer (d) and the applied potential drop (ϕ_A).

From the experimental values of d and applied voltage ϕ_A, we obtained a plot of ϕ_{dl} versus ϕ_A, which is shown in fig. 4.16. This shows a saturating trend at large relative bias voltages, with an initial linear increase. This plot very closely resembles the behaviour of the profile of the double layer potential obtained from the experimental observations with respect to the applied potential, shown in fig. 4.5. Similar trends in the potentials were obtained by Stenzel et al. (1982), wherein they had also obtained a saturating trend in potential at larger relative beam voltages, after an initial linear increase at lower applied voltages.

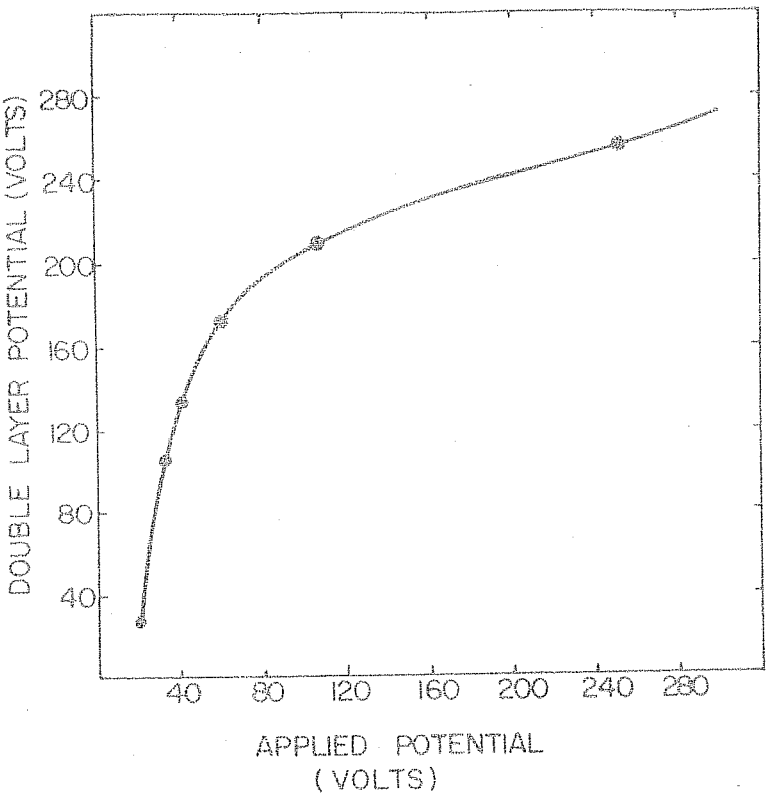

Figure 4.16 Double layer potential drops obtained from the derived empirical relation given by Eq. 4.8 with respect to the applied relative bias potential. This profile exhibits the same trend as that obtained from the experimental observations.

4.3.3 Double layer thickness and strength of double layers (Comparison with computer experiments)

From the plot of fig. 4.5 we find that in our experimental results the thickness of the double layer initially increases in accordance with the ideal theory (Carlquist 1972), but later reduces, with the formation of the knee like structure, to increase again to a saturation value. This phenomenon of initial reduction and again increasing in thickness has also been observed by other experimenters (Coakley and Hershkowitz, 1979; Sato et al. 1981; Stenzel et al. 1981).

Computer simulations of Joyce and Hubbard (1978) on double layers, have shown that the shock thickness ($L_{dl} = L/\lambda_D$) measured in terms of Debye length can be related to the dimensionless shock amplitudes as

$$L/\lambda_D = L_{dl} = 6\left(e\Delta\phi/T_e\right)^{1/2} \qquad 4.9$$

From his computer experiments, Singh (1980) obtained a general relation between the two to be

$$L_{dl} = \gamma\left(e\Delta\phi/T_e\right)^{1/2} \qquad 4.10$$

where γ is termed as the normalised width. From

Table 4.1, we find that the width of the double layer increases from about 15.5 λ_D to 54 λ_D and settles down to a constant value of 51.1 λ_D, as the potential drop increases. This is also shown in fig. 4.5. From the experimental observations, we calculated the value of Υ, which yields an average value of 12, for $e\Delta\phi/T_e < 20$. This is similar to the observations of Coakley and Hershkowitz (1979), where they have obtained a value of 12 at $e\Delta\phi/T_e \approx 14$. At $e\Delta\phi/T_e \gtrsim 50$, our value of Υ reduces to about 6.5. This is in very good agreement with the computer simulations of Joyce and Hubbard (1978). The width of the double layer in their computer simulation at $e\Delta\phi/T_e \approx 50$, was about 40 λ_D, whereas our experimental results reveal a double layer thickness of 40 ~ 50 λ_D.

Torven (1979) in order to compare the various results of different experiments has, defined Γ, a measure of the space charge strength within the layer as

$$\Gamma = \left(\lambda_D/L\right)\left(e\Delta\phi/T_e\right)^{1/2} \qquad 4.11$$

Till about $e\Delta\phi/T_e \lesssim 20$, the value of Γ obtained from our experimental observations is ≈ 0.08. At $e\Delta\phi/T_e \gtrsim 40 \sim 50$, we obtain a value of $\Gamma = 0.17$. The computer

TABLE 4.1

ELECTRON TEMPERATURE (T_e) = 2eV, DEBYE LENGTH (λ_D) = 20 mm

No	Applied Potential ϕ_A (volts)	Potential Drop across the double layer ϕ_{dl} (volts)	$\frac{e\Delta\phi}{T_e}$	Width of the double layer: L (mms)	$\frac{L}{\lambda_D}=L_{dl}$	Normalised Width $\Upsilon = \frac{L_{dl}}{(e\Delta\phi/T_e)^{1/2}}$	Strength of the double layer $F=\left(\frac{\lambda_D}{L}\right)\left(\frac{e\Delta\phi}{T_e}\right)^{1/2}$
1	20	3.5	1.75	31	15.5	11	0.08
2	30	22.5	11.25	88	44.0	13	0.1
3	40	33.3	16.65	100	50.0	12.25	0.08
4	60	46.6	23.3	108.3	54.13	11.23	0.09
5	100	83.3	41.65	108.3	54.13	8.39	0.13
6	200	97.1	48.55	82.1	41.05	5.9	0.17
7	250	105 (82.2)	52.5 (41)	102.1 (92.8)	51.1 (46.4)	7.0 (7.25)	0.14 (0.17)
8	300	120 (96)	60 (48)	101 (78.5)	51.1 (46.4)	6.6 (6.65)	0.15 (0.17)
Computer simulation of Joyce and Hubbard (1978)							
				50.0		6	0.17

Quantities in parenthesis indicate observations after the formation of the knee in the potential profile.

results of Joyce and Hubbard (1978) have also yielded a value of $\Gamma = 0.17$, at $e\Delta\phi/T_e \approx 50$ as calculated by Torven (1979).

From the comparisons, we find that our results are in good agreement with the computer simulations.

4.3.4 Role of neutral gas pressures and G2 bias voltages

The neutral gas pressure has been observed to play a crucial role in the formation of double layers (Chapter 3). Similar results were also observed by different experimenters (Coakley and Hershkowitz 1979 ; Leung et al. 1980; Stenzel et al. 1981).

Strong double layers were observed in most of the experiments only at low pressures for eg. 6×10^{-5} to 1×10^{-4} Torr. Beyond about 2×10^{-4} Torr, the double layers, tended to become unstable, and the entire plasma potential was rendered uniform. From the results of fig. 4.7 we find that it is true also in our experiments on strong double layers. One physical possible explanation, for this reduction in amplitude could be as follows:

After a double layer is formed, addition of neutral gas increases ionisation. The additional ions

formed, together with those, that are accelerated from the high potential region, reduce the excess negative space charge required on the low potential side. Since the electrons injected from the source region creates the negative potential well on the low potential side, the additional ions neutralise the space charge of the excess electrons. This leads to a reduction of the depth of the potential well. Beyond a certain value of pressure, the electron density on the low potential side is no more greater than the ion density. At this instant, the entire plasma potential in the target chamber becomes uniform.

Coakley and Hershkowitz (1979) were able to shift the position of the double layer in the target region by varying the G2 bias, when it was biased positive with respect to the source. In our present configuration, we were unable to shift the double layer position to the same extent as that of Coakley and Hershkowitz (1979). This is probably due to the presence of an additional source on the high potential side, in their experiment.

At low pressures Coakley and Hershkowitz (1974) were able to obtain larger potential drops with the grid

G2 biased positive with respect to the target, but the strength of the double layer was observed to reduce, since the electron temperatures increased at very low pressures.

In our experimental observation, we find that the amplitude of the double layer reduces with increase in G2 bias. This could be due to reduction in electron current flowing into the target region at positive G2 bias voltages. Hence we monitored the grid current with G2 bias, and observed that a large current flows in the grid G2, at larger G2 bias voltages. This leads to a cut off in the electron current flowing in the target region. Hence based on the observation presented in 4.3, we can deduce that the magnitude of the electron current in the target region decreases with G2 bias and hence lowers the amplitude of the potential drop in the double layer.

4.3.5 Stability of the double layers

The experimental results showed that the strong double layers in our experiments were very stable in contrast to those of Coakley and Hershkowitz (1979) and Leung et al. (1980), wherein the double layers were

rendered unstable beyond $e\Delta\phi/T_e \geq 18$.

As shown in fig. 4.12, we obtained low frequency fluctuations at a threshold relative bias voltage of 20 volts, which increased both in amplitude and frequency at a relative bias of about 40 volts. These ion acoustic fluctuations are probably created by the beam current when V_d (electron drift velocity) approached V_{the} (electron thermal velocity). These fluctuations can in turn scatter particles from localised regions, leading to a depression in particle density. These fluctuations are not present once the double layer is formed. Hence we find that there exists an ion acoustic type of instability, before the formation of the double layer, but after the formation, these instabilities are absent. Since the amplitude of these fluctuations is also very small compared to the total d.c. potential drop, they may not play a significant role in disrupting the double layer.

The 3- dimensional double layers presented in fig. 4.14, very closely resemble the U shaped double layers observed in the space experiments along the magnetic field lines, and also theoretically predicted by Block (1972). Similar observations were reported by

Baker et al. (1981) in an unmagnetized plasma. As observed in their results we have also obtained plasma potentials positive with respect to the walls, to reduce the electron losses.

Hence we have obtained stable 3-dimensional double layers in the present modifications.

4.4 Circuit analysis of the two configurations I & II

To justify our conclusion, that a layer current flows in the configuration II, than in configuration I, and also verify our experimental observations, we have carried out an approximate circuit analysis of the two configurations.

Fig. 4.17 shows the two configurations I and II, along with the directions of the independent currents, flowing in the system. Denoting the currents flowing in the different loops by the following :

I_{SG1} = current flowing between the source and grid G1

I_{G2} = Current flowing in the grid G2

I_T = Current flowing in the target region

I_{S-T} = current in the entire target region

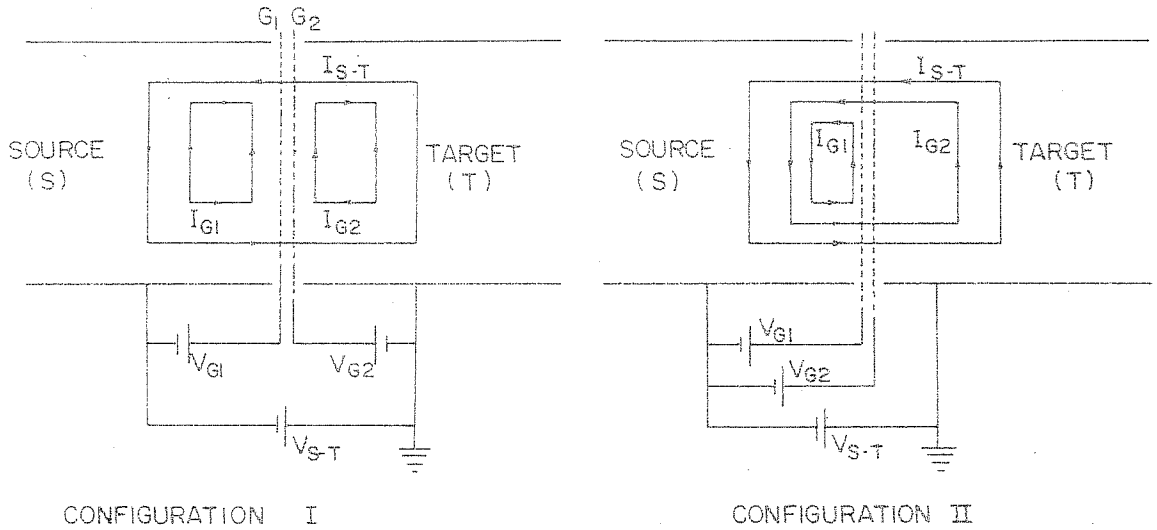

Figure 4.17 Diagram of an approximate circuit analysis carried out to verify the flow of current in the target chamber in the two configurations. The arrows indicate the direction of flow of current.

Configuration I corresponds to the weak double layer case (Chapter 3).

Configuration II corresponds to the strong double layer case with modified configuration.

we find, by analysing the circuit that the current flowing in the target section in configuration I is

$$I_T = I_{S-T} - I_{G2} \qquad 4.12$$

Hence, we find that the current flowing in the target region is reduced by I_{G2}, from the total current.

Now, considering the configuration II, we find that the total current flowing in the cource-target region turns out to be

$$I_T = I_{ST} \qquad 4.13$$

This shows that there is no reduction in the current, which flows into the target region. This is quite in agreement with the observation.

In configuration I, we find that I_T decreases, with increase in V_{S-T}, due to increase in the current flowing in G2. This was verified by monitoring the grid G2 current with respect to the V_{S-T} potential. The same effect was not observed in case of configuration II, wherein the grid G2 current, practically remained constant throughout, the increase in V_{S-T} potential.

Hence, we have proved that there is a largercurrent flow in configuration II, which in turn aids in obtaining strong double layers compared to configuration I. This model quite well agrees with the experimental observation for the currents in the target section for the two different configurations, shown in fig. 4.15. As a result, it also helps us in concluding, that the magnitude of the double layer amplitude, depends on the current flowing in the system, and not on the ionisation potential or the electron temperatures.

4.5 Comparison of the results with other previous experiments

In this section we present the comparison of our results of configuration II with configuration I, and also other experiments on strong double layers. Table 4.2 contains the comparison of configuration I and II, Table 4.3 presents the comparison of the results of Coakley and Hershkowitz (1979), and Leung et al. (1980) with those of ours in a multiple plasma device. Table 4.4 presents a comparison of the results of different experiments on strong double layers in different devices.

TABLE 4.2

COMPARISON OF CONFIGURATION I AND II

	Configuration I	Configuration II
1.	Only weak double layers $e\Delta\phi/T_e < 10$ were possible	Strong double layers with $e\Delta\phi/T_e > 10$ were obtained
2.	Potential drops were almost limited to ionisation potential	No limitation by ionisation potential
3.	Free electron current decreases, beyond a critical value of relative bias	Free electron current increases with relative bias
4.	Potential drop between source and grid G2 increases with relative bias	Potential of G2 was about 1 volt less than the source potential
5.	Current in G2 increased with relative bias	Current in G2 was practically constant
6.	Electron distribution function revealed a beam component close to the grid G2	Only a drifting electron distribution of the free electron species was observed
7.	Ion sheath like structure not observed close to grid G2	At large potential jumps, an ion sheath, helps in forming a virtual cathode like potential structure and hence trap ions

TABLE 4.3

COMPARISON OF THE EXPERIMENTAL OBSERVATIONS OF COAKLEY AND HERSHKOWITZ (1979), LEUNG ET AL. (1980) AND OURS IN A MULTIPLE PLASMA MACHINE

No.	Experimental details	Observations of Coakley and Hershkowitz (1979)	Observations of Leung et al. (1980)	Present Work
1.	Experimental setup	Triple Plasma machine. Obtained weak double layers in double plasma mode, with one source off	Triple plasma mode. Operated throughout in double plasma mode	Double plasma machine
2.	Surface magnetic fields to confine primary ionising electrons	Yes	No	No
3.	Role of primaries	Not significant	Not significant	Not significant
4.	Maximum limit on the potential drop ϕ	Obtained larger than 20 volts, but were unstable. At low pressures, obtained larger potential drops, but reduction in $e\Delta\phi/T_e$ was observed.	Limited to ionisation potential of the neutral gas	Obtained stable double layers, with potential drops of about 80-90 volts
5.	Electron temperature	1eV	2eV	2eV
6.	$e\Delta\phi/T_e$	≈ 14	$\lesssim 5 \sim 7$	$\gtrsim 50.0$

No.	Experimental details	Coakley & Hershkowitz	Leung et al.	Present Work
7.	Grid G2 biased positive with respect to the source	Could move the double layers, by increasing the G2 bias, probably due to additional plasma source	Not attempted	Strong double layers were obtained. Amplitude reduced with increase in G2 bias.
8.	Variation of $e\Delta\phi/T_e$ with V_{S-T}	Not measured	Not done	Obtained strong double layers, which move towards G2 as amplitude of potential drop increases.
10.	Variation of electron beam current with V_{S-T}	Not measured	Not done	Current increases
11.	Pseudo double layers	Observed in double plasma machine	Not observed	Were observed. Detailed investigations revealed moving double layers in an expanding plasma.

TABLE 4.4

COMPARISON OF STRONG DOUBLE LAYER EXPERIMENTS IN DIFFERENT DEVICES

No.	Experimental Details	Coakley and Hershkowitz (1979)	Torven (1981)	Sato et al. (1981)	Baker et al. (1981)	Stenzel at al. (1981)	Present work
1.	Potential drop ϕ (Volts)	14 ~ 18	1000	400	15	30	80 ~ 100
2.	Electron temperature-T_e	1.0 eV	2.0 eV	0.1 eV	0.1 to 0.3 eV	2 eV	2 eV
3.	$e\Delta\phi/T_e$(Max)	18	400~500	$1 \sim 2\times10^3$	50	22	40 - 50
4.	Magnetic Fields	Surface magnetic fields to contain primary ionising electrons	Strong axial magnetic fields	Strong axial magnetic fields	Strong axial magnetic fields	Magnetic dipole experiment with converging magnetic fields	No magnetic fields
5.	Role of primary electrons	Not significant	No primaries	No primaries since Q machine was used	No primaries since Kaufman source was used	Not significant	Not significant
6.	Effect of one source off	Weak double layers were obtained	No double layers	-	No double layers	-	No additional source was used

No.	Experimental Details	Coakley and Hershkowitz (1979)	Torvén (1981)	Sato et al. (1981)	Baker et al. (1981)	Stenzel et al. (1981)	Present work
7.	Limitation of ionisation potential	Potentials larger than ionisation potentials were unstable	No	No	No	No	No
8.	Electron drift velocity V_d greater than electron velocity	Yes	Yes	Yes	Yes	Followed as a result of double layer formation	Yes

4.6 Physical model for strong and weak double layers observed in our device

4.6.1 Strong Double Layers

From the circuit model explained in 4.9, we can deduce that in configuration II, strong double layers can be generated by drawing large currents into the target plasma. These current carrying electrons create a deep potential well, by providing the excess negative space charge. As it is a steady state, there is a constant influx of electrons, which provide these negative space charges. As we increase V_{S-T} bias, the density of the excess electrons increases, and hence the dip in the potential well increases. As described in section 4.2.1, we have three different types of potential profiles after the formation of the double layer. These are illustrated in fig. 4.18 a,b and c. Fig. 4.18 a corresponds to the case where the potential minimum in the target chamber is below the source potential. Fig. 4.18 b corresponds to the case where the potential minimum in the target chamber is above the source potential. Fig. 4.18 c corresponds to the case where a knee like structure appears in the potential profiles. Since the Grid G2 potential in this configuration was always 1 volt less than source

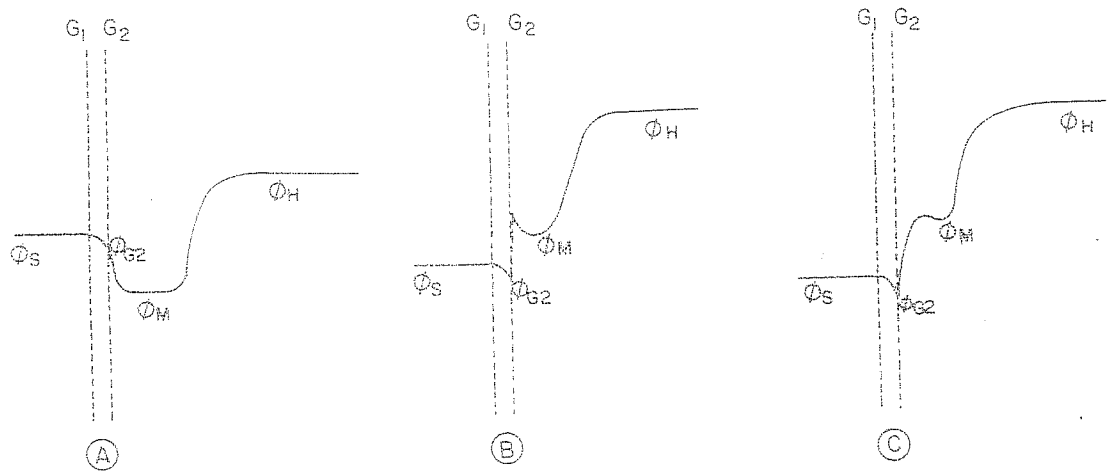

Figure 4.18 Model of the strong double layer potential profiles to explain the different experimental observations.

Case A: Double layer profile obtained with the potential minimum in the target chamber less than the source potential.

Case B: Double layer profile with the potential minimum more positive than source potential

Case C: Double layer profile similar to case B, but with the presence of knee like structure.

potential the electrons entering the target chamber are initially decelerated, very close to the grid G2, where they create a negative potential well by lowering the plasma potential, before the potential rises monotonically, to form a double layer.

Taking into account the initial deceleration, the free electron density obtained from the steady state equations of motion for electrons is

$$N_{ef} = N_0 \exp[\phi_s - \phi_M] \qquad 4.14$$

ϕ_s is the source plasma potential, ϕ_M is the potential minimum near grid G2. Both ϕ_s and $\phi_M < 0$.

From the above equation, we find that, the density of the free electrons increases with larger values of ϕ_s. This equation holds good atleast till V_{S-T} bias ≈ 40 volts, whence the target plasma potential minimum is more negative than the source potential as shown in fig. 4.18 a. Fig. 4.18 b corresponds to the second case, where the plasma potential minimum is slightly positive compared to the source electron density, we still have a double layer, maintained by the free electrons that are accelerated from the source, by the negative relative bias.

This situation holds good even at higher relative bias voltages, but as seen in fig. 4.18 c, when a potential of about 200 volts was applied, a knee like structure is observed in the potential profile. But in this case an ion sheath like structure commencing at G2 is present, with a large potential drop across it. This sheath like structure, aids in two ways to provide excess negative space charge on the low potential side. First of all it provides an accelerating structure for the electrons near G2 and also reflects electrons from reaching the grid G2, which would otherwise constitute to an additional grid G2 current. These two electron components apparently give rise to the knee like structure. This sheath like structure is even more prominent at higher relative bias potentials of about 300 volts. At this instant a clear negative potential dip is observed, after the initial transition from the grid and beyond the potential dip, a double layer profile is evident as seen from fig. 4.18 c. This entire profile is almost similar to the multiple double layer structure observed by Chan and Hershkowitz (1983).

The presence of ions on the low potential side can be accounted for by two processes. Since the G2

potential, was alwyas one volt negative with respect to the V_{S-T} voltage, this could give rise to the prominent ion sheath around G2 at large negative potentials. This could be formed from the ions accelerated from the high potential regions as well as ions entering the target from the source. As a result of this sheath, the electrons decelerated at the grid G2, would again experience an equal acceleration, and thus lead to a localisation of the excess negative charges beyond the sheath. This could give rise to the negative potential dip observed in the potential profiles, followed by the double layer transition.

Hence, we have obtained a density relation which could lead to strong double layers, as long as $\phi_M < \phi_S$. At $\phi_M > \phi_S$, the formation of an ion sheath like structure near G2, enables the formation of a negative potential well, on the low potential side, by providing the necessary electron space charge, required to sustain this structure. This could also resemble a multiple double layer as proposed by Block (1972) and observed in case of weak double layers by Chan and Hershkowitz (1983).

4.6.2 Weak Double Layers

In the case of weak double layers, we found from the circuit model for configuration I, that the current and hence the well near grid G2, reduce with V_{S-T} bias. Leung et al. modelled their observed double layers on the basis of a triode and obtained, a relation for the free electron density to be

$$N_{ef} = N_0 \left[exp - (\phi_S - \phi_M) \right] \qquad 4.15$$

from the Boltzman relation. Where ϕ_S is the source potential and ϕ_M is the potential minimum near G2 in the target region. From this it can be seen that if the potential drop is high, $(\phi_S - \phi_M)$ is large and the number of free electrons in the low potential region will be small. This perhaps could lead to weak double layers.

Eqn. 4.15 derived Leung et al. (1980), may hold good in our experiment also, on weak double layers (Chapter 3), wherein it was observed that the free electron density reduces beyond a certain value of V_{S-T}.

The above phenomena could be due to the following process:

From Fig. 4.19 it is evident that grid G2 in configuration I is always held at zero potential. Increasing V_{S-T} bias lowers ϕ_S and hence the difference between $(\phi_{G2} - \phi_S)$ increases. As a result almost the entire potential drop occurs between G1 and G2. Until the difference is below the ionisation potential, electrons can be accelerated across the grids and presence of the beam component can give rise to a double layer of a small amplitude. But once the difference exceeds the ionisation potential, it must be producing a large ionisation in the region between the grid assembly as well in the target region close to grid G2. This apparently increases grid current in G2, and thereby reduces excess electron space charge on the low potential side. The experimental observation of increase in G2 current confirms this process. The presence of an accelerated electron beam component (Chapter 3) in the distribution function, near G2 agrees well with our explanation that, below the ionisation potential, electrons could be accelerated across G1 and G2, which provides the necessary negative space charge required on the low potential side, to form a double layer.

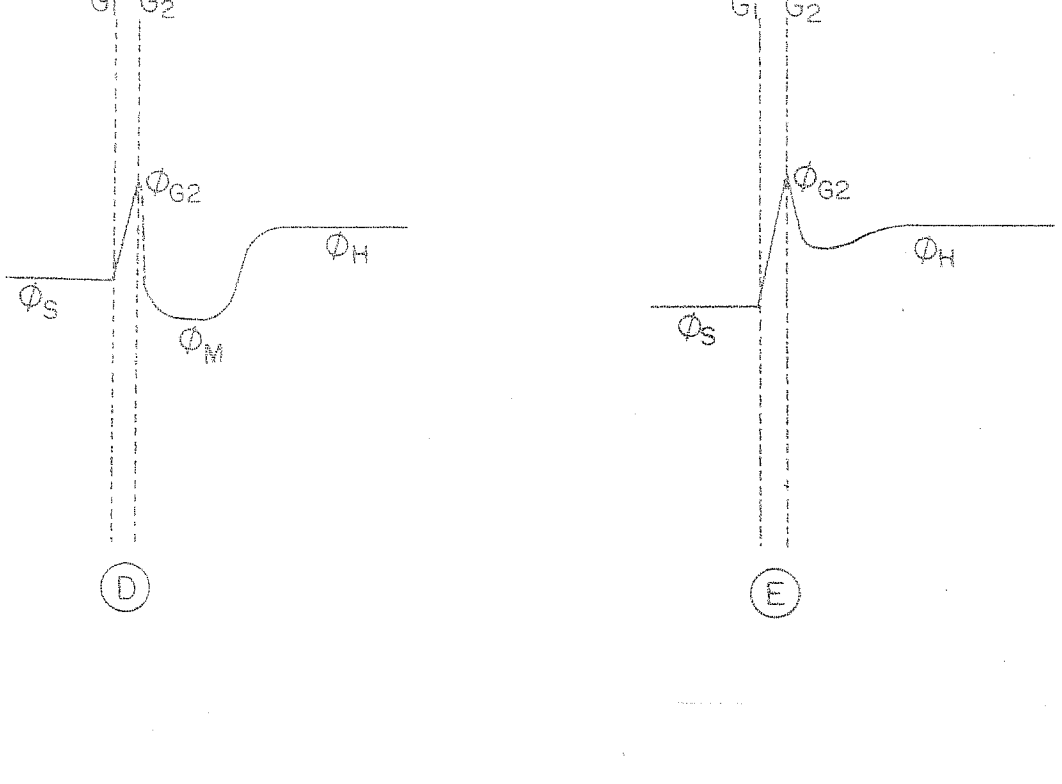

Figure 4.19 Models of the weak double layer profiles (similar to those in Chapter 3).

Case D: Double layer profile obtained with potential minimum in the target chamber less than the source potential though similar to case A of fig. 4.18, only weak double layers were obtained.

Case E: The almost uniform plasma potential in the target plasma, when no double layer was present at high relative bias potentials.

As a consequence of the depletion of excess negative space charge, near G2, the double layers obtained in configuration I are always weak double layers, with a potential drop, of the order of or less than the ionisation potential.

We have thus shown, that by modifying the bias configurations, it is possible to generate strong double layers with $e\phi/T_e \geq 10$. We have also shown, that irrespective of the device, it is possible to obtain strong double layers without being limited by the ionisation potential or electron temperature. The strength of the double layer has been found to depend on the currents involved. Through the circuit model, we have been able to establish the fact, that a larger current, and hence formation of strong double layers is possible with the modifications incorporated by us. The relation we have derived, between applied voltage and the double layer potential agrees quite well for the experimental observations. We have also presented a physical model which quite well explains the observations. An intercomparison has been made between the different experiments, and found that it is possible to obtain strong double layers, where ionisation potential should not be the limiting amplitude of the double layer.

Chapter 5

PROPAGATION OF NONLINEAR ION ACOUSTIC PULSE IN A HOMOGENEOUS PLASMA, AND THE EVOLUTION OF AN ION ACOUSTIC DOUBLE LAYER, FROM AN ION ACOUSTIC RAREFACTION INSTABILITY

Non-linear ion acoustic waves in plasmas have been the subject of intense study, for a considerable period of time. Weakly non-linear ion acoustic waves are described in terms of Korteweg-de-Vries equation (KdV) which possesses interesting stability properties in terms of having infinite number of constants of motion. In the past only compressive ion acoustic pulses have been studied in depth due to their interesting characteristics arising out of the balance of nonlinearity and dispersion,

giving rise to coherent solitary structures.

Such a balance of nonlinearity and dispersion is not possible for the case of the rarefactive ion acoustic pulse and as such the rarefactive pulse does not evolve into a solitary wave. Instead it suffers decay into a wavetrain. The rarefactive ion acoustic wave has, therefore not been paid much attention both in theoretical as well as in experimental works. Interesting behaviours in the propagation of rarefactive waves might, however arise due to the fact that negative potentials associated with these waves might a) trap a part of ion population and b) reflect low energy electrons. Recently some theories have been suggested that nonlinear steepening of a wave can arise due to trapping of particles(Kono and Mulser,1983) Such wave particle interactions might lead to effects which have not been properly understood.

Numerical simulations (Sato and Okuda 1980, 1981; Okuda and Ashour-Abadalla 1982; Smith 1982) and theoretical models (Hasegawa and Sato 1982; Schamel 1982; Hudson et al. 1983; Lotko 1982) present a scenario in which the ion acoustic double layers evolve from a

rarefactive negative potential in a current carrying plasma. Experimental evidence is however lacking, though recently there have been evidences of such structures observed in satellite measurements.

In view of the above, we have carried out experiments on the propagation of nonlinear ion-acoustic rarefactive pulse in homogeneous, current free, as well as current carrying plasma.

In this chapter, we first describe our results on the propagation of a rarefactive ion acoustic wave in a homogeneous plasma and then the evolution of a double layer from an ion acoustic rarefaction in the presence of an electron beam/current in the plasma.

5.1 Evolution of a rarefactive ion acoustic wave in a homogeneous plasma

5.1.1 Experimental setup and diagnostics

The experiment was performed in a large volume plasma devices 125 cms long and 50 cms diameter, as shown in fig. 5.1. The entire plasma chamber was evacuated to a base pressure $\leq 10^{-5}$ Torr. Tungsten filaments each about 8 cms long, were uniformly distributed throughout the device. The filaments were heated to thermionic

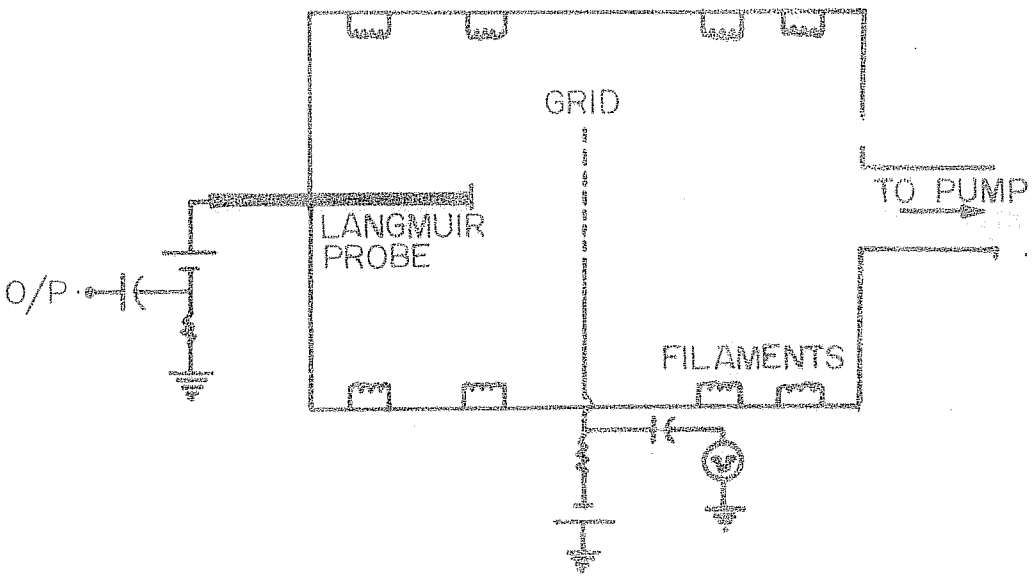

Figure 5.1 Schematic diagram of the experimental set up. The input pulse is applied to a negatively biased grid. Density perturbations are monitored by a Langmuir probe biased to collect electron saturation current.

emission and the emitted electrons were accelerated to maintain a steady state discharge, by electron-neutral impact ionisation of argon neutrals. The working pressure was maintained at about 10^{-4} Torr.

A cold Langmuir probe was deployed for the measurement of density and temperature. It was also used to monitor the density perturbations, by biasing it to collect electron saturation current. The plasma in the system was uniform over the chamber dimensions. The plasma parameters were $N_e \approx 2 \times 10^8$ cm^{-3}, $T_e \approx 1$eV, $T_i \approx T_e/20$. The ion acoustic speed measured through a low amplitude ion acoustic wave propagation was $\approx 1.66 \times 10^5$ cm/sec.

A grid of 20 cms diameter was immersed in the plasma and biased negative with respect to the plasma potential. In addition a negative step potential was applied to launch a rarefactive pulse. These perturbations were detected by the Langmuir probe and recorded on a storage oscilloscope, triggered in synchronization with the applied potential.

5.1.2 Experimental Results

The waves were launched into the plasma, by pulsing

the negatively biased grid with both positive (compressive) pulses and negative (rarefactive) pulses. The density perturbations monitored by the collecting Langmuir probe are shown in fig. 5.2. The compressive pulse evolved into well known solitons as displayed in fig. 5.2a, exhibiting the characteristic relationship between amplitude, width and speed.

For the case of a negative pulse, no rarefactive soliton was observed close to the grid, but outside the sheath, the negative pulse was observed to be a symmetric single pulse. Fig. 5.2b shows such a pulse of initial amplitude $\leqslant 0.5\%$. These pulses were observed to broaden as they move away from the launching grid, with a speed less than, but close ion acoustic velocity. At farther distances, these low amplitude pulses were linearly Landau damped.

Fig. 5.3 shows the density perturbation of initial amplitude $\approx 3.6\%$ as a function of time at different axial positions from the launching grid. The rarefactive pulse starts out as a symmetric negative pulse, together with a wavetrain, consisting of a prominent compressive pulse at the rising end of the rarefactive pulse. Further propagation leads to (i) broadening of the trough and

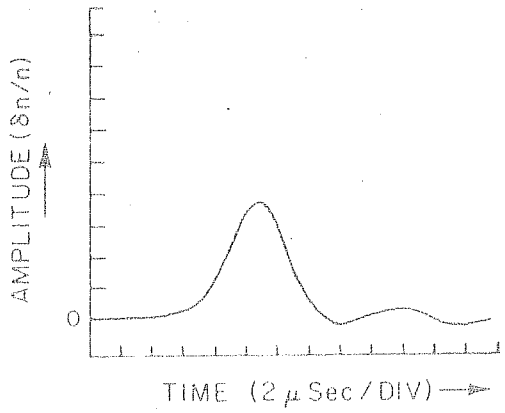

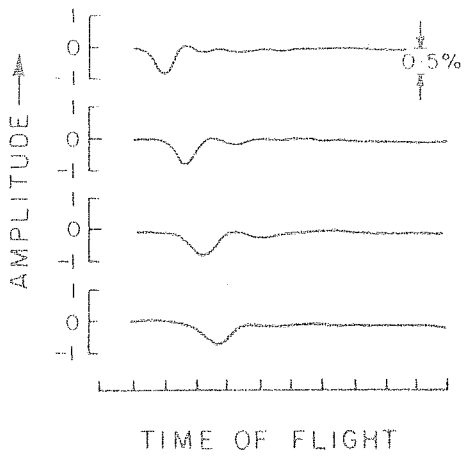

Figure 5.2 (a) Top Trace: Typical example of a compressive soliton formed by applying a positive step potential to the grid.

(b) Bottom Trace: Typical example of a low amplitude rarefactive pulse $\simeq$ 0.5% obtained by applying a negative step potential to the grid.

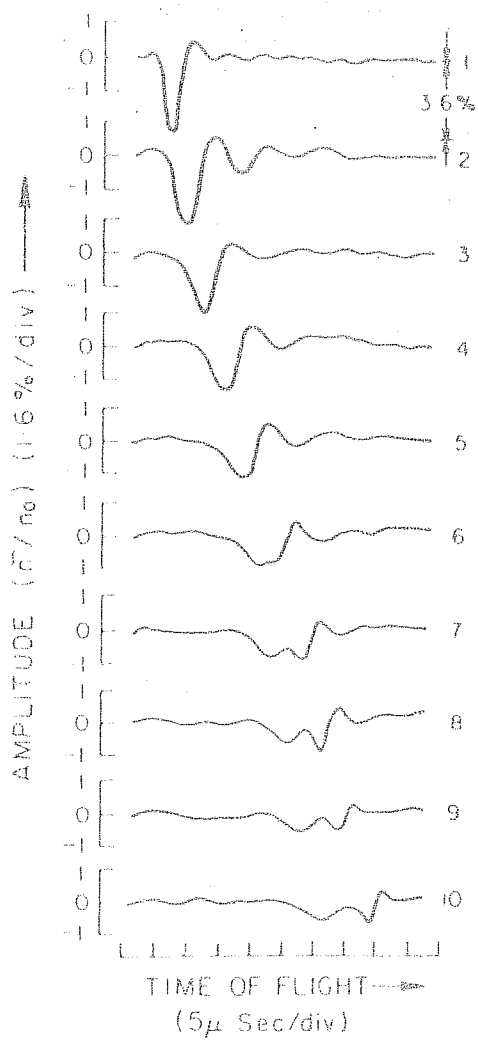

Figure 5.3 Typical example of rarefaction pulse propagation in the plasma. Successive traces (1-10) are time records taken at axial positions separated by 12.5 λ_D. Horizontal axis is time of flight in 5 μ sec/div and vertical axis gives amplitude ($\tilde{n}/n_o$) in 1.6% per division. Amplitude of the step potential applied to grid for all traces is 1 volt.

(ii) steepening of the rising part of the density and generation of the wavetrain at the trailing edge. The broadened trough next fissions near the minimum, resulting in the generation of two minima separated by a local maximum.

After this fissioning or breaking, the two troughs travel at different speeds and move away from each other. The wavetrain at the trailing edge also separates along with the newly created trough. The process of broadening of the trough and steepening at the trailing edge (near the rising part of the density) continues for both the troughs, as they propagate further, after the fissioning.

Similar results were observed for an initial amplitude of 4.5%, which is shown in fig. 5.4. For pulses of initial amplitudes $> 5\%$, the fissioning process, is observed to occur more than once, where each of the troughs undergoes this process, as the perturbation propagates further. A typical example is shown in fig. 5.5 for a pulse of initial amplitude of $\simeq 10\%$. Ultimately the entire population breaks up into a small amplitude wavetrain which damps out as it propagates in the plasma.

In fig. 5.6, we have plotted the time of flight

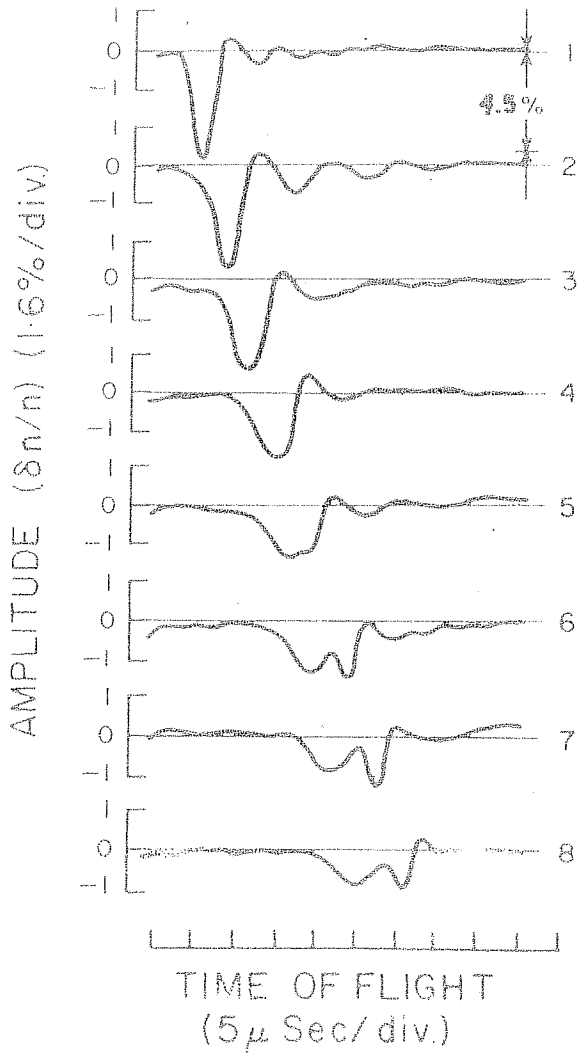

Figure 5.4 Typical example of the rarefaction pulse propagation similar to fig. 5.3, but for an input amplitude of 1.4 volts.

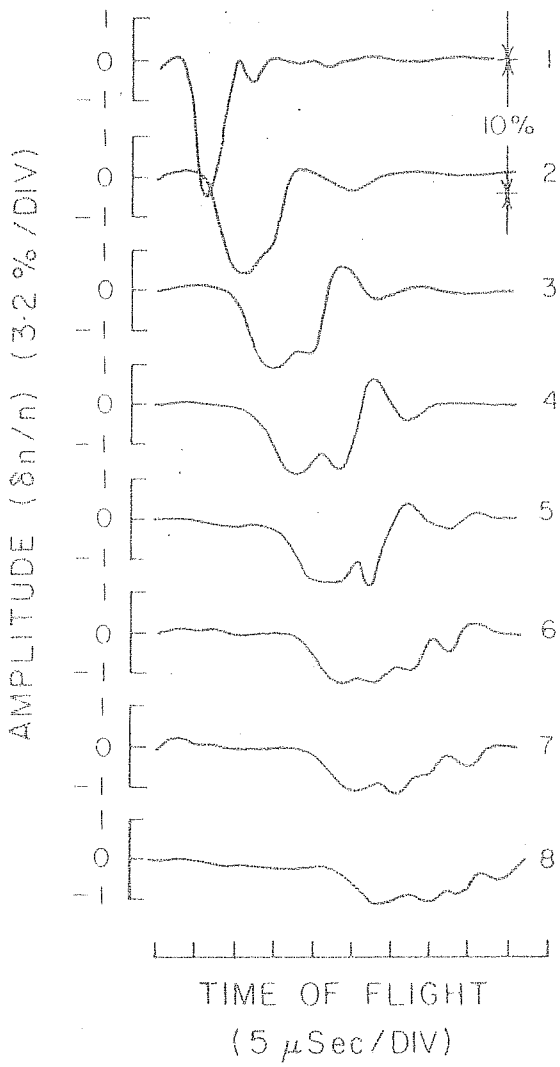

Figure 5.5 Example of multiple fissioning of a rarefactive pulse (traces 5 to 8). Successive traces are at 12.5 λ_D from each other. The input amplitude applied to the grid is 6 volts.

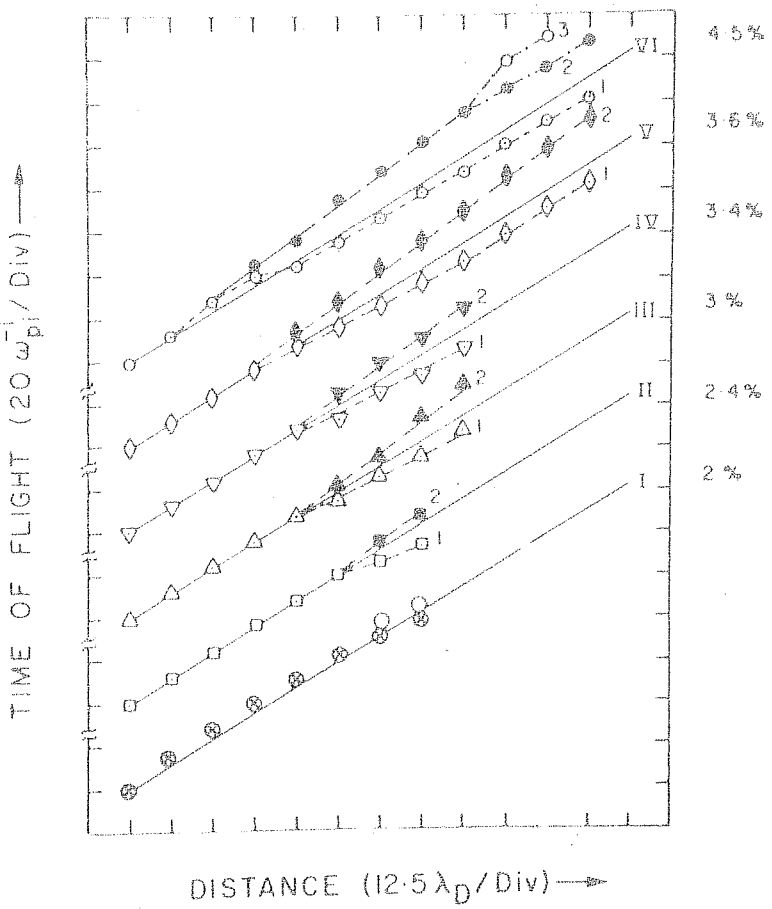

Figure 5.6 Time of flight versus axial position for the rarefactive pulses of different initial amplitude 2% to 4.5%. The initial amplitudes are indicated on the right hand side.

of the pulse minimum, for the different amplitudes of 2% to 4.5%. The path followed by the newly created trough after fissioning is shown by the dashed line. The side line in each plot represents, the path which the trough would have followed, if it travelled with ion acoustic velocity. An examination of the plot reveals the following.

(i) The rarefaction pulse travels with a speed $\leq C_s$ initially, and this speed depends upon the initial amplitude of the pulse. The speed decreases with increase in amplitude.

(ii) After fissioning, the first trough acquires a supersonic speed $> C_s$ (branch I) while the newly created trough and the wavetrain, which separated along with the newly created trough, travel at a subsonic speed $< C_s$, (branch 2) as seen in fig. 5.6.

(iii) For pulses of initial amplitudes between 2% and 4.5%, the speeds of the two troughs, created through the fissioning of the original pulse are 1.2 C_s and 0.8 C_s. Hence, there is a separation of $\pm$ 0.2 C_s, in the speeds of fast and slow troughs, from the ion acoustic velocity.

(iv) As seen in fig. 5.5, the distance to which the rarefaction pulse propagates before fissioning reduces as the initial amplitude of the pulse increases. This is illustrated in fig. 5.7, which gives the time of flight versus position for rarefactive pulses of larger initial amplitudes. Moreover, the separation of 0.2 C_s in the velocities from C_s, is also not obtained in this case. In one of the typical cases, the faster trough propagates at a speed of 1.12 C_s, whereas the slower trough propagates at a speed of 0.6 C_s. Hence it is observed that one of the troughs acquire a supersonic speed, while the other propagates at a subsonic speed. It is further observed, that the rarefactive wave with supersonic speeds survives for longer distances, while those travelling at lesser velocities damp.

Fig. 5.8 shows the variation of the amplitude of the rarefactive pulses as they propagate in the plasma. The amplitude of the newly created trough, after the fissioning is indicated by the dashed line, on each curve. It is seen that

(i) The attenuation of the pulse amplitude is not characterised by a single attenuation length, for the pulses of different amplitudes.

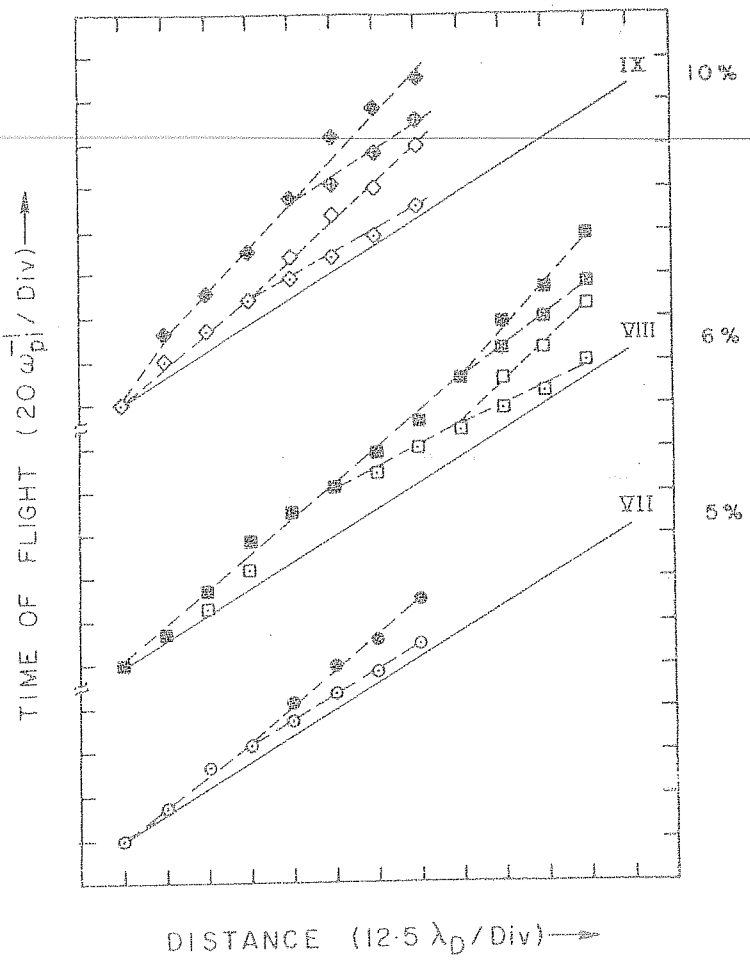

Figure 5.7 Time of flight versus axial position for larger initial amplitude 5% to 10% as indicated on the right hand side.

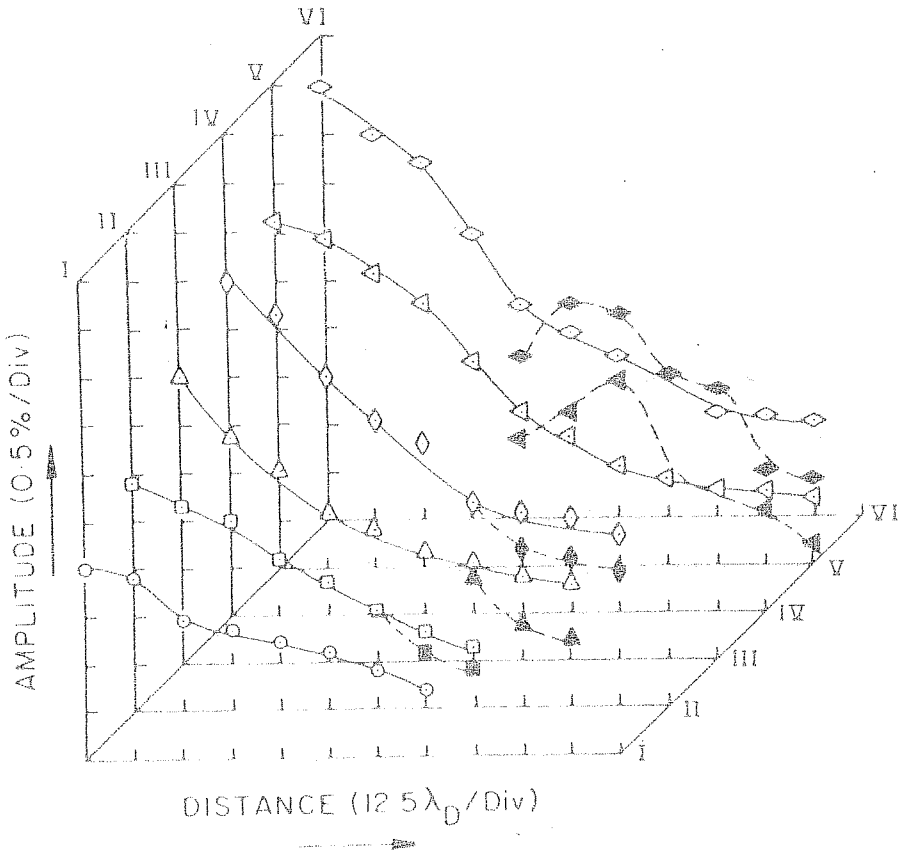

Figure 5.8 Amplitude versus axial position for rarefactive pulses of different initial amplitudes. Case I to VI corresponds to case I to VI to Fig.5.6. Open points represent the amplitude of the original pulse and the darkened points denote the amplitude of the new trough created after the fissioning.

(ii) The slower trough generated after the fissioning attenuates faster, and

(iii) For pulses of larger amplitudes, the slower trough grows in amplitude over a certain length before attenuation sets in.

5.1.3 Discussion

The results of the experiment show that the rarefaction wave in a homogeneous plasma does not evolve into a double layer. Instead we observe that the low amplitude wave $\lesssim 0.5\%$ are found to be Landau damped, whereas the rarefactive waves of larger amplitudes present some new features, like the fissioning of the original wave trough into two, following the nonlinear steepening, and the observation of the difference in the velocities of the two minima.

Okutsu and Nakamura (1979) carried out a numerical and experimental study of the temporal development of weakly nonlinear, broad ion-acoustic pulses. They were mainly interested in the experimental observation of the train of ion acoustic compressive peaks that evolved from three kinds of initial perturbations, pure compressive, pure rarefactive and one-cycle sinusoidal pulse in which

the rarefactive leading part is followed by a compressive part.

Their experiment was performed in a large volume plasma machine, and the waves were launched by grids, immersed in the plasma. In case of the compressional initial pulse, the leading edge was found to steepen and then develop into a train of compressive peaks. These peaks moved at speeds faster than ion acoustic velocity.

Similar train of compressive peaks were also generated by introducing a rarefactive part in front of the compressive part. But in this case the velocity of the peaks was not faster than ion-acoustic velocity. It was observed that these peaks did not evolve into solitons as in the previous case. The spatial plots exhibited a broadening at the minimum and a new rarefaction was observed, but this was not reproducible.

Their numerical solution of the KdV equation with an initial one cycle sinusoidal perturbation consisting of a compressive and a rarefactive part and also a pure rarefactive wave did not exhibit the formation of the new rarefaction wave at the minimum of the perturbation.

Though the observation of the second rarefaction

in their experiment is similar to those of ours, they do not attribute it 'fissioning' and moreover they have not been able to reproduce the results.

Apart from these there are quite a few essential differences between the two experiments.

The main difference between the observations of Okutsu and Nakamura (1979) and ours is in the shape and the width of the initial perturbation. While in the former case, the initial perturbation is close to a single sinusoidal pulse of widths $\lesssim 100\,\lambda_D$, the initial perturbation in our experiment, is better approximated by $\mathrm{Sech}^2(\xi/\lambda_D)$, with a typical width $\approx 10\,\lambda_D$. The rarefactive pulse in the present case, thus contains higher k-numbers and hence subjected to larger dispersive effects than broader pulse in the experiments of Okutsu and Nakamura (1979). It thus appears that the steepening of these narrow pulses at the trailing edge results in the generation of higher k-numbers, and higher order dispersive terms, neglected in deriving the KdV equation, may start becoming important. Further, as the potential associated with the density depletion is an attractive potential for ions, the ion distribution function taking into account the finite temperature effects, may be getting modified

within the wave. This could lead to trapping of ions in the wave troughs and hence lead to the observed results.

5.2 Numerical solution of the KdV (Korteweg-de-Vries) Equation

Since the weakly nonlinear ion acoustic waves are described by the KdV equation, we carried out a numerical solution of the KdV equation, as an initial value problem, to verify the experimental observations.

The KdV equation in a frame moving with the ion acoustic velocity C_s, is given as

$$\partial\phi/\partial\tau + \phi\cdot\partial\phi/\partial\xi_\eta + 1/2\ \partial^3\phi/\partial\xi_\eta^3 = 0 \qquad (5.1)$$

where ϕ is the normalised density or potential perturbation, and $\xi_\eta = \varepsilon^{1/2}(x-t)$ and $\tau = \varepsilon^{3/2}t$ are the stretched coordinates. In this equation, the convective term $\phi\cdot\partial\phi/\partial\xi_\eta$ describes the nonlinearity and the third derivative term $1/2\ \partial^3\phi/\partial\xi_\eta^3$ reflects dispersion.

The numerical technique deployed to solve the above equation is a hybrid method, where time integration is done using the partially corrected Adams-Bashforth scheme (Gazdag 1976), and the space operator is split up

into a linear and nonlinear part (Tappert 1974). The space integration is mainly carried out in the Fourier space, but the nonlinear terms are computed by getting back into the real space representation. To prevent aliasing, when computing the nonlinear term, only the n/2 lowest Fourier modes are retained, where n is the number of grid points in the space coordinates. The accuracy of the integration is gauged by keeping a check on how well the constants of motion are conserved.

5.2.1 The Algorithm

The KdV equation defined in Eqn. (5.1) may in general be written as

$$\partial\phi/\partial\tau + \beta\phi\cdot\partial\phi/\partial\xi + \delta^2\partial^3\phi/\partial\xi^3 = 0 \qquad (5.2)$$

where τ is the time variable and ξ is a suitably constructed space variable. β and δ are constant coefficients (e.g. $\beta = 1$ and $\delta^2 = 1/2$ for ion acoustic waves in plasmas). Eqn. (5.2) is invariant under the scaling transformation

$$\xi \to \lambda\xi \;;\; \tau \to \lambda^3\xi \text{ and } \phi \to \lambda^{-2}\phi \qquad (5.3)$$

This invariance is useful for example, to normalise the scale length λ in the ξ direction to unity. There is an alternate scaling given by Berezin and

Karpman (1966) which can convert all initial conditions to an unit amplitude, unit width type of initial condition. To see this let us consider a class of initial conditions of the form

$$\phi(\xi, 0) = \phi_0 f(\xi, L) \tag{5.4}$$

where ϕ_0 is the initial amplitude, L is the width and $f(\xi, L)$ is the functional form of the initial pulse (viz. a square pulse; a half sine pulse, seeant hyperbolic pulse etc.). The following new set of variables

$$\tilde{\xi} = \xi/L \; ; \; \tilde{\tau} = \phi_0 \frac{\tau}{L} \text{ and } \tilde{\phi} = \phi/\phi_0 \tag{5.5}$$

changes the KdV equation (5.2) to

$$\partial\tilde{\phi}/\partial\tau + \beta\tilde{\phi}\frac{\partial\tilde{\phi}}{\partial\xi} + \frac{\sigma^2}{\sigma^2}\partial^3\phi/\partial\xi^3 = 0 \tag{5.6}$$

where $\sigma^2 = \phi_0 L^2$

Under the given transformation, all initial conditions are transformed to the same initial condition i.e. unit amplitude, unit width functions. Initial conditions with same numerical value evolve identically in the scaled coordinate system, though differently in the laboratory system. This scaling applies for all times and not merely in the asymptotic region. With the use of appropriate scaling parameter, the initial condition

can be simply described by the functional form of unit width and the behaviour in the laboratory coordinates can be recovered by multiplying the space, time and amplitude in the scaled coordinate by the scaling parameters given below :

Scaling parameter for amplitude	=	ϕ_o
Scaling parameter for time	=	L/ϕ_o
Scaling parameter for space	=	L

In case, the calculations are to be carried out without this scaling, the scaling parameter δ may be set equal to unity and the initial condition may be specified by its constant amplitude and width.

Fourier transforming Eqn. (5.2) gives us

$$\partial\Phi_k/\partial\tau - ik^3\delta^2\Phi_k + ik\langle\phi^2\beta/2\rangle_k = 0 \qquad (5.7)$$

where

$$\Phi_k = \int_{-\infty}^{\infty} \phi(\xi,\tau)\exp(-ik\xi)\,d\xi \qquad (5.8)$$

is the k_{th} Fourier component of $\phi(\xi,\tau)$ and

$$\langle\phi^2\beta/2\rangle_k = \beta/2\int_{-\infty}^{\infty}\phi^2(\xi,\tau)\exp(-ik\xi)\,d\xi \qquad (5.9)$$

is the k_{th} component of the nonlinear term. Eqn. (5.6) consists of a linear part

$$\partial \phi_k / \partial \tau - i k^3 \delta^2 \phi_k \tag{5.10}$$

and a nonlinear part

$$-ik \langle \beta \cdot \phi^2 / 2 \rangle_k \tag{5.11}$$

which can be treated as a source term. Thus we can treat the linear part exactly by writing

$$\phi_k(\tau) = \bar{\phi}_k(\tau) \exp(i \Omega \tau) \tag{5.12}$$

where $\Omega = k^3 \delta^2$

From Eqn. (5.10) we get by Taylor's expansion

$$\phi_k(\tau+\Delta\tau) = \left[\bar{\phi}_k(\tau) + \frac{\partial \bar{\phi}_k}{\partial \tau} \Delta\tau + \frac{1}{2} \frac{\partial^2 \phi_k}{\partial \tau^2} \Delta\tau^2 + \cdots \right] \exp\left[i \Omega (\tau+\Delta\tau) \right] \tag{5.13}$$

The derivatives can be evaluated from the equation for $\bar{\phi}_k(\tau)$ which can be obtained by substituting Eqn. (5.12) in Eqn. (5.7) to be

$$\partial \bar{\phi}_k / \partial \tau = -ik S_k(\tau) \exp(-i \Omega \tau) \tag{5.14}$$

where $S_k(\tau) = \langle \phi^2 \beta / 2 \rangle_k$ If $\Delta\tau$ is chosen such that $S_k(\tau)$ does not vary significantly in this interval then Eqn. (5.14) can be integrated to yield

$$\bar{\phi}_k(\tau+\Delta\tau) = \bar{\phi}_k(\tau) + \frac{k}{\Omega} S_k(\tau) \left[\exp(-i \Omega \Delta\tau) - 1 \right] \cdot \exp\left[-i \Omega \Delta\tau \right] \tag{5.15}$$

Hence the second term of Eqn. (5.13) may be written as

$$\partial \bar{\phi}_k/\partial\tau\Big|_\tau \exp(i\Omega\Delta\tau)\cdot\Delta\tau = \left[\bar{\phi}_k(\tau+\Delta\tau) - \bar{\phi}_k(\tau)\right]\cdot \exp(i\Omega\Delta\tau)$$

$$= \frac{k}{\Omega}\left[1-\exp(i\Omega\Delta\tau)\right] S_k(\tau)\exp(-i\Omega\Delta\tau) \quad (5.16)$$

Similarly, the higher order derivatives can be evaluated by using the equation (5.15). It is to be noted that the nonlinear term $S_k(\tau)$ is a convolution term and hence it is convenient to first go back into real space, construct the nonlinear term and then take its Fourier transform. To prevent aliasing errors only the n/2 lowest Fourier modes are retained. The solution to Eqn. (5.7) can then be obtained in terms of the Taylor series of Eqn. (5.13), by truncating the series at an appropriate term. An increase Fourier transform then yields the solution of the KdV equation. The method involves single step time differencing scheme.

It has however been shown (Gazdag, 1973) that this method of using truncated Taylor series is unstable if the truncation is effected by neglecting time derivatives higher than the first $\partial\bar{\phi}_k/\partial\tau$ and second $\partial^2\bar{\phi}_k/\partial\tau^2$; however it is stable if the truncation is done by neglecting derivatives of order higher than $\partial^3\bar{\phi}_k/\partial\tau^3$ and $\partial^4\bar{\phi}_k/\partial\tau^4$. Thus, for stable calculations it would

be necessary to calculate second and third time derivatives at each step, which may become rather involved.

In order to avoid this difficulty, following Gazdag (1976), we have used a two-step time differencing scheme, which yields stable accurate solutions, with the evalution of only the first time derivatives. The scheme consists of (1) a predictor step, followed by (2) a corrector step.

For this purpose we write Eqn. (5.16) as

$$\left.\frac{\partial \bar{\phi}_{lk}}{\partial \tau}\right|_{\tau} \exp(i\Omega\Delta\tau)\cdot\Delta\tau = G_{lk}(\tau)$$

$$= \frac{lk}{\Omega}\left[1-\exp(i\Omega\Delta\tau)\right]\cdot S_{lk}(\tau)\cdot\exp(-i\Omega\Delta\tau) \qquad (5.17)$$

Then if the results obtained from the predictor step are denoted by super-script p, then the predictor step according to partially corrected second order Adams-Bashforth scheme (Gazdag, 1976) is given by

$$\phi^{p}_{lk}(\tau+\Delta\tau) = \bar{\phi}_{lk}(\tau)\exp(i\Omega\Delta\tau) + \left(3G^{p}_{lk}(\tau) - G^{p}_{k}(\tau-\Delta\tau)\right)/2 \qquad (5.18)$$

and the corrector step

$$\bar{\phi}_{k}(\tau+\Delta\tau) = \bar{\phi}_{lk}(\tau)\exp(i\Omega\Delta\tau) + \left(G^{p}_{k}(\tau) + G^{p}_{lk}(\tau+\Delta\tau)\right)/2 \qquad (5.19)$$

Eqs. (5.18) and (5.19) correspond to Eqs. (5.12)

and (5.13) of Gazdag (1976) respectively. In the first time step the predictor is calculated according to the equation

$$\bar{\Phi}_{|k}^{p}(\tau+\Delta\tau) = \bar{\phi}_{|k}(\tau)\exp(i\Omega\Delta\tau) + G_{|k}(\tau) \tag{5.20}$$

and for subsequent time steps Eqs. (5.18) and (5.19) are used to obtain predicted and corrected values for $\bar{\phi}_k$. Inverse transform according to the equation

$$\phi(\tau+\Delta\tau,\xi) = \frac{1}{\sqrt{2\pi}} Re \int_{-\infty}^{\infty} \bar{\phi}_{|k}(\tau+\Delta\tau)\exp\left[i(-\Omega\tau+k\xi)\right] dk \tag{5.21}$$

then yields the solution of KdV equation at a given time step $(\tau + \Delta\tau)$.

To check the accuracy of the integration, the conservation of the following invariant quantities are monitored

$$I_1 = \int_{-\infty}^{\infty} \phi(\xi,\tau)\, d\xi \tag{5.22}$$

$$I_2 = \int_{-\infty}^{\infty} \phi^2(\xi,\tau)\, d\xi \tag{5.23}$$

$$I_3 = \int_{-\infty}^{\infty} \left[\phi^3(\xi,\tau)/3 - \left(\partial\phi/\partial\xi\right)^2\right] d\xi \tag{5.24}$$

These constants are evaluated using FFT routine. These constants are conserved to better than 1 part in 10^6 and are sensitive to the time step used. The time

step should be chosen to satisfy $\pi^2 \delta^2 k^3 \max \Delta\tau \lesssim 1$ (Abe and Inuoue, 1980).

5.3 Numerical Results and discussion

We solved the KdV equation for compressive pulses and rarefactive pulses, keeping the amplitude ($\delta n/n$) constant at 10%, and varying the widths. The shape of the initial pulse in all these cases, was taken to be $\mathrm{Sech}^2 (\xi/\xi_0)$. The amplitude was positive for compressive pulses and negative for rarefactive pulses.

Fig. 5.9 illustrates the results of the KdV equation for an initial compressive pulses of a width of $\sqrt{60}$. This pulse being an almost exact solution of a soliton is found to maintain its shape and width for long times. It travels to the right at a velocity of about 1.04 C_s. Fig. 5.10 shows the evolution of an initial pulse of width $\approx \sqrt{30}$. This also propagates to the right at a velocity of 1.03 C_s. But this solution not being an exact soliton solution does not maintain its shape in the process of its propagation. Since nonlinearity and dispersion are not exactly balanced, the wave suffers a distortion. A nonlinear steepening is observed at the negative slope of the perturbation and as it propagates, the amplitude reduces, by generating

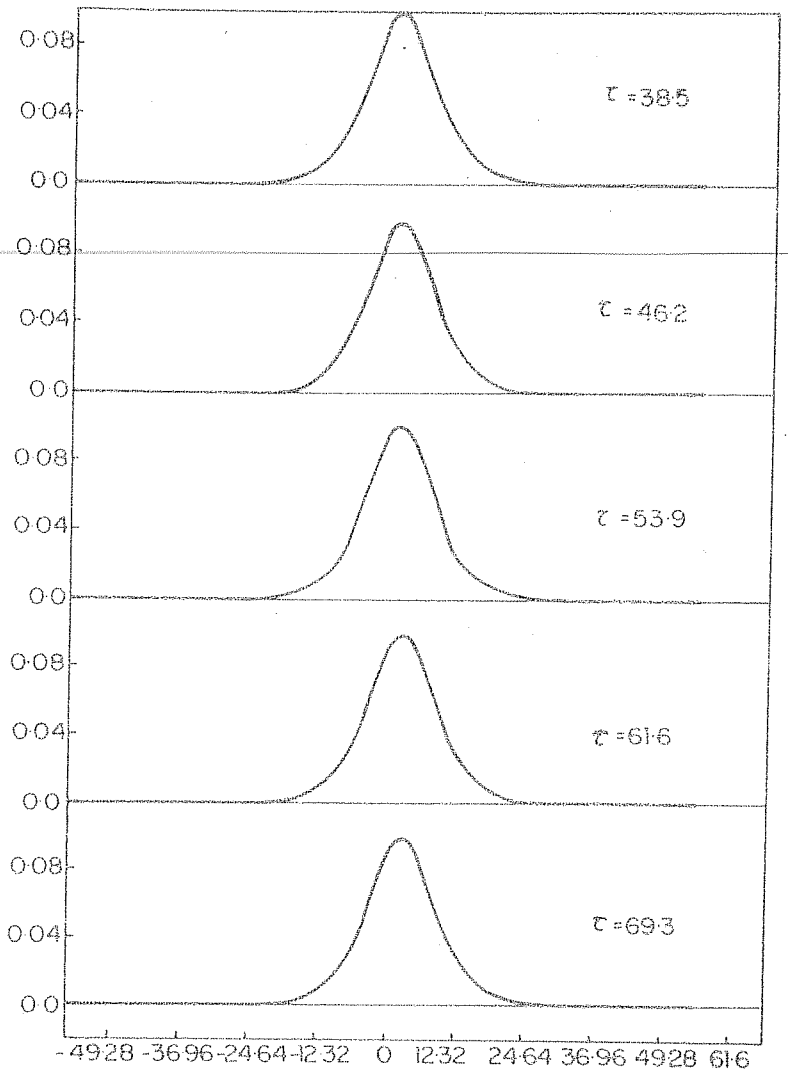

Figure 5.9.a Time evolution of the compressive pulse according to the calculations based on the KdV equation. The vertical axis represents the amplitude ($\delta n/n_o$) and horozontal axis represents the distances normalised to the Debye length. The figures on the right represent the time normalised to ω_{pi}. The initial amplitude and width of the pulse are 10% and 60 λ_D respectively.

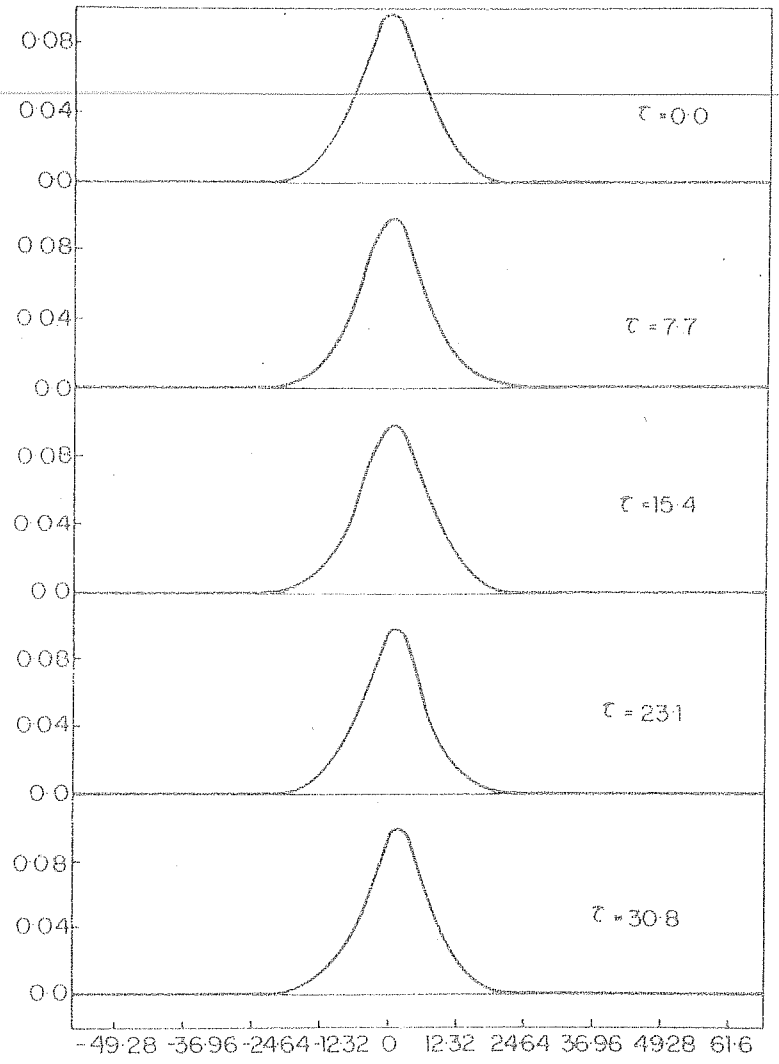

Figure 5.9.b Further propagation of the compressive pulse shown in fig. 5.9.a.

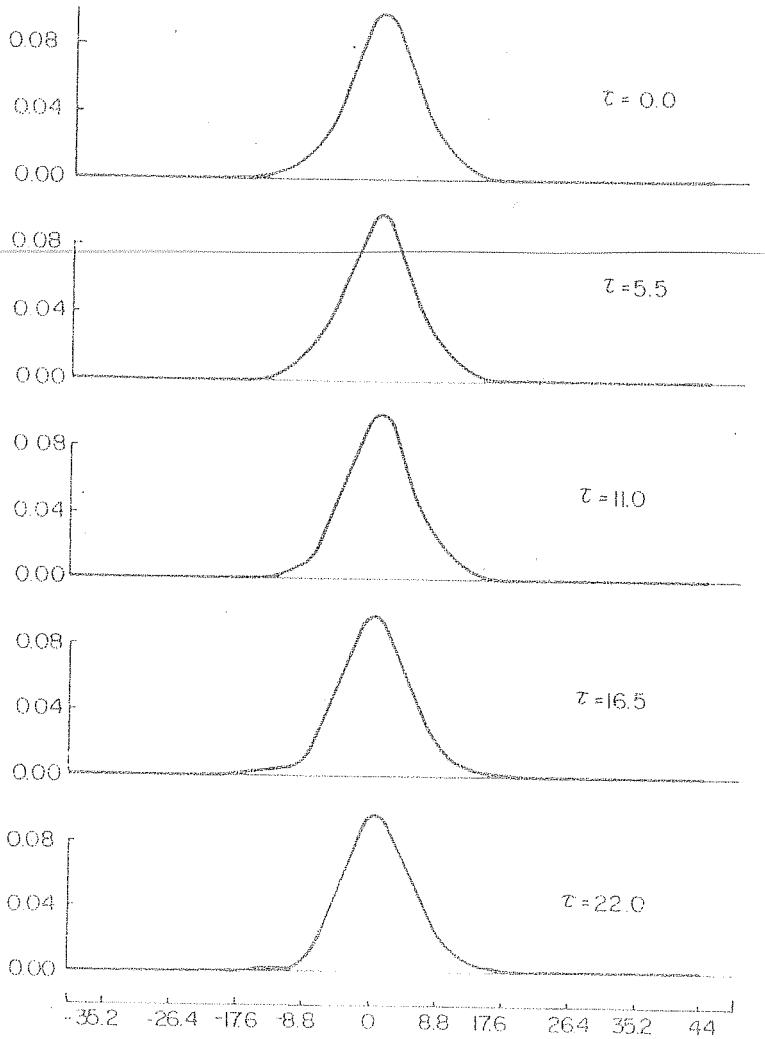

Figure 5.10.a Time evolution of the compressive pulse of amplitude 10%, and width of $30\lambda_D$. The wave exhibits a nonlinear steepening and damping by generating and ion acoustic wavetrain.

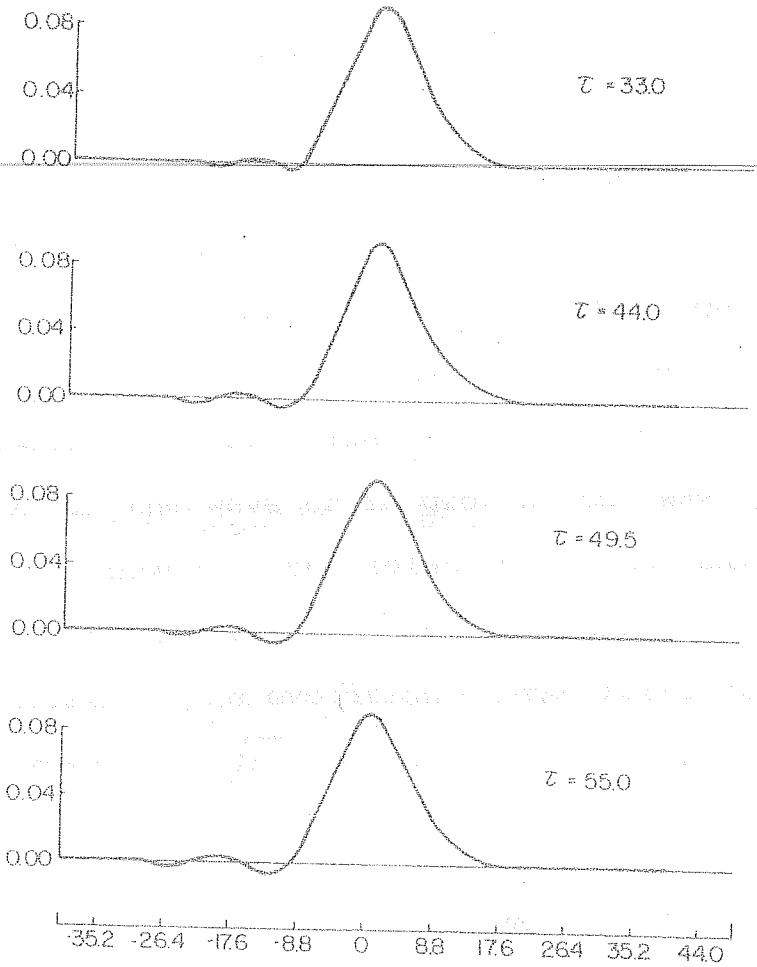

Figure 5.10.b Further propagation of the compressive pulse shown in fig. 5.10.a.

an ion acoustic wave train.

The evolution of a rarefactive wave for an initial amplitude of $(\delta n/n_o) \approx$ 10% and width $\approx \sqrt{60}$ is shown in fig. 5.11. These pulses propagate to the left in the ion acoustic frame, implying a speed less than ion acoustic speed in the laboratory frame. The velocity observed in this case is about 0.9 C_s. Further while the leading edge gets stretched, the trailing edge steepens and a wavetrain is generated at this edge. The number of peaks in the wave train grow as the wave propagates further. However, the solutions do not exhibit the experimental observation of the fissioning of the wave at the minimum. The evolution of the rarefaction for smaller width $\approx \sqrt{30}$ is shown in fig. 5.12 which is almost similar to that observed in fig. 5.11.

From the above results, it is apparent that the KdV equation given by Eqn. (5.1) alone, exhibits only some of the experimental observations, but does not predict the results such as the fissioning of the wave at the minimum since the rarefactive wave launched in this experiment is very narrow, it may be subjected to larger dispersion, due to the generation of higher order k-numbers.

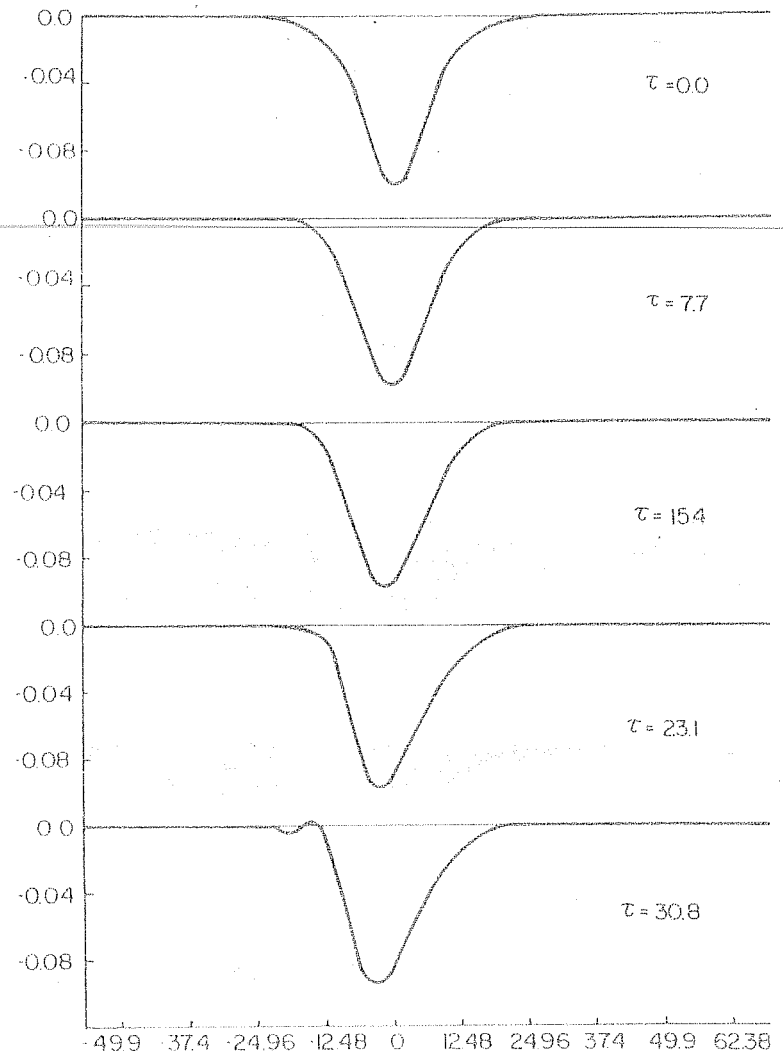

Figure 5.11.a Time evolution of the rarefactive pulse according to the calculation based on the KdV equation. The initial amplitude and width of the pulse are 10% and 60 λ_D respectively. The wave steepens on the negative slope edge and damps by generating an ion acoustic wave train.

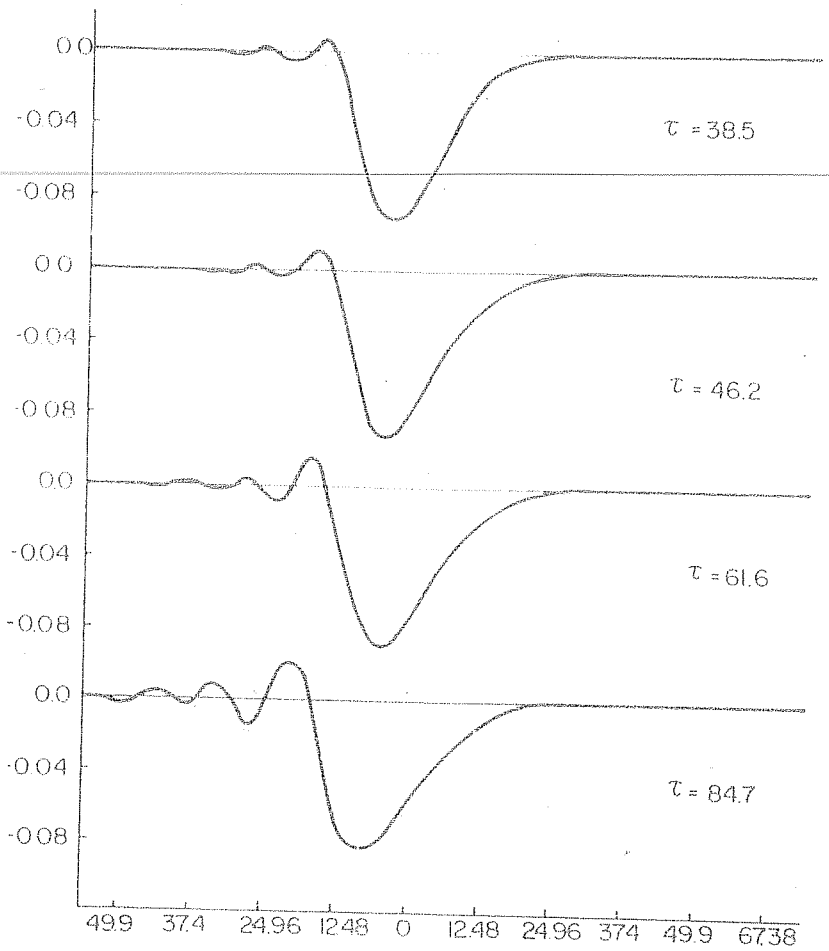

Figure 5.11.b Further propagation of the rarefactive pulse shown in fig. 5.11.a.

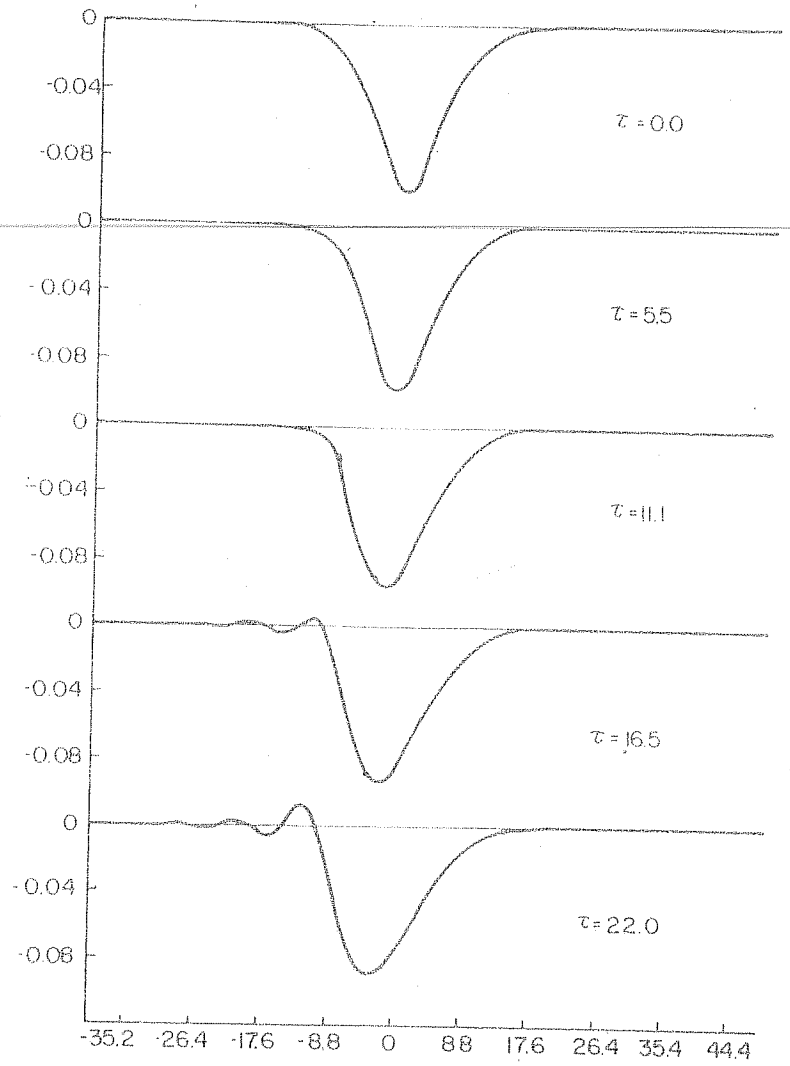

Figure 5.12.a The evolution of the rarefactive pulse similar to fig. 5.11 but a reduced width of $30\lambda_D$. It exhibits similar phenomena as that shown in fig. 5.11.

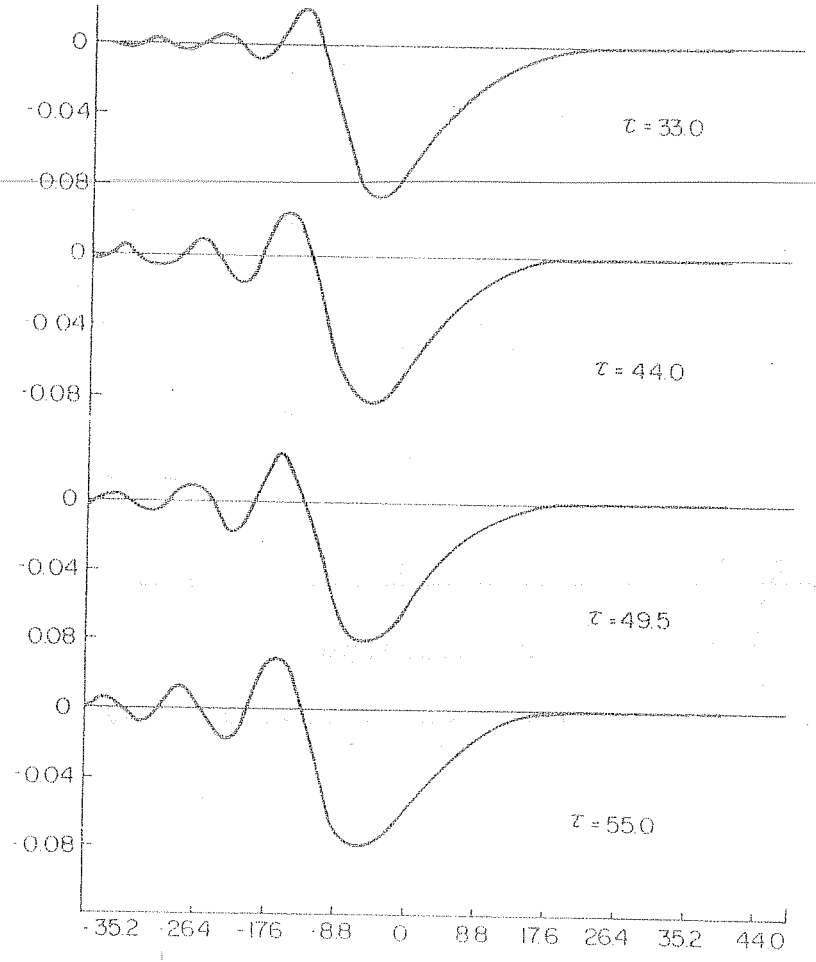

Figure 5.12.b Further propagation of the rarefactive pulse shown in fig. 5.12.a.

Taking into account the higher order nonlinearities and dispersion, Ichikawa et al. (1976, 1977) obtained a coupled set of the first order KdV equation and the linear inhomogeneous equation for the second order perturbed quantity. The steady state solution of the coupled set of equations gives rise to a Dressed soliton, of which the stable core is determined as a soliton solution of the KdV equation and the clouds surrounding the core is determined as a solution of the second order equation.

5.3.1 Effect of higher order nonlinarity and dispersion

The coupled set of equations for the first order potential $\phi^{(1)}$ and the second order potential $\phi^{(2)}$ are given by

$$\partial/\partial\tau\,\phi^{(1)} + \frac{1}{2}\,\partial^3\phi^{(1)}/\partial\xi_1^3 + \phi^{(1)}\,\partial/\partial\xi_1\,\phi^{(1)} = 0 \tag{5.25}$$

$$\partial/\partial\tau\,\phi^{(2)} + \frac{1}{2}\,\partial^3/\partial\xi_1^3\,\phi^{(2)} + \partial/\partial\xi_1\left(\phi^{(1)}\phi^{(2)}\right) = S\left(\phi^{(1)}\right) \tag{5.26}$$

where $$S\left(\phi^{(1)}\right) = -\frac{3}{8}\,\partial^5/\partial\xi_1^5\,\phi^{(1)} + \frac{1}{2}\,\phi^{(1)}\,\partial^3/\partial\xi_1^3\,\phi^{(1)} - \frac{5}{8}\,\frac{\partial}{\partial\xi_1}\left(\partial/\partial\xi_1\,\phi^{(1)}\right)^2 \tag{5.27}$$

The KdV equation (5.25) possesses an infinite number of conservation laws, thus ensuring the existence of an arbitrary number of stable solitons, while the

linear-inhomogeneous equation for $\phi^{(2)}$ describes the hebaviour of the second order potential affected by the nonlinear interaction of the wave $\phi^{(1)}$. The second order potential is also influenced by the distortion of the nonlinear wave $\phi^{(1)}$.

The steady state solutions of the coupled set of equations (5.25) and (5.26) are given by

$$\phi^{(1)}(\eta) = 3\lambda \, \mathrm{Sech}^2(D\eta) \tag{5.28}$$

$$\phi^{(2)}(\eta) = 9/4 \, \lambda^2 \, \mathrm{Sech}^2(D\eta) \left\{ 2D\eta \tanh(D\eta) - 1 + 7 \, \mathrm{Sech}^2(D\eta) \right\} \tag{5.29}$$

with

$$D = (\lambda/2)^{1/2} \tag{5.30}$$

$$\eta = \xi - \lambda t - \delta \tag{5.31}$$

Here δ, defines the initial position of the soliton, and determines the amplitude and velocity of the soliton. The perturbed potential calculated upto the second order is given by

$$\phi(\eta) = \phi^{(1)}(\eta) + \phi^{(2)}(\eta) \tag{5.32}$$

We carried out a numerical solution of Eqns. (5.28) and (5.29), by the technique similar to that explained in section 5.4, for both compressive and rarefactive pulses as an

initial value problem.

Fig.5.13a shows the results obtained in case of an exact soliton solution (eqs. 5.28-5.31). It is observed that the steady state clouds of Eqn. (5.27) moves stably with the KdV soliton, confirming the reliability of our numerical technique.

Fig.5.13b exhibits the temporal evolution of the soliton solution $\phi^{(1)}(\xi)$ with an initial condition

$$\phi^{(2)}(\xi, 0) = 0 \qquad (5.33)$$

When the KdV equation travels to the right, the second order clouds (shown by dotted lines) start to develop themselves around the soliton core.

The evolution of a rarefactive wave with these second order corrections is shown in fig. 5.14. It is observed that the inclusion of higher order effects has also not reproduced the experimental observation such as the fissioning of the wave. The rarefactive wave unlike the compressive pulses do not maintain the initial shape. They exhibit a nonlinear steepening, followed by a reduction in amplitude, by generation of ion acoustic wave train.

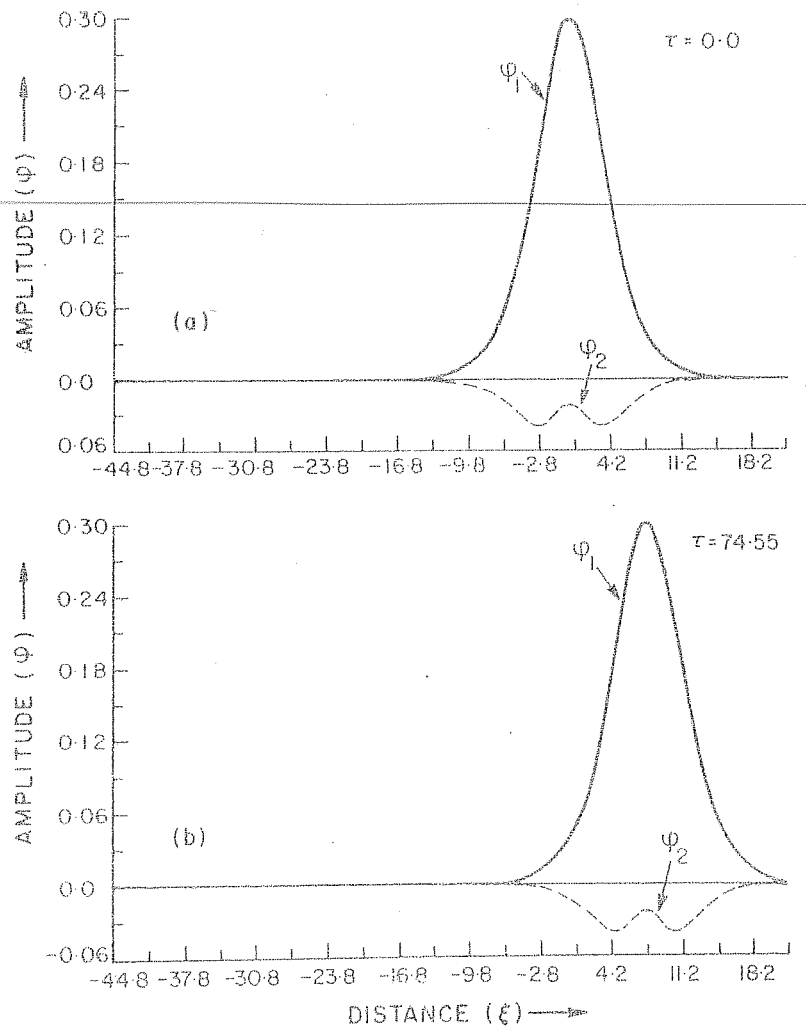

Figure 5.13.a Time evolution of the exact compressive soliton solution given by eq. 5.28, for the coupled set of KdV equations.

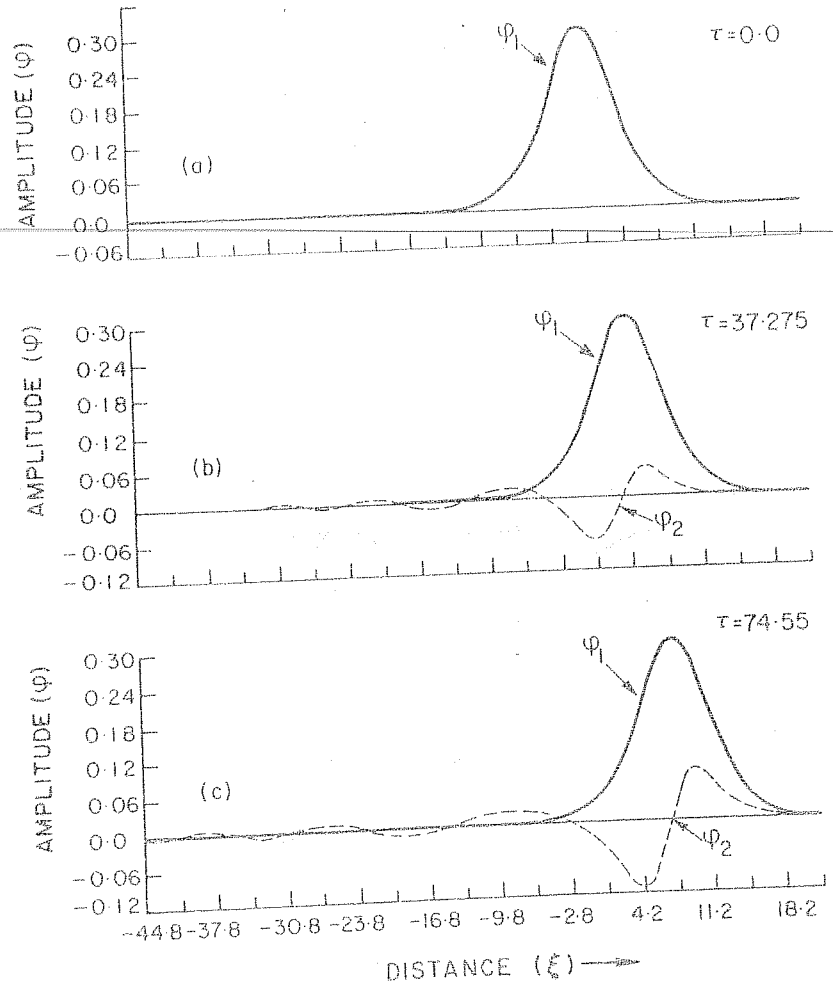

Figure 5.13.b Time evolution of the compressive soliton solution similar to fig. 5.13.a, but with condition

$$\phi^{(2)}(\xi, o) = o$$

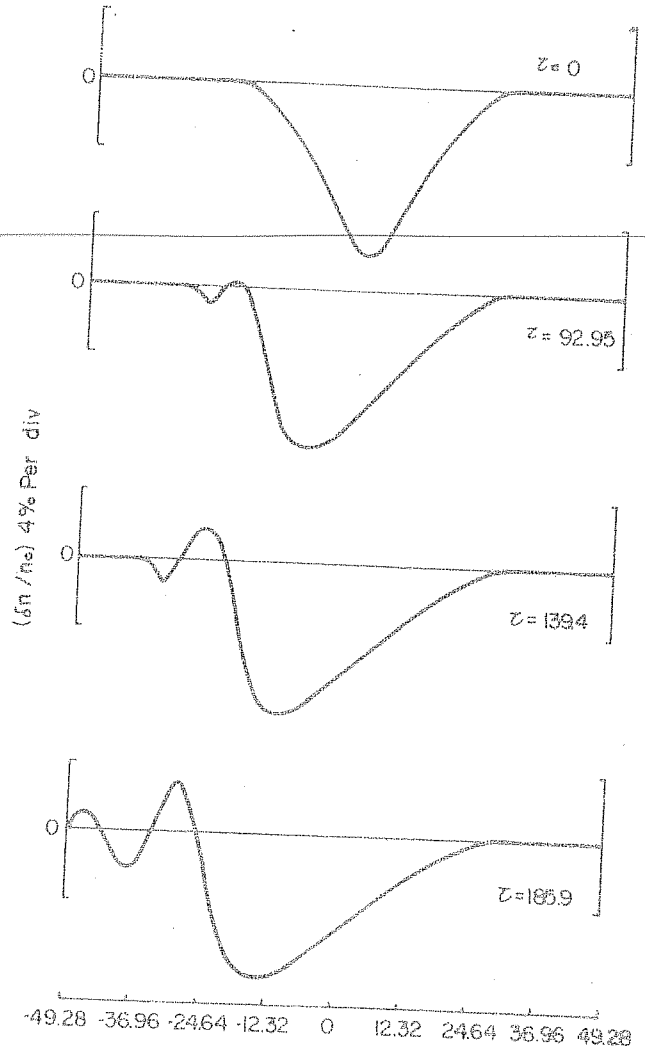

Figure 5.14 Time evolution of the rarefactive pulse based on the coupled set of KdV equations. The rarefactive pulse does not maintain its initial shape, but damps, by generating ion acoustic waves preceded by a nonlinear steepening.

Our experimental results do not show as many peaks in the wave train as expected on the basis of numerical calculation of the fluid equations. This is understandable in view of the fact that while a slow wave train is subjected to Landau damping in the actual experiment, the KdV equation does not account for this effect.

Since the potential associated with the density depletion is an attractive potential for ions, the ion distribution may be getting modified in the presence of the wave. It may be possible that in the process of launching the waves, a slug of ions travelling at ion acoustic velocity could be created, which is eventually trapped in the negative potential of the wave. These trapped ions probably lead to a localised density increase between the two density minima.

So it is clear that the wave particle interactions may be important to explain the experimental observations. In order to verify this we intend solving numerically, the nonlinear Vlasov-Poisson euqations for the ions, as a future work.

5.4 Evolution of an ion-acoustic double layer from an ion acoustic rarefaction instability

Of recent a widespread interest has been generated towards the formation of ion acoustic double layers, which originate from an ion acoustic instability. An electron current drawn through a plasma can cause a number of low-frequency instabilities that may give rise to anomalous resistivity, and thus limiting the current. Recent investigations, however have shown a different behaviour namely, the formation of a double layer.

Block (1972) and Carlquist (1972) proposed theoretical models to explain the formation of double layers in the ionosphere regions. In both these models a rarefaction in density in a localised region was found to evolve into a double layer. Block (1972) suggested that in a current carrying plasma, a rarefactive instability tended to grow, and finally evolve into a double layer. The condition that was required for this was that the drift velocity of current carrying electrons should be greater than the thermal velocity i.e.

$$m_e u_d^2 > k(T_e + T_i) \qquad (5.34)$$

It was also shown that under the same conditions compressive modes would be damped out.

Computer simulations by De Groot et al. (1977) revealed the formation of double layers preceded by a negative potential well. The double layers they had obtained had $e\Delta\phi/T_e < 4$ in a short system (length $\simeq 141\lambda_D$, where λ_D is the Debye length), when the electron drift velocity v_d against an ion background satisfied $v_d \geq v_e$, where v_e is the electron thermal velocity. Ion acoustic double layers were later obtained by Sato and Okuda (1980, 1981) in simulations with slower drift velocity ($v_d < v_e$) and a longer system ($L > 512\lambda_D$). The ion

acoustic double layers were small amplitude ($e\Delta\phi/T_e \ll 1$) and were found to evolve from a subsonic negative potential pulse propagating in the direction of the electron drift. The computer simulation of Okuda and Ashour - Abdalla (1982) revealed that weak double layers similar to those observed by Sato and Okuda (1980) could be obtained in systems of shorter lengths of $128\,\lambda_D$, in the presence of a continuous plasma source.

Hasegawa and Sato (1982) constructed a BGK solution of an ion acoustic double layer, from a negative potential well. They supposed a stationary negative potential spike to be formed in an electron stream. Then those streaming electrons whose kinetic energies are less than the peak potential energy can be reflected by the negative potential spike, thus leaving an electron void in the velocity space on the downstream side of the spike. With this electron void, the potential would swing to a positive value on the downstream side forming a double layer structure.

The ion density they had assumed in the presence of a negative potential well is given by

$$n_i = 2n_0/\sqrt{\pi}\; e^{-e\phi/kT_i} \int_{\sqrt{-e\phi/kT_i}}^{\infty} e^{-t^2}\,dt \quad \text{for } \phi \leq -\phi_0 \qquad (5.35)$$

$$n_i = n_0 e^{-e\phi/kT_i} \quad \text{for } \phi > -\phi_0 \qquad (5.36)$$

where ϕ_0 is the rms potential of ion fluctuations or something equivalent.

From the flux and energy conservations, the density of the beam electrons were obtained to be

$$n_b = n_1 \left(1 + \phi/\phi_s\right)^{1/2} \qquad (5.37)$$

The density of thermal electrons was assumed to be

$$n_e = n_2 \exp\left(e\phi/kT_e\right) \qquad (5.38)$$

With these density values for both electrons and ions, they obtained a BGK solution resembling a double layer with a negative potential on the low potential side.

Schamel (1982) constructed two types of double layers one symmetric monotonic double layer and the other an asymmetric ion hole double layer. The potential profiles and the phase space diagrams are explained in figs. 1.3 and 1.4 of Chapter 1. From this model, it was observed that in order to form an asymmetric double layer from a symmetric ion hole, two processes play a dominant role. The negative potentials created in a plasma would favour ion trapping and further due to electron reflection,

electron density balance on the two sides is disturbed and as a consequence, the symmetric ion hole evolves into an asymmetric ion hole double layer.

Though the Ion acoustic double layers had not been observed in laboratory plasmas, satellite observations (Temerin et al. 1982) revealed that coherent asymmetric double layer like structures with $e\triangle\phi/T_e < 1$ did exist in space plasmas. Based on these results, Hudson et al. (1983) and Lotko (1982) proposed theoretical models for such structures, as solutions of Vlasov-Poisson equations. They had also predicted that, while rarefactive modes would amplify in a current carrying plasma, compressive modes on the other hand would damp out.

There have been some laboratory experiments, wherein a negative potential well was observed following a double layer (Leung et al. 1980; Iizuka et al. 1982). But these experiments do not exactly resemble the theoretical models mentioned above. The experimental observation of Iizuka et al. (1982) is virtually similar to the expansion of a plasma from a high density region into a low density region.

However, very recently Chan et al. (1984) reported the observation of the first ion acoustic double layers

originating from an ion acoustic instability. In the following sections we present our experimental observations of the formation of a double layer from a rarefactive ion acoustic instability. Though similar in some respects to the observations of Chan et al. (1984), there are some striking differences which we shall discuss later.

5.4.1 Experimental set up and diagnostics

This experiment was performed in the modified double plasma machine, the schematic of which is shown in fig. 5.15. The details of plasma production in the source and target chambers are similar to those explained in section 4.1, of Chapter 4. A constant relative bias V_{S-T} was maintained between the source and the target, to inject a steady electron current into the target region. Above a critical relative ($V_d > V_{th}$), this configuration leads to the formation of strong ($e\phi/kT_e > 10$) monotonic double layers, in the target section. Hence, the steady bias was kept at a value below this critical value.

The diagnostics deployed for the density and potential measurements were a cold Langmuir probe and a hot emissive probe respectively. Simultaneous measurements of density and potential fluctuations was carried out at

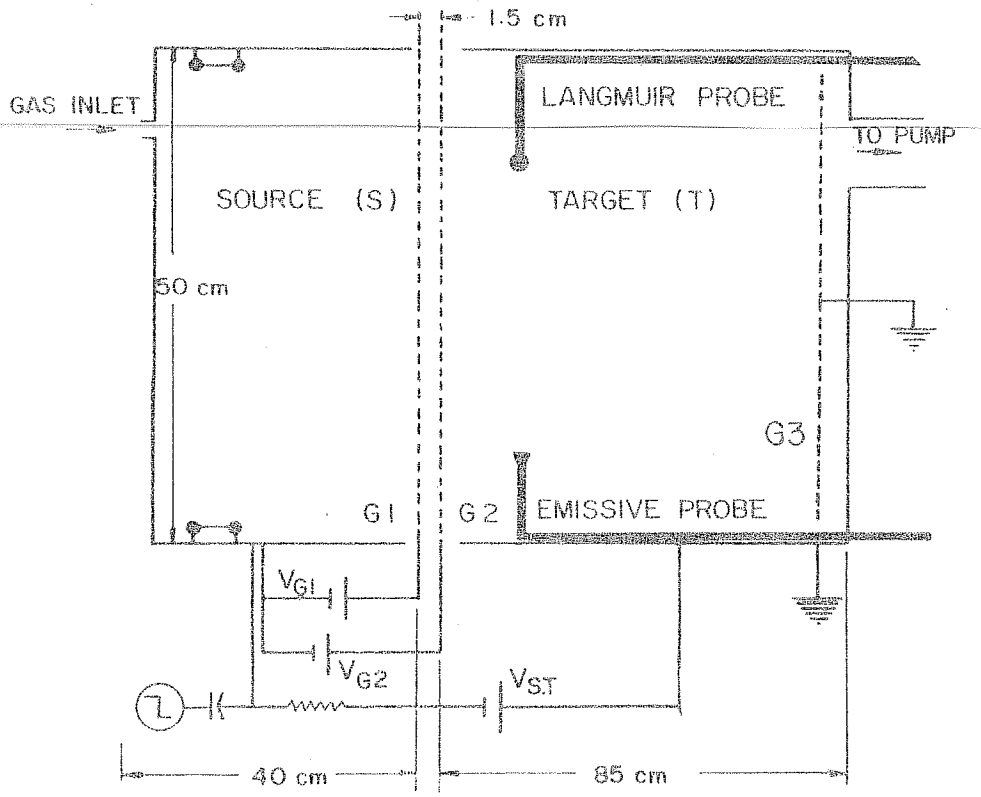

Figure 5.15 Schematic of the experimental setup used to obtain ion acoustic double layers. A negative pulse is superimposed on the steady relative bias potential.

various axial positions from the grid G2, by mounting them on the same shaft. The plasma parameters in the target region were $N_e \simeq 10^7$ cm^{-3}, $T_e \simeq$ 2eV, $T_i/T_e \leq \frac{1}{10}$, $\lambda_D \simeq 0.3$ cms and C_s (ion acoustic speed) $\simeq 2 \times 10^5$ cm/sec.

5.4.2 Experimental Results :

A steady relative bias between source and target (V_{S-T}) was maintained below the critical value above which strong monotonic double layers were formed. This bias resulted in a steady electron beam with $V_d < V_{th}$ entering from the source side into the target region. A step potential was superimposed on the applied relative bias at the source, which resulted in the modulation of the electron-beam density/velocity. As a result of this modulation, an ion acoustic fluctuation growing in space away from the grids was observed. Both the density and potential fluctuations were monitored simultaneously and a typical example of these at various spatial locations are shown in Fig. 5.16.

The profiles on the left correspond to fluctuations in electron saturation current, while those on the right are corresponding potential fluctuations monitored by the emissive probe. Close to the grids the potential exhibits a solitary negative pulse. Farther away from the

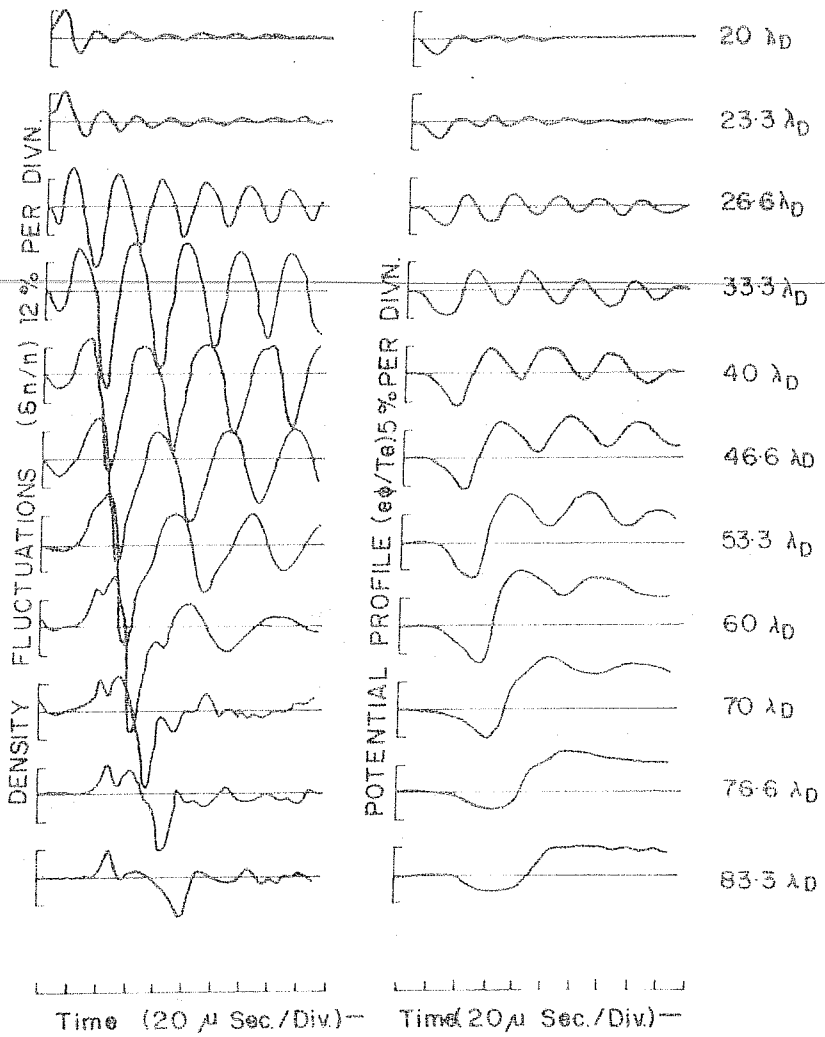

Figure 5.16 Typical example of the development of the ion acoustic rarefactive fluctuations into an asymmetric double layer on applying a negative potential pulse to the source.

a) density fluctuations corresponding to the potentials shown on the right.

b) Figures on the right indicate various spatial points away from grid G2.

grid ($\simeq 26\lambda_D$) ion acoustic fluctuations ($\simeq 30$ kH_z frequency) are observed, on the trailing edge of the leading negative pulse. At farther distances, the ion acoustic fluctiations grow in amplitude and this is accompanied by cascading down in frequency. The leading pulse still maintains the negative potential character and undergoes steepening at its trailing edge, developing into a shock like structure. At about $46\lambda_D$, following the shock formation, ion acoustic fluctuations are seen on the high potential side. These modes are observed to propagate at ion thermal velocities and damp out at farther distances. At about $76\lambda_D$ away from the grid G2, the fluctuations on the high potential side damp out, leaving behind an asymmetric potential structure, with a negative dip on the low potential side. This structure resembles an ion hole double layer. The negative potential dip is found to persist till the end of the system. The maximum amplitude, was $e\Delta\phi/kT_e \simeq 0.4$. The shapes of the potential and density profiles at a fixed location in the target region away from grid G2 is shown in fig. 5.17.

Density fluctuations close to the grids are similar to the fluctuations in the potential. At about $20.0\lambda_D$,

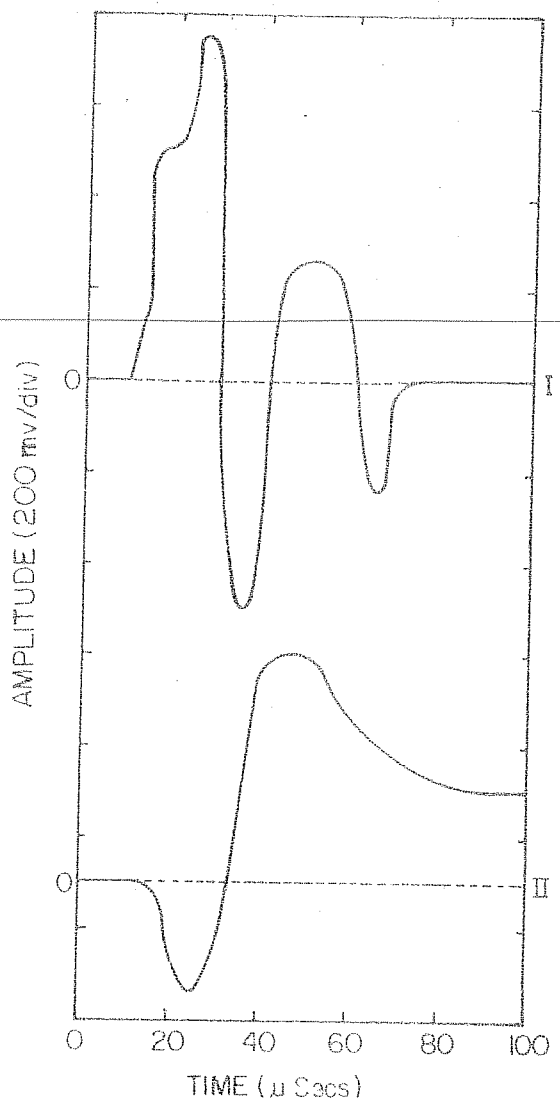

Figure 5.17 Maximum amplitude of the density and potential perturbations

Top Trace - Density perturbation ≈ 60 - 80%

Bottom Trace - Potential perturbation ≈ 40%.

small amplitude ion-acoustic fluctuations are seen. The fluctuations grow in amplitude accompanied by reduction in frequency. The fluctuations grow such that the density depletion are enhanced and density humps are reduced. A maximum amplitude ($\delta n/n_o$) of $\simeq$ 0.8 is obtained on the leading rarefactive part of density fluctuation at about $50\lambda_D$. The leading rarefactive pulse undergoes steepening at its trailing edge and at the point, where the potential assumes a shock like structure, a density hump is observed at the leading edge followed by a density depletion at the transition region, of the potential. High frequency fluctuations are seen in the density profiles beyond the density depletion as seen in fig. 5.18. The density hump is present at the negative transition of the potential and density depletion at the transition to high potential side of the double layer.

The time of flight plot for the leading potential dip is shown in fig. 5.19, and the corresponding plot for the leading density depletion is shown in fig. 5.20. The change of slope in fig. 5.20 indicates the slowing down of the wave to 1.3×10^5 cm/sec from an initial ion acoustic speed of 2×10^5 cm/sec. The fluctiations on the high potential side travel at much lower speeds and are

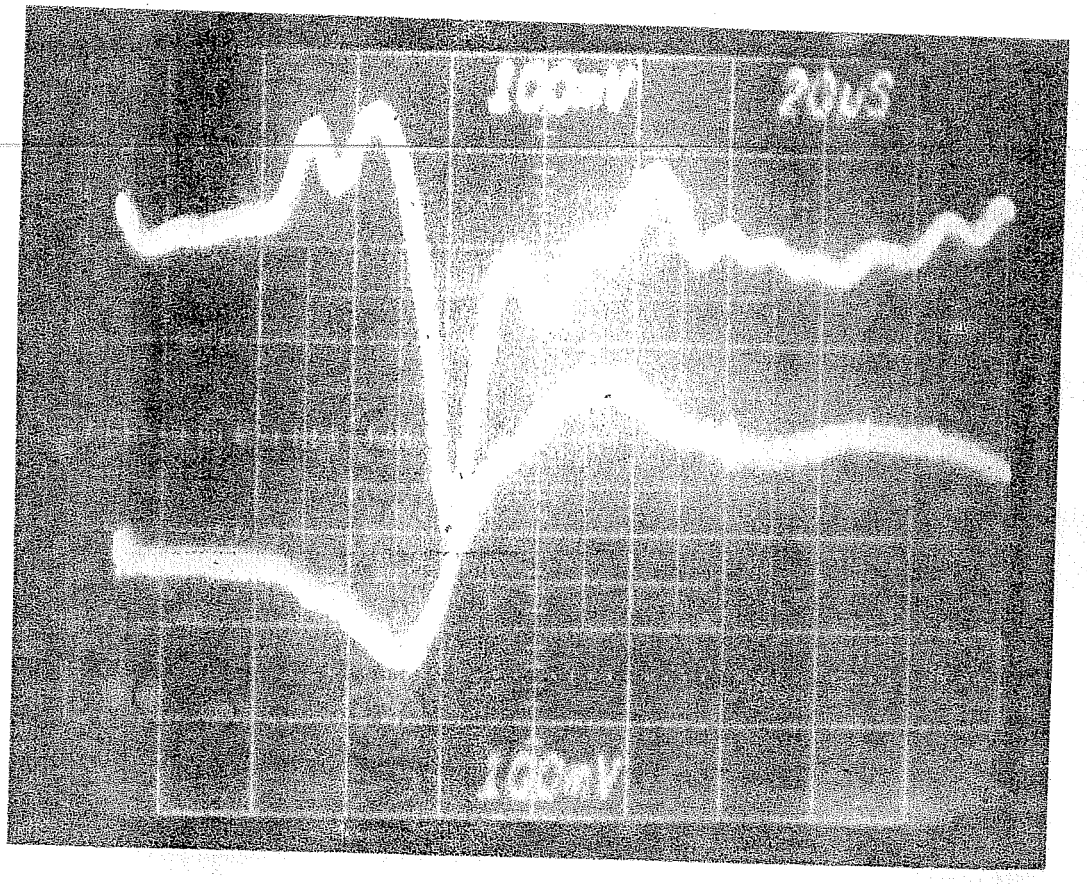

Figure 5.18 Oscilloscope trace of the high frequency fluctuation in the density profile, developed after the formation of the double layer.

Top Trace - Density perturbations

Bottom Trace - Potential profile of the asymmetric double layer.

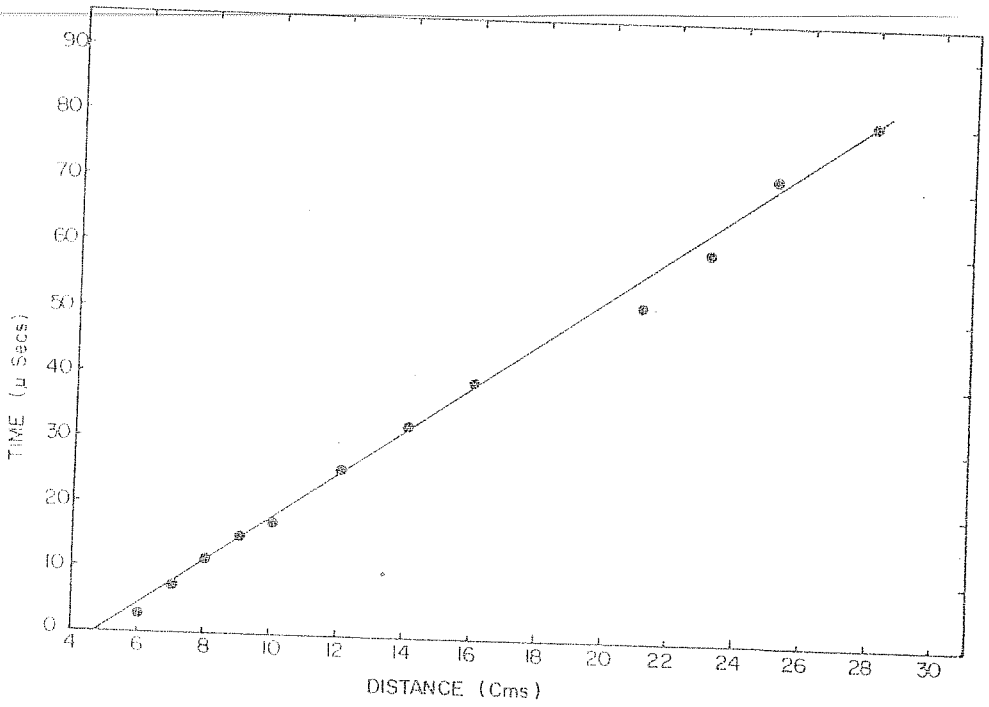

Figure 5.19 Time of flight versus axial position for the dominant negative potential well.

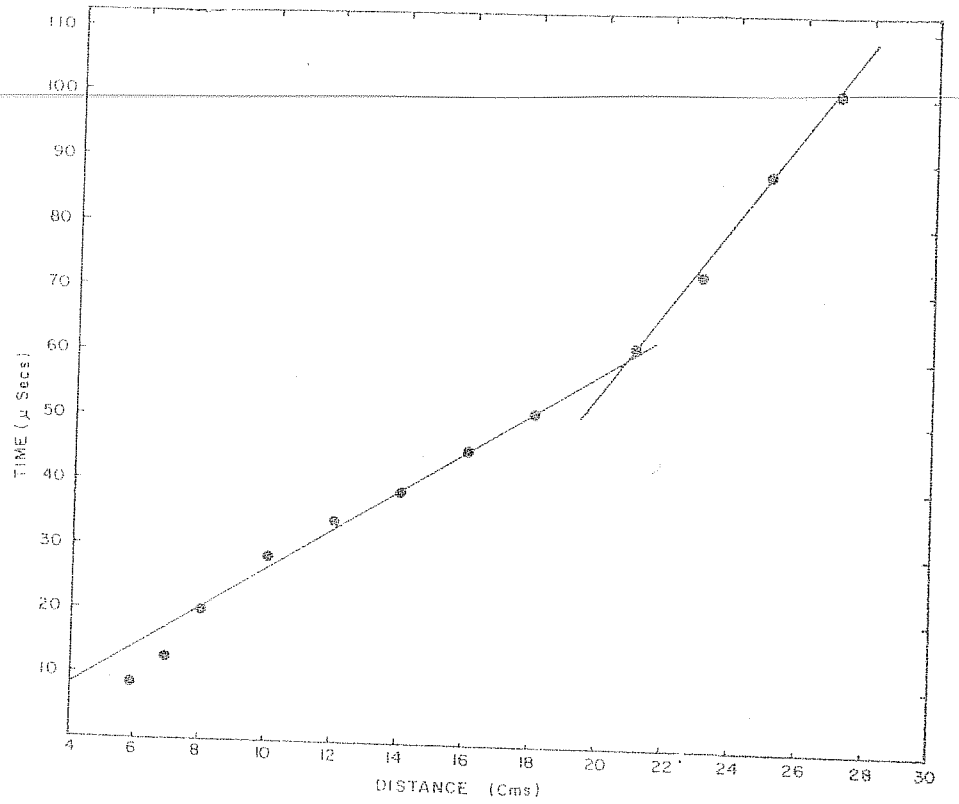

Figure 5.20 Time of flight versus axial position for the dominant rarefactive density perturbation. The change of slope indicates the slowing down of the wave after the double layer formation.

damped out. The leading density minimum travels initially with a velocity close to ion acoustic speed, but later slows down as the double layer like potential structure is formed. The widths of the double layer obtained in our case was found to be $\simeq 42\,\lambda_D$ and that of the associated potential dip on the low potential side to be $\simeq 20\lambda_D$. The amplitude of the potential drop of the double layer was about $\simeq$20%.

Similar results were obtained when a positive step potential was superimposed on the relative bias potential applied to the source as shown in fig. 5.21. There are a few minor differences observed in this case like a compressive wave is observed in the density profiles, very close to the grid and at about 6 cms away from G2 a rarefactive wave separates out from the compressive pulse. At farther distances, the compressive wave damps out leaving behind only the prominent density depletion associated with the transition of the potential profile.

5.4.3 Discussion

The results presented above indicate that modulation of electron beam density/velocity leads to ion acoustic fluctuations which grow in the direction of the electron drift. The rarefactive waves undergo preferen-

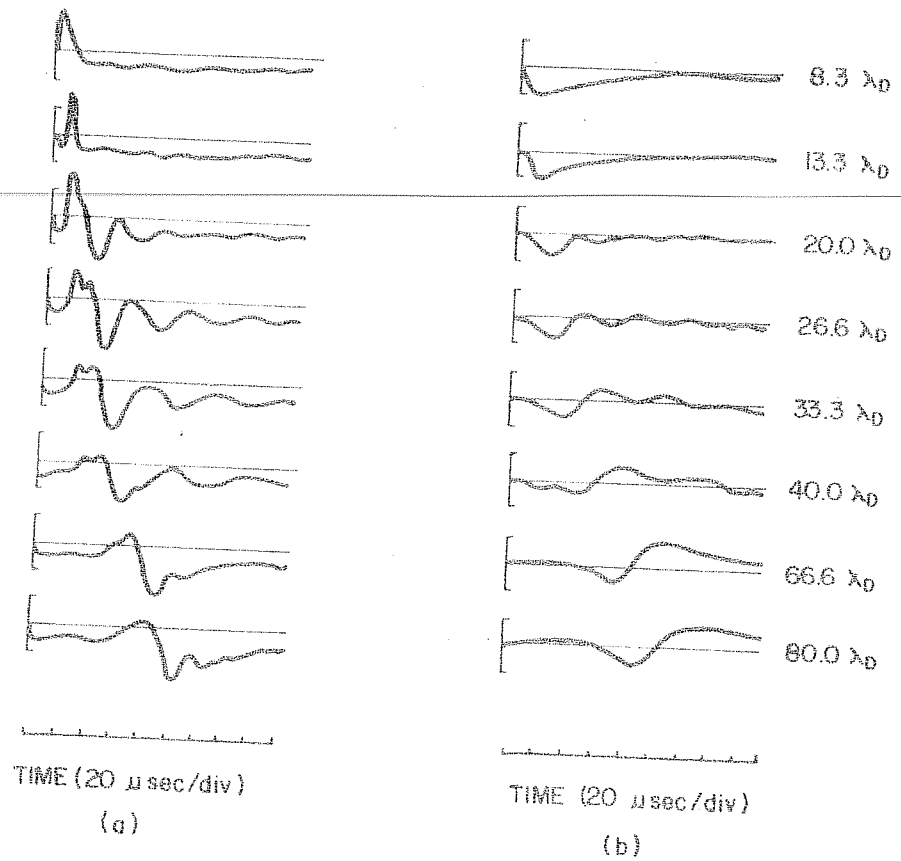

Figure 5.21 Typical example of the development of ion acoustic double layer, by modulation of the electron beam density/velocity with a positive potential pulse applied to the source.

a) density fluctuations corresponding to the potentials shown on the right.

b) Figures on the right indicate various spatial points away from grid G2.

tial amplification and the associated potential evolves into an asymmetric ion-acoustic double layer with a negative potential dip on the low potential side. The observations are very similar to the scenario envisaged in numerical simulations and analytical treatments (Sato and Okuda, 1980, 1981; Hudson et al., 1983; Kindel et al. 1981; Nishihara et al. 1982; Hasegawa and Sato, 1982; Schamel, 1982). According to this scenario the growth of the ion hole was triggered by current driven ion-acoustic fluctuations, leading to the formation of non-linear coherent state. The negative (rarefactive) potential pulse propagated initially at ion-acoustic speed and subsequently grew by exchange of energy with drifting electrons. The propagating velocity finally decreased to almost zero. Two processes appeared to play important role in the evolution of the asymmetric ion-hole viz. partial reflection of streaming electrons and trapping of ions in the negative potential well.

In our experiment we see that the perturbation triggered by beam modulation is driven strongly by the electron beam leading to growing ion-acoustic fluctuation travelling along the direction of electron drift. The fluctuations attain a level of 20 to 40% and are of

sufficient amplitude to trap the ions locally. The trapping velocity is found to be $\simeq 10^5$ cm/sec., which is less but of the order of ion acoustic velocity. As a result of particle trapping, the waves grow at the cost of energy of the free streaming electrons. The consequence of the growth of these waves is that almost periodic nature of the wave gets modified. A prominent negative potential well is left behind and later partial reflection of streaming electrons causes different plasma states on either side of the double layer. The potential structure almost becomes stationary after the double layer formation. An important feature of our results is the existence of the negative potential dip till the end of the pulse.

Spatial plots for the potential and density fluctuations at different times, after the application of the pulse are shown in figs. 5.22 and 5.23 respectively. The figures illustrate clearly the formation of steady asymmetric ion acoustic double layer with an electron density hump associated with the negative potential dip and an electron density dip at the transition to high results.

Our results resemble the results obtained in

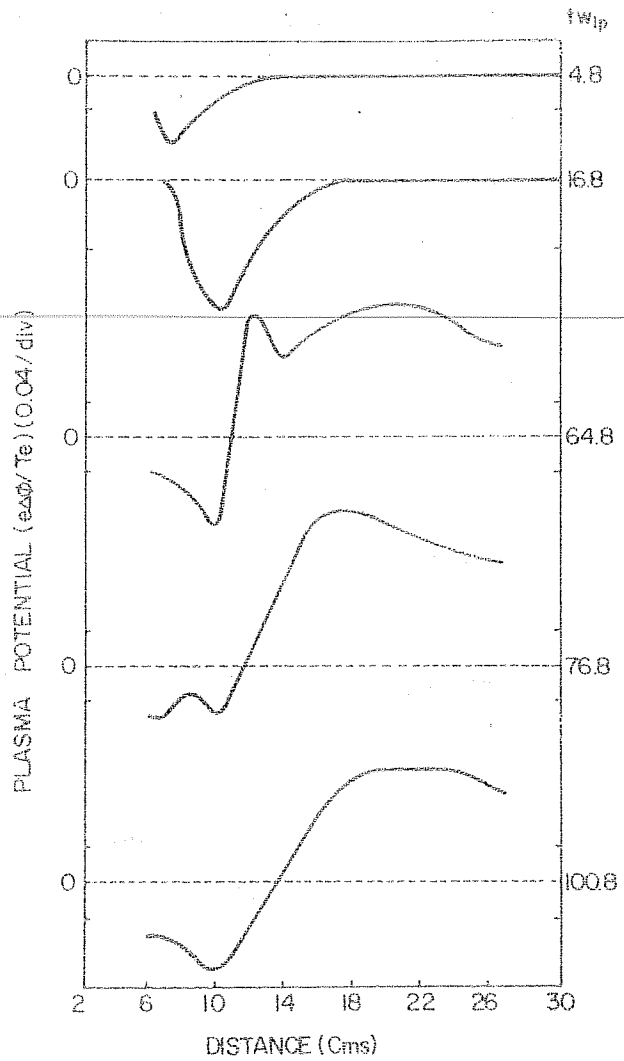

Figure 5.22 Spatial development of the ion acoustic double layer. The figures on the right indicate the different times normalised to ion plasma period.

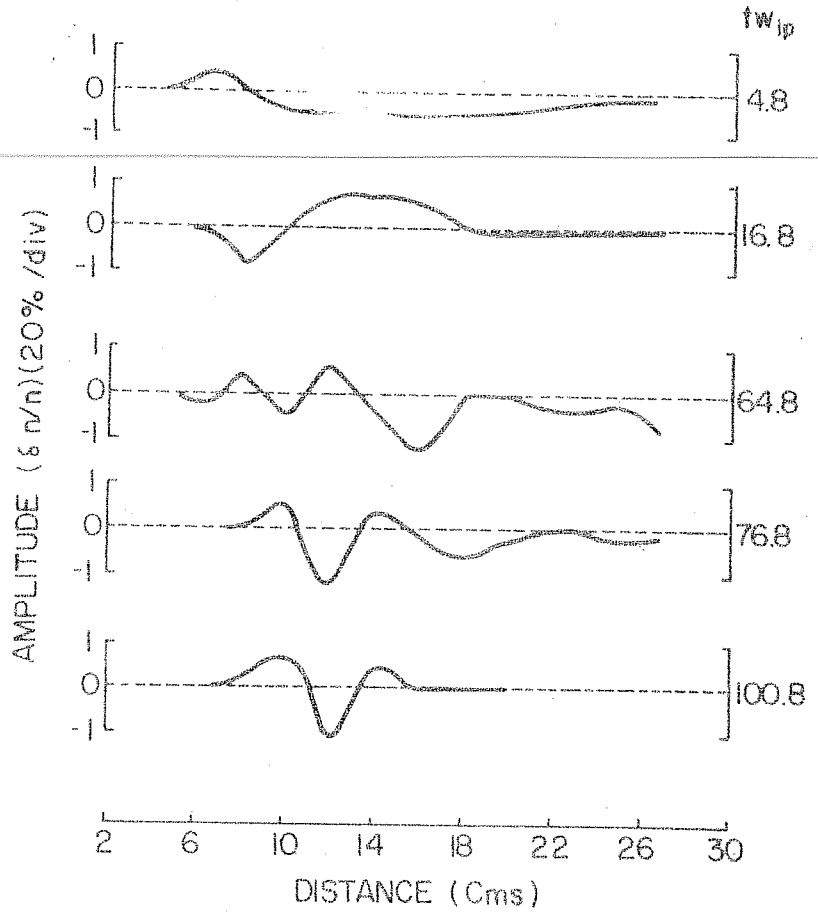

Figure 5.23 Spatial development of the density perturbation corresponding to the potential profiles shown in fig. 5.22.

numerical and analytical works in many important aspects viz. the growth of the ion-acoustic fluctuations in a current carrying plasma accompanied by the cascading of the frequency, growth of the negative potential dip and subsequent formation of asymmetric potential structures. The width of the double layer in our experiment is 42 λ_D which is quite close to the numerical results of 50 λ_D obtained by Sato and Okuda (1980, 1981) and Okuda and Ashour-Abdulla (1982). The amplitude of the potential drops in our result is 0.4, while those obtained in the numerical experiments is also 1.

5.4.4 Comparison with the result of Chan et al. (1984)

Comparing our results with those of Chan et al. (1984) we find quite a few interesting differences between the two, apart from minor differences in the mode of excitation of ion-acoustic instability, that leads to the formation of the double layer.

Chan et al. (1984) observed that on pulsing the grid, the entire plasma potential becomes positive to enable acceleration of the Maxwellian tail electrons. This appears to be very similar to the observations related to plasma expansion as reported by Iizuka et al. (1979) and Mattoo et al. (1981). In our experiment a constant electron current was injected by a steady relative bias and the additional pulse modulated this

current, which is similar to the theoretical predictions of Hasegawa and Sato (1980). In our results, the modulation results in the negative potential well growing from the ion acoustic instability. The experiment of Chan et al. (1984) does not reveal explicitly, the growth of the rarefactive wave. They instead, observed fluctuations on both the low and high potential sides. In our experiment we clearly observe the growth of shock like structure leading to the formation of asymmetric potential structure. We also explicitly observe the damping of compressional modes, as predicted from the theoretical analysis of Lotko (1982)

The negative potential dip accompanying the double layer, is observed till the end of the system i.e. about 30 cms, and persists till the presence of the input pulse that is applied to the source plasma i.e. about 1 msec. This is contrast to the observations of Chan et al. (1984) and Iizuka et al. (1982) wherein, the negative potential dip is filled up as the wave propagates towards the end of the system. Similar results of the presence of the negative potential dip have been observed in the computer simulations of Okuda and Ashour- Abdalla (1982) in the presence of a continuous plasma source.

There are many common features in the two experimental observations viz. the growth of the ion acoustic

fluctuations in a current carrying plasma, cascading down of the frequency coupled with the growth and formation of asymmetric potential structures.

Ion distribution function measurements within the potential wells would have clearly pinned down the observations of ion holes in phase space vortices are being planned for the future work.

We have thus experimentally demonstrated the formation of ion acoustic double layer in a laboratory plasma, beginning from the growth of an ion-acoustic instability in a current carrying plasma. The results are in good agreement with the predictions of numerical simulations and theoretical models.

Chapter 6

CONCLUSIONS

In this thesis, studies of some nonlinear phenomena, like double layers and evolution of nonlinear ion acoustic waves have been presented. The experimental observations of the so called pseudo-double layers, its causes etc., have been discussed in detail. The role of currents in generating weak and strong double layers have been investigated. The time evolution study of rarefaction ion acoustic waves, in quiescent plasmas and in a current carrying plasma have yielded a wealth of information on the nonlinear dynamics of some plasma systems. The conclusions drawn from the results of our experiments are presented below.

6.1 Summary of the experimental results

6.1.1 Moving double layers in an expanding plasma

The detailed investigations on the so called pseudo double layers (Coakley and Hershkowitz, 1979) revealed that the phenomon was essentially due to the ionisation of additional neutral gas that leaked into the system during probe movement. From the velocity measurements it was observed that a high density plasma blob formed near grid G2 as a result of the additional ionisation, expanded into the low density region towards end of the system. The difference in the thermal energies of the charged species led to formation of fast moving double layers, and as a consequence ions were accelerated to very high velocities $\simeq 5\ C_s$. (C_s is the ion acoustic velocity). The thermodynamic model and the self similar expansion model for this phenomena, agree quite well with the experimental observations.

6.1.2 Weak double layers ($e\triangle\phi/kT_e < 10$)

Initially, we were able to form stable and stationary weak double layers with $e\phi/kT_e \simeq 4$ to 5 in the double plasma machine. It was not necessary to provide a separate plasma source on the high potential side, nor

was it necessary to have specially designed sources with surface magnetic fields. The amplitude of the potential drops across the double layers, was observed to reduce beyond a critical value of relative bias potentials, especially beyond values close to ionisation potentials.

6.1.3 Strong Double Layers ($e\Delta\phi/kT_e > 10$)

By suitably modifying the bias configurations, it was possible to generate strong double layers of amplitude $\leqslant$ 100 volts, corresponding to $e\Delta\phi/kT_e \leqslant 50$, in the double plasma machine itself. This was in contrast to the earlier experiments in double plasma and triple plasma machines, where the double layers were rendered unstable beyond the ionisation potential.

Detailed investigation revealed that in the modified version (Chapter IV), we were able to increase the current in the target system by increasing the relative bias voltages, whereas in the other configuration (Chapter 3) the current in the system decreased beyond a critical relative bias voltage. We carried out a circuit analysis which agrees quite well with the experimental observations. We have presented a detailed comparison of the different experiments especially on strong double layers.

6.1.4 Evolution of rarefaction waves

The experiments on rarefactive ion acoustic waves yielded some interesting results contrary to the expectations of fluid theory. In a homogeneous plasma, the rarefaction pulse, after propagating some distance, broadened at the minimum, and then split into two minima, preceded by a nonlinear steepening of the rising edge. One of the troughs propagated at a supersonic speed, while the other propagated at a subsonic speed.

In order to verify the experimental observations, we carried out some computer experiments, by solving the time dependent KdV equation. First we solved the equation without the higher order nonlinearities and dispersion. Next we solved the coupled set of equations including the second order nonlinearities and dispersion. Though the fissioning of the rarefaction into two minima, was not exhibited, some of the results like the nonlinear steepening and generation of ion acoustic wave train etc. were exhibited.

6.1.5 Evolution of an ion acoustic double layer

To study the time evolution of a double layer, we applied a step potential to the source plasma. This modulated the electron beam density/velocity, which gave rise to ion acoustic fluctuations, and at farther distances from G2, there was a preferential growth of ion acoustic rarefactions. The compressive modes damped out leaving an asymmetric potential double layer resembling an ion hole double layer.

6.2 Scope of future work

The experimental results, of the present investigation, provides the basis to pursue further detailed experimental, theoretical and numerical work, to acquire a more complete and thorough understanding of some of the nonlinear processes in plasma physics. The research work intended to be pursued in the immediate future are listed below.

6.2.1 Instabilities associated with the formation of a double layer

We observed in our experiments that at a critical value of relative bias voltages, ion acoustic instability was triggered before the onset of double layers. An

increase in frequency was observed with increasing relative bias. Correlation measurements are being planned, to verify frequency shift observations, and ascertain trapping of particles associated with this phenomena.

6.2.2 Measurement of ion distribution functions

It has been observed in our experiments on rarefactive ion acoustic waves, that trapping of charged particles, especially ions in the potential wells lead to different results. This would probably be reflected in the modification of the ion distribution functions. Monitoring these ion distribution functions in the presence of such structures have been planned. The study of these distribution functions would also throw light on the phenomena like ion phase space vortices etc.

6.2.3 Evolution of a double layer due to resonant effects of an electron beam and a negative potential well

Our experimental results on rarefactive waves in a homogeneous plasma showed that these waves do not damp, as expected from fluid theory. In the presence of an electron current, the rarefactive ion acoustic fluctuations were observed to evolve into a double layer. Though there exist theories, that a negative potential wave ought to grow in the presence of an electron beam, not many experiments have been carried out to verify this phenomena.

We intend studying the effect of an electron beam injected continuously, on a rarefactive wave launched through a grid. It is our conjecture that this should also lead to the formation of ion hole type of double layers.

6.2.4 Transmission and Reflection of Waves across a potential structures

Though the properties of a transmitted and a reflected wave have been studied across the sheath potential of a grid immersed in a plasma, no experimental observation has been carried out, on the propagation of waves in the presence of free potential double layer. This if investigated further, could also serve as a diagnostic for many of the space plasma experiments, to detect the presence of such potential structures.

Though one has to surmount many difficulties in this experiment, due to the presence of instabilities generated by the accelerated charged particles across the double layers, the study of this phenomena would be interesting from Tokamak plasma point of view also, wherein wave propagation in the presence of density fluctuations due to instabilities has been very little understood.

6.2.5 Computer Experiments

We intend carrying out further, the numerical computation to verify some of the above mentioned phenomena, especially the fissioning of the rarefaction wave and the time evolution of the double layer from a rarefactive wave in the presence of a current.

REFERENCES

Abe, K. and Inoue, O. : 1980, J. Comput. Phys. 34 202

Akasofu, S. I. : 1969, Nature, 221 1020

Albert, R.D. and Lindstorm. : 1970, Science, 170 1398

Alfvén, H., and Fälthammar, C.G.: 1963, Cosmical Electrodynamics, Fundamental Principles, Clarendon Press, Oxford.

Alfvén, H. and Carliquist, P.: 1967, Solar Phys. 1 220

Alfvén, H.: 1968, Ann. Geophys. 24 1

Alfvén, H.: 1975 in Physics of the Hot Plasma in the Magnetosphere, eds. B.Hultquist and L. Stenflo, Plenum Publ. Co., New York.

Alfvén, H. and Arrhenius, G.: 1976, Evolution of the Solar Systems, Chapter 15, NASA, p-345

Alfvén, H.: 1976, J. Geophys. Res. 81 4019

Alfvén, H.: 1977, Rev. Geophys. Space Sci. 15 271

Alfvén, H.: 1978, Astrophys. Space Sci. 54 279

Ames, W.F.: 1972, Nonlinear Partial Differential Equations in Engineering (Academic Press)

Andersson, D.: 1977, J. Phys. D : Appl. Phys. 10 1549

Andersson, D.: 1981, J. Phys. D : Appl. Phys. 14 1403

Babić, M., Sandahl, S., and Torvén, S.: 1971, X Conf. on Phenomena in ionised gases, Oxford, p.120

Babić, M. and Torvén, S.: 1974, Trita-EPP-74-02, Dept. of Plasma Phys. Royal Inst. of Tech., Stockholm, Sweden.

Baker, K.D., Singh, N., Block, L.P., Kist, R., Kampea and Thiemann, H.: 1981, J. Plasma Phys. 26 1

Baldwin, D.E. and Logan, B.G.: 1977, Phys. Rev. Lett. 43 1318

Belova, N.G., Galeev, A.A., Sagdeev R.Z. and Sigov, Yu, S.: 1980, JETP. Lett. 31 518

Berezin, Yu, A., and Karpman, V.I.: 1966, J. Expt. Theor. Phys. 51 1557, (Sov. Phys. JETP, 24 1049 (1967)

Bernstein, I.B., Greene, J.M. and Kruskal, M.D.: 1957, Phys. Rev. 108 546

Biskamp, D.: 1969, J. Plasma Phys. 3 411

Block, L.P.: 1969, Rep. No.69-30, Deptts. of Electron and Plasma Phys. Royal Inst. of Tech. Stockholm, Sweden.

Block, L.P.: 1972, Cosmic Electrodyn. 3 349

Block, L.P.: 1975, in Physics of Hot Plasma in the Magnetosphere, eds. B.Hultquist and L.Stenflo, Plenum Press, New York, 229.

Block, L.P. and Falthammar, C.G.: 1976, Ann. Geophys. 32 161

Block, L.P.: 1978, Astrophys. Space Sci. 55 59

Borovsky, J.E. and Joyce, G.: 1981a, U. Iowa Prep. 81-31

Borovsky, J.E. and Joyce, G.: 1981b, U. Iowa Prep. 81-34

Buneman, O.: 1969, Phys. Rev. 115 503

Buti, B.: 1980, Phys. Lett. 76A 251

Carlquist, P.: 1969, Solar Phys. 7 377

Carlquist, P.: 1972, Cosmic Electrodyn. 3 377

Carlquist, P.: 1979, Solar Phys 63 353

Carlquist, P.: 1979, in Wave Instabilities in Space Plasmas, eds. P.J.Palmadesso and K.Papadopoulos, D.Reidel Publ. Co., Holland 83

Chan, C., and Hershkowitz, N. and Longren, K.E.: 1983, Phys. Fluids 26 1587

Chan, C., Cho, M.H., Hershkowitz, N., Intrator, T.: 1984, Phys. Rev. Lett. 52 1782

Chauteur, G., Adam, J.C., Pellat.: 1982, Proc. Int. Conf. on Plasma Phys. Goteborg/Sweden.

Chen, F.F.: 1965, Plasma Diagnostique Techniques. (Ed. Huddlestone, R.H.) Academic Press, New York

Cheng, C.Z. and Knorr, G.: 1976, J. Comput. Phys. 22 330

Coakley, P., Hershkowitz, N., Hubbard, R. and Joyce, G.: 1978, Phys. Rev. Lett. 40 230

Coakley, P., and Hershkowitz, N.: 1979, Phys. Fluids 22 1171

Dahiya, R.P., John, P.I. and Saxena Y.C.: 1978, Phys. Lett. 65A 323

Danielsson, L.: 1973, Astrophys. Space Sci. 24 459

De Groot, J.S., Barnes, C., Walstead, A.E., Buneman, O.: 1977, Phys. Rev. Lett. 38 1283

Fälthammar, C.G.: 1977, Rev. Geophys. Space Phys. 15 457

Fälthammar, C.G., Akasofu, S.I. and Alfven, H.: 1978, Nature, 275 185

Forsythe, E.G., Malcolm, A.M., Molev, B.C.: 1977 Computer Methods for Mathematical Computation (Prenfice-Hall Inc.)

Fowler, T.K. and Logan, B.G.: 1977, Comments on Plasma Phys., Cont. Fusion 2 167

Fujita, H., Yagaura, S. and Matsuo, K.: 1983, Phys. Lett. 99A 317

Gardner, C.S., Greene, J.M., Kruskal, M.D., Miura, R.M.: 1972, Phys. Rev. Lett 19 1095

Gazdag, J.: 1973, J. Comput. Phys. 13 100

Gazdag, J.: 1976, J. Comput. Phys. 20 196

Ghielmetti, A.G., Sharp, R.D., Shelly, E.G., and Johnson, R.G.: 1979, J. Geophys. Res. 84 5781

Goldenbaum, G.C. and Gerber, K.A.: 1973, Phys. Fluids, 16 1289

Goertz, C.K. and Joyce, G.: 1975, Astrophys. Space Sci. 32 165

Goertz, C.K.: 1979, Rev. Geophys. Space Phys. 17 418

Gurevich, A.V. and Pitaevsky, L.P.: 1975, Prog. Aerospace, Sci. 16 227

Haerendel, G., Reiger E., Valenzula, A., Foppl, H., Stenbeck-Nielson, H.C. and Wescott, E.M.: 1976, in European Programmes on Sounding Rocket and Balloon Research in Auroral Zone. ESA-SP 115, European Space Agency, Neuilly, France.

Hasan, S.S. and Ter Haar, D.: 1978, Astrophys. Space Sci. 56 89

Hasegawa, A. and Sato, T.: 1982, Phys. Fluids 25 632

Hatakeyama, R., Iizuka, S., Mieno, T., Rasmussen, J.J. Saeki, K., Sato, N.: Proc. of 1980 Autumn Meeting of Physical Society of Japan, Fukui, 62

Hatakeyama, R., Saeki, K., and Sato, N.: 1982, Phys. Rev. Lett. 48 145

Hendel, H.W. and Reboul, T.T.: 1962, Phys. Fluids 5 360

Hershkowitz, N., Romesser, T., and Montgomery, D.: 1972, Phys. Rev. Lett. 29 1586

Hollenstein, Ch., Gyot, M., and Weibel, E.S.: 1980, Phys. Rev. Lett. 45 2110

Hollenstein, Ch. and Gyot, M.: 1983, Phys. Fluids 26 1606

Hubbard, R.F. and Joyce, G.: 1979, J. Geophys. Res. 84 4297

Hudson, M.K. and Potter, D.W.: 1981, in Physics of Auroral Arc formation (Ed. S.-I. Akasofu and J.R. Kan), American Geophysical Union, Washington, 260

Hudson, M.K., Lotko, W., Roth, I. and Witt, E.: 1983, J. Geophys. Res. 88 916

Ichikawa, Y.H., Mitsuhashi, T., Konno, K.: 1976, J. Phys. Soc. Japan 41 1382

Iichikawa, Y.H., Mitsuhashi, T., Konno, K.: 1977, J. Phys. Soc. Japan, 43 675

Iizuka, S., Saeki, K., Sato, N., Hatta, Y.: 1979, Phys. Rev. Lett. 43 1404

Iizuka, S., Michelsen, P., Rasmussen, J.J., Schritweiser, R., Hatokeyama, R., Saeki, K. and Sato, N.: 1982, Phys. Rev. Lett. 48 145

Ikezi, H., Taylor, R.J. and Baker, D.: 1970, Phys. Rev. Lett. 25 11

Ikezi, H.: 1978 in Solitons in Action, Ed. K.E.Longren and A. Scott, Academic Press.

John, P.I. and Saxena, Y.C.: 1976, Phys. Lett. 56A 385

John, P.I., Saxena, Y.C. and Dahiya, R.P.: 1977, Phys. Lett. 60A 119

Johnson, L.E.: 1980, J. Plasma Phys., 23 433

Jovanovic, D., Lynov, J.P., Michelsen, P., Pecseli, H.L., Rasmussen, J.J., and Thomsen, K.: 1982, Proc. of Symp. on Plasma Double Layers, Riso National Laboratory, Denmark, 147

Joyce, G., and Hubbard, R.F.: 1978, J. Plasma Phys. 20 391

Kan, J.R. and Akasofer, S.I.: 1978, J. Geophys. Res. 83 735

Kan, J.R. Lee, L.C. and Akasofu, S.-I.: J. Geophys. Res. 84 4305

Kanazawa, T., Hatakeyama, R., and Sato, N.: 1981, Proc. of Autumn Meeting of Physical Society of Japan, Niigata, 93

Kaw, P.: 1982, Private communication.

Kemp, R.F., and Sellen, J.M.: 1966, Rev. Scient. Instrumn. 37 455

Kim, K.Y.: 1983, Phys. Lett. 97A 45

Kindel, J.M., Barnes, C., and Forslund, D.W.: 1981, in Physics of Auroral Arc Formation (ed. S.-I. Akasofu and J.R. Kan), AGU Monograph 25 296

Knorr, G. and Goertz, C.K.: 1974, Astrophys. Space Sci. 31 209

Kono, M. and Mulser, P.: 1983, Phys. Fluids 26 3004

Langmuir, I.: 1929, Phys. Rev. 33 954

Leung, P., Wong, A.Y. and Quon, B.H.: 1980, Phys. Fluids 23 992

Levine, J.S. and Crawford, F.W.: 1980, J. Plasma Phys. 23 223

Longren, K.E.: 1977, Recent Advances in Plasma Physics (ed. B. Buti) Indian Academy of Sciences, 39

Longren, K.E.: 1983, Plasma Phys. 25 943

Lotko, W., and Kennel, C.F.: 1981, in Physics of Auroral Arc Formation (ed. S.-I. Akasofu and J.R. Kan) AGU Monograph, 25 437

Lotko, W.: 1982, Preprint No. SSL-82-110, Space Sciences Laboratory, University of California, Berkeley

Lotko, W. and Kennel.: 1983, J. Geophys. Res. 88 381

Lutsenko, E.T., Sereda, N.D., and Kontsevoi, L.M.: 1975, Zh. Tekh. Fiz. 45 789 (Sov. Phys. Tech. Phys. 20 498 (1976)

Mason, R.J.: 1970, Phys. Fluids 13 1042

Mattoo, S.K., Saxena, Y.C. and Sekar, A.N.: 1980, Pramana 15 525

Mattoo, S.K., Saxens, Y.C. and Sekar, A.N.: 1981, Fusion Energy - Spring College on Fusion Energy, Trieste, 305

Moiseev, S.S. and Sagdeev, R.Z.: 1963, Plasma Phys. (J. Nucl. Energy, part C) 5 43

Montgomery, D., and Joyce, G.: 1969, J. Plasma Phys. 3 1

Mozer, F.S., Carlson, C.W., Hudson, M.K., Torbert, R.B., Parady, B., Yatteau, J., and Kelly, M.C.: 1977, Phys. Rev. Lett. 38 292

Nakamura, Y.: 1982, IEEE Trans. Plasma Sci. PS-10, 180

Okuda, H., and Ashour-Abdalla, M.: 1982, Phys. Fluids 25 1564

Ott, E. and Sudan, R.N.: 1969, Phys. Fluids 12 2388

Okutsu, E. and Nakamura, Y.: 1979, Plasma Phys. 21 1053

Perkins, F.W., Sun, Y.C.: 1981, Phys. Rev. Lett. 46 115

Pierce, J.R.: 1944, J. Appl. Phys. 15 721

Quon, B.H. and Wong, A.Y.: Phys. Rev. Lett. 37 1393

Raadu, M.A. and Carlquist, P.: 1981, Astrophys. Space Sci. 74 189

Sagdeev, R.Z.: 1966, Reviews of Plasma Phys. 4 New York

Sato, N., Hatakeyama, R., Iizuka, S., Mieno, T., Saeki, K., Rasmussen, J.J. and Michelsen, P.: 1981, Phys. Rev. Lett. 46 1330

Sato, N.: 1982, Proc. of Symp. on Plasma Double Layers, Riso National Laboratory, Denmark, 116.

Sato, T., and Okuda, H.: 1980, Phys. Rev. Lett. 44 740

Sato, T. and Okuda, H.: 1981, J. Geophys. Res. 86 3357

Saxena, Y.C., Mattoo, S.K., Sekar, A.N. and Chandua, V.: 1981, Phys. Lett. 84A 71

Schamel, H. and Bujarbarua, S.: 1980, Phys. Fluids 23 2498

Schamel, H.: 1982, Proc. of Symp, on Plasma Double Layers, Riso National Laboratory, Denmark 13

Sekar, A.N.: 1982, Proc. Indian Natn. Sci. Acad. 48A 256

Sekar, A.N., Mattoo, S.K., Mohan, M. and Saxena, Y.C.: 1982, Proc. Int. Conf. on Plasma Phys. Goteborg, Sweden, 141

Shawhan, S.D., Goertz, C.K., Hubbard, R.F., Gurnett, D.A., and Joyce, G.: 1975, in V. Formisano (ed). The Magnetospheres of Earth and Jupiter, Reidel. Co. Dordreeht, Holland, 375

Shawhan, S.D.: 1976, J. Geophys. Res. 86 3373

Sherman, J.C.: 1973, Astrophys. Space Sci. 24 487

Singh, N.: 1980, Plasma Phys. 22 1

Singh, N.: 1982, Plasma Phys. 24 639

Singh, N. and Schunk, R.W.: 1982, J. Geophys. Res. 87 3561

Smith, J.R., Hershkowitz, N. and Coakley, P.: 1979, Rev. Sci. Instrumn. 50 210

Smith, R.A., and Goertz, C.K.: 1976, J.Geophys. Res. 83 2617

Smith, R.A.: 1982, Physica Scripta 25 413

Stenzel, R.L., Ooyama, M., Nakamura, Y.: 1980, Phys. Rev. Lett. 45 498

Stenzel, R.L., Ooyama, M., Nakamura, Y.: 1981, Phys. Fluids, 24 708

Stenzel, R.L., Gekelman, W., and Wild, N.: 1982, Proc. of Symp. on Plasma Double Layers, Riso National Laboratory, Denmark 181

Swift, D.W.: 1975, J. Geophys. Res. 80 2096

Tanuiti, T. and Wei, Ch. Ch.: 1968, J. Phys. Soc. Japan 27 941

Tappert.: 1974, Lectures in Appl. Math. 15 215

Temerin, M., Cerny, Lotko, W. and Mozer, F.S.: 1982, Phys. Rev. Lett. 48 1175

Torvén, S.: 1971, Physica Scripta 4 65

Torvén, S. and Babic, M.: 1975, in J.G.A. Holscher and D.C. Schroum (eds), Proc. 12th Int. Conf. on Phenomena in ionised gases, American Elsevier Publ. Co., New York, 124

Torvén, S.: 1979, in Wave Instabilities in Space Plasmas (Eds. P.J. Palmadesso and K. Papadopoulos), D. Reidel Publ. Co., Dordrecht, Holland, 109

Torvén, S. and Andersson, D.: 1979, J. Phys. D : Appl. Phys. 12 717

Torvén, S.: 1980, Trita-EPP-80-02, Dept. of Plasma Phys., Royal Inst. of Tech. Stockholm, Sweden.

Torvén, S. and Lindberg, L.: 1980, J. Phys. D : Appl. Phys. 13 2285

Torvén, S.: 1981, TRITA-EPP-81-05, Dept. of Plasma Physics, Royal Inst. of Tech. Stockholm, Sweden.

Torvén, S, and Litting, S.: 1982, Proc. of 1982 Int. Conf. on Plasma Phys. Goteborg, Sweden, 26

Wahlberg, C.: 1979, J. Plasma Phys. 22 303

Washimi, H. and Tanuiti, T.: 1966, Phys. Rev. Lett. 17 266

Watanabe, S.: 1975, J. Plasma Phys. 14 353

Wescott, E.M., Stenbeck-Nielson, H.C., Halliman, T.J., Davis, T.N., and Peek, H.M.: 1976, J. Geophys. Res. 81 4495

Whitham, G.B.: 1974, Linear and Nonlinear Waves (Wiley-Interscience, New York)

Yabe, T., Mima, K., Yoshikawa, K., Takabe, H., Hamano, M.: 1981, Nucl. Fusion 21 803

Yajima, N., Tanuti, T. and Outi, A.: 1966, J. Phys. Soc. Japan, 21 757

Zabusky, N.J. and Kruskal, M.D.: 1965, Phys. Rev. Lett. 15 240